Development of an *In vitro* Test Using Dendritic Cells to Assess the Hazard of Food-borne Nanomaterials

---

Dissertation

zur

Erlangung der naturwissenschaftlichen Doktorwürde
(Dr. sc. nat.)

vorgelegt der

Mathematisch-naturwissenschaftlichen Fakultät

der

Universität Zürich

von

Hans Christian Winkler

aus

Zürich ZH und Basel BS

Promotionskomitee

Prof. Dr. Hanspeter Nägeli (Vorsitz und Leitung)

Prof. Dr. Barbara Rothen-Rutishauser

Prof. Dr. Cornel Fraefel

Zürich, 2016

Table of Content

Summary

The development of nano-materials is viewed as one of the most important technological advances of the 21st century and new applications of nano-sized particles in the production, processing, packaging or storage of food are expected to emerge soon. This trend of growing commercialization of engineered nanoparticles (NPs) as part of modern diet will substantially increase oral exposure due to their deliberate or accidental incorporation in food. After oral uptake, NPs encounter dendritic cells (DCs), which constitute first-line biological sensors of foreign materials invading the organism. These specialized sentinel cells are necessary to launch immune reactions against pathogens but also to mediate tolerance to self-antigens and, in the intestinal milieu, to nutrients and commensals. A key question in the safety evaluation of orally ingested nanomaterials is, therefore, whether their contact with DCs in the intestinal mucosa disrupts this delicate homeostatic balance between pathogen defense and tolerance.

Here, we monitored the response of steady-state DCs exposed to food-grade synthetic amorphous silica (SAS) to examine the potential ability of this common nanomaterial to trigger adverse immune reactions. The differential display of molecular maturation markers shows that SAS particles are able to activate completely immature, unprimed DCs differentiated from hematopoietic progenitors. A concomitant internalization of particles by endocytic uptake into the DCs fails to elicit cytotoxicity. However, this endocytic uptake of SAS particles leads to induction of the pro-interleukin-1β (pro-IL-1β) cytokine precursor, subsequently cleaved by the inflammasome to secrete highly inflammatory IL-1β. In contrast, neither pro-IL-1β induction nor IL-1β secretion is triggered upon internalization of TiO_2 or $FePO_4$ nanoparticles. Pharmacologic inhibitors of the endosomal pathogen recognition process like chloroquine and bafilomycin A1 suppress the observed pro-IL-1β induction, indicating that expression of this cytokine precursor takes place in DCs because the nanostructured surface of SAS materials mimics a microbe-associated molecular pattern.

This activation of immature DCs with a direct *de novo* induction of a potent inflammatory cytokine, by a novel and unexpected mechanism, implies that the currently massive use of SAS materials as food additives should be reconsidered.

Zusammenfassung

Die Entwicklung von Nanomaterialien wird als eine der bedeutendsten Errungenschaften des 21. Jahrhunderts angesehen und neue Anwendungen von Nanopartikeln in der Lebensmittelproduktion, -verarbeitung, -verpackung und -aufbewahrung werden in naher Zukunft erwartet. Durch diesen Trend wachsender Kommerzialisierung wird die orale Exposition durch bewusste oder unbeabsichtigte Beimischung von synthetisch hergestellten Nanopartikeln (NP) in Lebensmitteln substanziell erhöht. Nach der oralen Aufnahme treffen NP auf dendritischen Zellen (DC), die als biologische Alarmgeber den Eintritt fremder Materialien überwachen. Diese spezialisierten Wächterzellen sind notwendig, um einerseits effektive Immunantworten gegen Pathogene zu initiieren, und andererseits um immunologische Toleranz gegenüber körpereigenen Antigenen und im Darm zusätzlich gegenüber Nahrungsmitteln und nützlichen Kommensalen zu vermitteln. Eine Schlüsselfrage in der Sicherheitsbeurteilung von Nanopartikeln in Lebensmitteln lautet daher, ob ihr Kontakt mit DC in der intestinalen Schleimhaut dieses Gleichgewicht zwischen Abwehr und Toleranz beeinträchtigt.

In dieser Arbeit wurde daher die Reaktion von unreifen dendritschen Zellen auf synthetisches amorphes Siliciumdioxid (SAS) getestet, um zu untersuchen, ob die dieses Material unerwünschte Immunreaktionen hervorrufen kann. Veränderungen der molekularen Maturationsmarker zeigen, dass SAS unreife, unstimulierte DC, die aus hämatopoetischen Vorläuferzellen differenziert wurden, aktivieren kann. Die Partikel werden bei diesem Prozess endosomal aufgenommen, lösen aber keine Zytotoxität aus. Allerdings wird durch diese endosale Aufnahme das Propeptid pro-Interleukin-1β (pro-IL-1β) induziert, das anschliessend vom Inflammasom enzymatisch gespalten und als hochentzündliches Zytokin IL-1β freigesetzt wird. Im Gegensatz dazu löste die Aufnahme von TiO_2 oder $FePO_4$ Nanopartikeln weder pro-IL-1β Induktion noch Sektretion von IL-1β aus. Pharmakologische Inhibitoren des endosomalen Mustererkennungssystems wie Chloroquin und Bafilomycin A1 unterdrücken die pro-IL-1β-Induktion, was darauf hinweist, dass das Propeptid pro-Interleukin-1β (pro-IL-1β) induziert wird, weil die nanostrukturierte Oberfläche von SAS-Materialien ein Pathogen-assoziiertes molekulares Muster imitiert.

Die Aktivierung von unreifen, unstimulierten DC mit direkter *de novo* Induktion eines hochentzündlichen Zytokins – über einen neuartigen und unerwarteten Mechanismus – impliziert, dass der allgegenwärtige, verbreitete Einsatz von SAS-Materialien als Lebensmittelzusatzstoff überdacht werden sollte.

Abbreviations

BET	Brunauer-Emmett-Teller theory
BSA	Bovine serum albumin
CD	Cluster of differentiation
CpG	Single stranded DNA containing an unmethylated cytosine-phosphatidyl-guanine motif
cDC	Conventional dendritic cell
DC	Dendritic cell
DNA	Desoxyribonucleic acid
E 551	Synthetic amorphous silica permitted as food additive
EDX	Energy-dispersive X-ray spectroscopy
ELISA	Enzyme-linked immuno sorbent assay
EU	Endotoxin unit
FBS	Fetal bovine serum
Flt3L	Feline McDonough sarcoma-like tyrosine kinase 3 ligand
FMO	Fluorescence-minus-one
FSC	Front scatter
GM-CSF	Granulocyte-macrophage colony-stimulating factor
HAADF	High angle annular dark filed detector
IL	Interleukin
kD	Kilodalton
LOD	Limit of detection
LPS	Lipopolysaccharide from *E. coli*
NOAEL	No observed adverse effect level
ODN	DNA oligonucleotide
PAGE	Polyacrylamide gel electrophoresis
PAMP	Pathogen-associated molecular pattern
PBS	Phosphate-buffered saline
pDC	Plasmacytoid dendritic cell
PS	Polystyrene
RNA	Ribonucleic acid

RPMI-1640	Roswell Park Memorial Institute 1640 medium
SAS	Synthetic amorphous silica
SDS	Sodium dodecyl sulfate
SSC	Side scatter
TBS	Tris-buffered saline
TBST	Tris-buffered saline Tween® 20
TEM	Transmission electron microscopy
TLR	Toll-like receptor
TNF	Tumor necrosis factor
WBC	White blood cell
WCE	Whole cell extracts

Units

°C	Degrees Celsius
Da	Dalton
h	Hour
L	Liter
min	Minute
rpm	Revolutions per Minute
U	Unit

1 Introduction

Although the respiratory toxicity of inhaled nanomaterials gained much attention (Warheit & Donner, 2015; Yazdi et al., 2010), the gastrointestinal tract is exposed to comparably much larger amounts of inorganic particles including nanostructured food additives (Evans et al., 2002; Lomer et al., 2002; Winter et al., 2011; Yada et al., 2014). Silica (silicon dioxide) has currently the highest production volume of all engineered nanomaterials worldwide (Yang et al., 2016). Common applications in the food industry use synthetic amorphous silica (SAS) as anticaking agent in powdered food products (Figure 1), as defoaming agent in beverages, as a thickener in pastes or carrier of flavorings (Dekkers et al., 2011; Peters et al., 2012). Titanium dioxide, containing up to 36% particles with a size below 100 nm, serves as a whitening agent in food and toothpastes (Weir et al., 2012). New emerging uses in the food industry include $FePO_4$ particles for iron fortification (Hilty et al., 2010).

Figure 1. Food products containing nano-structured synthetic amorphous silica (SAS) particles (E551) or titanium dioxide (E171) as a food additive. Several food products containg the food additives E171 and/or E551 as ingredients are shown.

1.1 Nano-structured silica in food

Section 1.2 and a part of section 5 constitute part of a review article. I wrote the manuscript together with H. Naegeli.

Winkler *et al. J Nanobiotechnol (2016) 14:44*
DOI 10.1186/s12951-016-0189-6

Journal of Nanobiotechnology

REVIEW Open Access

Critical review of the safety assessment of nano-structured silica additives in food

Hans Christian Winkler[1], Mark Suter[2] and Hanspeter Naegeli[1*]

Abstract

The development of nano-materials is viewed as one of the most important technological advances of the 21st century and new applications of nano-sized particles in the production, processing, packaging or storage of food are expected to emerge soon. This trend of growing commercialization of engineered nano-particles as part of modern diet will substantially increase oral exposure. Contrary to the proven benefits of nano-materials, however, possible adverse health effects have generally received less attention. This problem is very well illustrated by nano-structured synthetic amorphous silica (SAS), which is a common food additive since several decades although the relevant risk assessment has never been satisfactorily completed. A no observed adverse effect level of 2500 mg SAS particles/kg body weight per day was derived from the only available long-term administration study in rodents. However, extrapolation to a safe daily intake for humans is problematic due to limitations of this chronic animal study and knowledge gaps as to possible local intestinal effects of SAS particles, primarily on the gut-associated lymphoid system. This uncertainty is aggravated by digestion experiments indicating that dietary SAS particles preserve their nano-sized structure when reaching the intestinal lumen. An important aspect is whether food-borne particles like SAS alter the function of dendritic cells that, embedded in the intestinal mucosa, act as first-line sentinels of foreign materials. We conclude that nano-particles do not represent a completely new threat and that most potential risks can be assessed following procedures established for conventional chemical hazards. However, specific properties of food-borne nano-particles should be further examined and, for that purpose, in vitro tests with decision-making cells of the immune system are needed to complement existing in vivo studies.

Keywords: Aerosil, Corona, Dendritic cells, E 551, Food toxicology, Lymphoid tissue, Nanomaterial, SAS, Synthetic amorphous silica, Silicium dioxide

Background

The use of nanotechnology has many potentially beneficial applications in food production, processing and storage. The largest share of predicted markets involves nano-sized coatings of food-packaging materials that optimize mechanical properties or exert antimicrobial activity. In the future, nano-sized additives may be deliberately included to modify food properties such as taste, sensation, color, texture, consistency or shelf life, to fortify basic foods with nutrients and vitamins or to enhance bioavailability. An emerging application in the food industry includes, for example, the use of nano-Fe particles for iron supplementation. Nano-sized materials might further be employed as indicators of food quality and freshness, or to ensure traceability [1–3]. In contrast to these novel developments, nano-structured silica has been on the market as a food additive since around 50 years. In the United States, the Food and Drug Administration allows up to 2 % by weight of such silica particles to be added to food [4]. Within the European Union (EU), Commission Regulation 1129/2011 sets a maximum level for silica of 1 % by weight in dried powdered foodstuffs [5]. Silica particles may thus be regarded as a paradigmatic case for the safety assessment of nano-material applications in the food industry.

A European Commission Recommendation defines nano-materials as having one dimension not exceeding 100 nm [6]. However, there is no solid scientific ground

*Correspondence: naegelih@vetpharm.uzh.ch
[1] Institute of Pharmacology and Toxicology, University of Zurich-Vetsuisse, Winterthurerstrasse 260, 8057 Zurich, Switzerland
Full list of author information is available at the end of the article

to propose a strict size boundary and the prefix "nano" does not make a substance automatically harmful. Nevertheless, the nano-size scale changes the material characteristics as compared to larger particles or the same substance in a dissolved state. Nano-sized materials display an increased surface-to-mass ratio that enhances their reactivity compared to larger structures [7, 8]. Also, nano-sized particles easily penetrate intact cell membranes thus conferring the potential for trafficking across biological barriers including the epithelium of the gastrointestinal tract [9–13]. Until now, the health effects of nano-particles have been studied mainly in relation to a respiratory uptake [14]. Considering their widespread food-related uses, however, there is an urgent need to review the suitability of oral toxicity and risk assessment studies addressing the long-term safety of nano-structured silica.

Synthetic amorphous silica

Silicon (Si) is a metalloid displaying an atomic weight of 28. The terms "silicium" and "silica" refer to naturally occurring or anthropogenic materials composed of silicon dioxide (SiO_2), which appears in two major forms, i.e., crystalline and amorphous. Synthetic amorphous silica (SAS) is widely applied to processed foods and registered by the EU as a food additive with the code E 551 [15]. The main purpose of SAS particles in the food industry is to prevent poor flow or "caking", particularly in powdered products. SAS particles are additionally employed as a thickener in pastes or as a carrier of flavors, and also to clarify beverages and control foaming [16–18].

Silica particles exist in large amounts in nature and it is acknowledged that that they have been dietary constituents throughout human evolution. However, the risk assessment of silica discussed in this review is limited to man-made materials introduced as food additives. In 1942, Harry Kloepfer (a chemist working at Degussa, now Evonik) invented the Aerosil procedure for the production of SAS particles intended for the food industry [19, 20]. Following a standard pyrogenic process, also known as flame hydrolysis, silicon tetrachloride is burned in a hydrogen flame at temperatures of 1000–2500 °C, generating silica nano-particles with a diameter of ~10 nm [21]. This material is denoted pyrogenic or fumed silica referring to the above production method. In an alternative wet route of synthesis, nanostructured SAS particles denoted as precipitated silica, silica gel or hydrous silica, are produced from alkali metal silicates dissolved in water and reacted with sulphuric acid. In the EU, only synthetic particles obtained by these pyrogenic or wet processes are allowed as food additive [15]. All SAS products aggregate into larger particles with sizes in the order of 100 nm, which further agglomerate to form micron-sized structures [14, 22]. The term "aggregate" describes an assembly of particles held together by strong forces such as covalent or metallic bonds. "Agglomerates" of particles appear as a consequence of weak forces like van der Waals interactions, hydrogen bonding, electrostatic attractions or adhesion by surface tensions. SAS materials are hydrophilic but can be rendered hydrophobic, thus reducing their moisture uptake, by subsequent surface modifications.

Oral toxicity studies using SAS particles

A synopsis of animal studies addressing the oral safety of SAS particles was published by the European Centre for Ecotoxicology and Toxicology of Chemicals (ECETOC) [23] and, more recently, by the Organization for Economic Co-operation and Development (OECD) [24]. No mortality or adverse signs resulted from acute exposure by single oral administrations of hydrophilic SAS particles to rodents at doses of up to 5000 mg per kg body weight. A sub-acute (28-day) study was carried out by oral gavage administration of hydrophilic SAS particles to Wistar rats. The daily doses ranged between 100 and 1000 mg/kg body weight. None of the monitored endpoints (clinical signs, food consumption, body weight, behavioral tests, hematology, clinical chemistry parameters, organ weights, macroscopic pathology and histological examinations) revealed any substance-related abnormalities [25].

In a sub-chronic (90-day) toxicity study carried out in Charles River rats with daily doses of up to 3500 mg/kg body weight, hydrophilic SAS particles included in the feed did not elicit systemic toxicity and did not affect growth rate, food consumption or survival [26]. Also, no macroscopic or microscopic changes were observed in post-mortem analyses of the organs of exposed animals. A more detailed 90-day toxicity study was conducted in Wister rats with in-diet administrations of hydrophilic SAS particles (up to 4000 mg/kg body weight daily). Endpoints included general condition and survival, behavior, water intake, food consumption, body weight, hematology, clinical chemistry, urinary analysis, organ weights, macroscopic pathology and histological examinations. As observed in the previous sub-chronic study, none of these parameters revealed any effects ascribed to SAS ingestion [27]. Sub-chronic dietary exposure studies were also carried out with hydrophobic SAS particles not permitted as food additive in the EU. In one case [28], no treatment-related abnormalities were reported except minimal changes in the thyroid gland morphology of male rats exposed to 2000 and 4000 mg/kg body weight daily. In another repeated dose toxicity study with hydrophobic SAS particles [29, 30], Wister rats were exposed

via the diet for 5 weeks at 0 (control), 500 or 1000 mg/kg body weight per day, and for 8 weeks at progressively increasing SAS doses from 2000 to 16,000 mg/kg body weight per day. Animals in these high-dose group developed severe atrophy of the liver detected by microscopic examination, which was also observed to a milder degree in the 1000-mg/kg dose group.

Further effects on the liver were described in more recent reports, thus converging on a potential systemic hazard of SAS particles (Table 1). In one repeated oral toxicity study, BALB/c mice were exposed for 10 weeks to hydrophilic nano- or micron-sized silica particles prepared from rice husk (not permitted as food additive in the EU) [31]. The inclusion rate in feed was 1 % (wt/wt) translating to an expected oral uptake of 1500 mg/kg body weight per day. The animal group fed the nano-particles showed a significantly higher serum level of alanine aminotransferase (a biomarker of liver injury) compared to untreated controls or animals tested with micro-sized silica. In the histologic examination of tissues from mice exposed to nano-particles, but not in those exposed to micro-particles, there was an appearance of fatty liver characterized by abnormally frequent lipid droplets in hepatocytes. Further liver reactions were detected in a repeated dose toxicity study in Sprague–Dawley rats [32]. The animals were exposed via feed to hydrophilic SAS particles obtained from Evonik (denoted "Evonik-SAS") or from the Joint Research Centre of the European Commission (denoted "JRC-SAS"). Both materials were produced by flame hydrolysis but differed in their surface area, i.e., 380 and 200 m^2/g for "Evonik-SAS" and "JRC-SAS", respectively. These particles were delivered with the feed at different daily doses (between 100 and 2500 mg/kg body weight) for 28 days, whereby the exposure was extended to 84 days for the highest dose groups. No treatment-related effects were observed after 28 days. However, following 84 days of exposure, the occurrence of periportal liver fibrosis was higher than in control animals (Table 1). This increase in the frequency of liver fibrosis was significant in the JRC-SAS-treated animals ($p = 0.02$) but slightly below statistical significance ($p = 0.07$) in the Evonik-SAS-treated group. The histological effects were not accompanied by changes in clinical chemistry. Notably, this experiment also included some immunological parameters like IgG and IgM levels in blood, lymphocyte proliferation, as well as cytokine release from in vitro activated lymphocytes. None of the tested immunological endpoints were affected in any of the dose groups.

Long-term dietary studies in rats [33] were used for the risk assessment of human exposure. Groups of 40 Fischer rats were fed 0 (control), 1.25, 2.5 and 5 % (wt/wt) hydrophilic SAS particles for 103 consecutive weeks. The design of this chronic bioassay is outlined for the high-dose group in Table 2. The feed was not examined for possible nutritional imbalances [34]. There were no test substance-related effects on food consumption, overall survival, clinical laboratory or hematologic results and microscopic pathology findings. Liver weights were significantly reduced in the females fed 2.5 and 5 % SAS particles and this effect might be a consequence of the lower body weight attained in these two higher dose groups relative to controls and animals in the 1.25 % inclusion group. It is retrospectively not possible to distinguish whether the effect on liver weight represents an adverse reaction to SAS ingestion or whether it is an indirect consequence of a possible nutritional imbalance not directly related to SAS exposure. Notably, SAS-treated males displayed isolated cases of hyperplastic nodules in the liver and pheochromcytomas in the adrenal gland, but none of the control animals had such rare lesions. A long-term study in B6C3F1 mice involved groups of 40 animals fed 0 (control), 1.25, 2.5 and 5 % (wt/wt) SAS particles for 93 weeks [33]. Again, the feed was not examined for nutritional imbalances. The growth rate was significantly reduced in the mice of the high-dose group only at the end of the first 10 study weeks. Food consumption was significantly increased in the males fed 2.5 and 5 % SAS particles but no other substance-related differences came to light. The treatment had no effect on clinical chemistry, hematologic results and macroscopic as well as microscopic pathology findings. Recently, the European Commission Scientific Committee on Consumer Safety pointed out that these long-term studies

Table 1 Oral repeated dose toxicity studies with amorphous silica yielding liver effects

Species	Study length	Effect	LOAEL	NOAEL	Reference
Wistar rats	5–8 weeks	Liver atrophy	1000 mg/kg body weight per day	500 mg/kg body weight per day	[29, 30]
Balb/c mice	10 weeks	Fatty liver	1500 mg/kg body weight per day	NA	[31]
Sprague–Dawley rats	12 weeks	Periportal liver fibrosis	810 mg/kg body weight per day	NA	[32]
Fischer rats	103 weeks	Reduced liver weight	1000 mg/kg body weight per day	500 mg/kg body weight per day	[33]

Delivery of particles was by inclusion into the feed. This table proposes *LOAEL* (lowest observed adverse effect level) and *NOAEL* (no observed adverse effect level) values that differ from those purported in previous risk assessment reports. Other oral repeated dose studies [25–27] did not elicit adverse effects

Table 2 Outline of the chronic toxicity study with SAS particles carried out in rats

	Weeks of feeding						
	0	**5**	**15**	**30**	**50**	**81**	**103**
Body weight (g)	108 ± 6	174 ± 9	223 ± 11	253 ± 10	310 ± 18	364 ± 26	359 ± 56
Feed intake (g/day)		11.1 ± 0.4	10.4 ± 0.4	10.2 ± 0.5	11.9 ± 0.8	13.2 ± 0.8	12.7 ± 2.7
SAS intake (g/kg body weight per day)		3.2	2.3	2.0	1.9	1.8	1.8

Summarized data from the oral chronic toxicity study in Fischer rats [33]. This table illustrates the relationship between body weight, feed intake and daily doses in the females of the highest dose group, where the feed was supplemented with 5 % (wt/wt) SAS particles. When corrected for the actual feed intake, the daily dose of SAS particles was between 1.8 and 2.0 g/kg body weight during most of the study period

in rodents cannot be considered as adequate for risk assessment because it is not clear whether the research was conducted under generally accepted guidelines and because the test material was not properly described [35].

To summarize, a critical analysis of existing oral repeated dose studies in rodents reveals data gaps and uncertainties limiting their predictive value for the risk assessment of human dietary exposure. Some studies were based on poorly characterized particles in terms of composition, impurities or physico-chemical properties, and most reports lacked an assessment of particle size distribution.

Oral bioavailability and systemic distribution

Little is known on the intestinal absorption of nano-sized SAS particles and the potential to disseminate into tissues. A limited systemic uptake following oral ingestion cannot be ruled out although none of the tested SAS particles were shown to bio-accumulate [19]. This is illustrated by a repeated dose kinetic study, in which rats were administered SAS particles via gavage at a low dose of 20 mg/kg body weight during 5 consecutive days [36, 37]. On the sixth day of the study, measurements by quadrupole inductively coupled plasma mass spectrometry (ICP-MS) revealed only slightly elevated silicon levels in liver and spleen. The gastrointestinal absorption after administration of SAS particles, estimated from these silicon measurements in tissues and not considering a concurrent excretion, ranged between 0.03 and 0.06 % of the total oral dose [38]. In another repeated dose study already presented above, rats were administered SAS particles via feed for 28 days, with continued administration in the high-dose group for up to 84 days. Silicon contents were measured at days 29 and 84 by ICP-MS in liver, spleen, kidney, brain and testis. Conversion of the resulting silicon levels to assumed silica concentrations in tissues, again not considering concomitant excretion processes, indicated an overall oral bioavailability of 0.02 % or less [32]. The highest silica concentration (up to ~300 mg/kg tissue against a physiologic background below the limit of detection) was found in the spleen of SAS-exposed animals. So far, no SAS particles have been detected in mesenteric lymph nodes or any other organ after oral uptake and, therefore, it is not clear whether the observed silicon residues exist in a particulate form or rather in a dissolved state, for example as orthosilicic acid.

Another key issue that has not yet been investigated with regard to bioavailability and systemic distribution is the effect of biomolecules bound to nano-particles changing their surface properties [38]. In particular, SAS nano-particles are known to be decorated by proteins, for example fibrinogen or apolipoprotein A1, as soon as they get in contact with biological fluids [39]. The term "protein corona" was introduced to describe the attachment of plasma proteins to the surface of nano-particles [40, 41]. One possible effect of this corona is that it mediates the uptake of nano-particles into cells and organs including the liver, thus influencing bioavailability and tissue distribution [42].

Human exposure

To obtain realistic dietary exposure values for a European population, Dekkers and colleagues [18] selected food products from a local supermarket (ready-to-eat meals, soups, sauces, coffee creamers, pancake mixes, seasonings and supplements) based on declarations for the presence of E 551. Next, the total silica concentration in these products was determined by inductively coupled plasma atomic emission spectrometry (ICP-AES). Then, dietary intake estimates of these products for the population were calculated using a Dutch food consumption survey [43]. Based on estimated consumption and silica levels, the resulting daily dietary intake was 9.4 mg SAS particles per kg body weight. This total daily quantity includes all SAS particles regardless of their degree of aggregation or agglomeration. Hydrodynamic chromatography with inductively coupled plasma mass spectrometry (HDC-ICPMS) showed that up to ~40 % of SAS particles detected in food products display an external diameter <200 nm [18].

The next question was whether the SAS particles in commercial food products would be destroyed in the digestive tract or rather withstand gastrointestinal

conditions. Using an in vitro system mimicking human gastric digestion, it could be demonstrated that nano-structured silica forms agglomerates under acidic conditions resembling the milieu of the stomach. By switching the conditions to those imitating the subsequent intestinal digestion stage, however, these large agglomerates disintegrate readily into nano-sized silica structures. In light of these in vitro findings, it was concluded that up to ~80 % of orally ingested SAS particles withstand gastric dissolution and display a nano-sized range once they reach the intestinal lumen [44].

Inadequacies of existing risk assessments

Nano-particles are neither inherently toxic nor inherently safe and possible adverse effects should be tested case-by-case. In principle, a standard assessment with risk = hazard × exposure, which includes hazard identification, hazard characterization, exposure assessment and risk characterization, is applicable to nano-materials in food [21, 45, 46].

The United Kingdom Food Standards Agency Expert group on Vitamins and Minerals (EVM) performed an assessment of the oral safety of SAS particles, yielding a safe upper dietary level for daily consumption of 1500 mg SAS particles per day for adults [34]. This upper safety limit was calculated from the only available long-term toxicity study in rats [33], despite its limitations recently reiterated by the Scientific Committee on Consumer Safety [35]. The EVM experts noted that oral exposure to SAS particles for 103 consecutive weeks elicited effects on body weight and absolute liver weight (concerning the groups with a 2.5 and 5 % dietary inclusion rate). However, they attributed this outcome to possible nutritional imbalances, not adjusted in these two higher dose groups and considered unlikely to be relevant for humans. On this basis, the EVM group concluded that the no observed adverse effect level (NOAEL) is equivalent to the highest dose tested, i.e. 5 % SAS (wt/wt) in the diet. In the absence of further information or studies explaining the reduction in body and liver weight, we advocate a more cautious approach by deriving from the same study a lower NOAEL equivalent to the 1.25 % inclusion rate, also in view of the emergence of liver hyperplastic nodules and adrenal pheochromcytomas recorded in a few SAS-treated males but never in controls [33]. This more cautious interpretation is supported by a recent, above-described study [32] revealing periportal liver fibrosis in SAS-exposed rats.

As indicated, the EVM expert group opted for a NOAEL of 5 % dietary inclusion and further estimated that this translates by default to a daily dose of 2.5 g/kg body weight. After introducing an uncertainty factor of 100 (to adjust for inter-species as well as inter-individual variations in sensitivity), the derived safe upper level for lifetime daily consumption of SAS particles was 25 mg/kg per day, equivalent to 1500 mg per day for a 60-kg adult. In terms of elemental silicon, the "safe" upper limit for daily consumption is 12 mg/kg body weight per day (equivalent to 700 mg for a 60-kg adult). In 2004, the Scientific Panel on Dietetic Products, Nutrition and Allergies (NDA Panel) at the European Food Safety Authority concluded for silicon that "there are no suitable data for dose—response for establishment of an upper level" [47]. In 2009, however, the Scientific Panel on Food Additives and Nutrient Sources added to Food (ANS Panel) took into consideration the risk assessment carried out by the EVM experts and adopted their proposed upper limit of 1500 mg per day when assessing silicon dioxide as food additive [46]. It remains to be mentioned that default intake calculations made by translating a 5 % inclusion in the feed of rats to an assumed ingestion of 2.5 g/kg per day seem incorrect as the actual daily dose of SAS particles, determined from feed consumption in the high-dose group, was around 1.9 g/kg body weight during most of the study period (Table 2). Similarly, the lower inclusion rates of 1.25 and 2.5 % correspond to daily oral doses of around 0.5 and 1 g/kg, respectively. To summarize, several gaps in both study design and interpretation of results diminish the predictability of the only available long-term bioassays in rodents addressing the oral safety of SAS particles.

Potential for local effects in the gastrointestinal tract

Depending on the nature of identified hazards that raise concerns, the canonical risk characterization may need to be complemented with endpoints that are not routinely assessed in the toxicological evaluation of chemicals. For example, a nano-Trojan horse hypothesis has previously been proposed in view of the observation that, in human lung epithelial cells exposed to Co_3O_4 or Mn_3O_4 nano-particles, the generation of reactive oxygen species (ROS) was higher than in controls exposed to an equivalent concentration of dissolved cobalt or manganese salts [10]. It is equally conceivable that the binding of luminal antigens to SAS particles could aid their delivery to reactive cells of the gastrointestinal tract. In this respect, we note in particular that none of the above-reviewed studies examined local effects on the lymphoid tissue of the gastrointestinal mucosa. Rather than causing ROS production, SAS particles have been implicated in the release of pro-inflammatory cytokines (see below).

Although the function of the immune system is to safeguard the host against invasive pathogens, the steady-state gastrointestinal tract is geared towards immune silencing or tolerance to avoid futile reactions

to innocuous food antigens and beneficial commensal microorganisms [48, 49]. Upon oral exposure, foreign particles encounter a single layer of mucous membrane lining the digestive tract. This large vulnerable surface is defended by the gut-associated lymphoid tissue, which consists of loosely organized clusters of lymphoid cells and more organized Peyer's patches. Nano-particles including those made of silica are known to penetrate this lymphoid tissue underlying the epithelial barrier [50–53], where they may disrupt the critical balance between tolerance to harmless food constituents and commensals on the one hand and inflammatory reactions towards pathogens on the other hand [54, 55]. Specific analyses of Peyer's patches are not mentioned in the available sub-chronic and chronic toxicity studies in rodents and, therefore, it is not possible to ascertain whether delayed local effects on the gut-associated lymphoid system were adequately excluded.

Previous studies highlighted the fact that there is one critical site in which food-borne nano-particles accumulate during lifelong exposure, i.e., in "pigment cells" of the gut-associated lymphoid tissue where the earliest signs of inflammatory bowel disease (IBD) are noted (reviewed in [56–58]). This is a wide group of chronic conditions ranging from Crohn's disease (affecting all segments of the digestive tract) to ulcerative colitis (restricted to the large bowel, [59]). The main gatekeepers of tolerance in the intestinal system, as well as major mediators of adverse reactions like IBD, are specialized antigen-presenting cells known as dendritic cells [60]. They act as scavengers of foreign materials by extending branched and rapidly changing projections across the epithelial barrier into the gut lumen and taking up particles by endocytosis [61]. Particles are also delivered directly to dendritic cells after their passage through microfold cells (M-cells) in the intestinal mucosa. In this way, dendritic cells filter out a volume of up to 1500 μm^3, which equals their own cell volume, per hour [62]. Unlike other antigen-presenting cells, dendritic cells constitutively express class II major histocompatibility complexes and, in response to pathogen recognition, display co-stimulatory surface glycoproteins and produce inflammatory cytokines. For these reasons, dendritic cells constitute potent activators of the innate immune system and also polyvalent drivers of T lymphocytes [63, 64]. As nano-particles are in the same size range as many proteins or common viruses, it is not surprising to find that, by virtue of their function in probing the environment for intruding insults, dendritic cells capture nano-particles in an efficient manner [65–67].

It was shown that endotoxin-activated dendritic cells release the potent pro-inflammatory cytokine interleukin-1β (IL-1β) upon incubation with SAS nano-particles [68]. Mechanistically, this response has been linked to activation of the inflammasome complex, which in turn cleaves the pro-IL-1β precursor protein to release active IL-1β. In view of this finding, it will be of pivotal importance to determine how steady-state dendritic cells like those residing in the normal non-inflammatory intestinal mucosa react to the presence of food-borne SAS particles. IBD has a multi-factorial origin with genetic susceptibility, gut microflora and a dysfunction of the mucosal immune system as main drivers [60]. Additionally, various dietary factors have been implicated in the increasing incidence of IBD and several authors raised the concern that food-borne nano-particles may contribute to initiating this chronic inflammatory disease [69–71]. Inadvertent stimulation of the immune system by nano-particles could trigger a reaction sequence that abrogates tolerance to food constituents and commensal bacteria and thereby favor immune-mediated conditions with the hallmarks of IBD (reviewed by [72]).

Conclusions

Previous and current controversies on hormone or antibiotic residues in food illustrate that nutrition is a highly emotional area in the public perception. The finding that SAS particles activate the inflammasome and, hence, are not biologically inert is intriguing because this type of nano-structured material has been employed since decades as food additive and is so far considered to be safe for consumers. Based on a critical review of existing oral toxicity studies, however, we consider that adverse effects from food-borne SAS particles cannot be excluded. Table 1 summarizes independent repeated dose studies that reached much the same conclusion with an oral NOAEL of 500 mg per kg body weight and a lowest observed adverse effect level (LOAEL) in the range of 810–1500 mg per kg body weight. Therefore, we advocate a prudent approach by taking the oral NOAEL of 500 mg/kg, based on body and liver weights in the 103-week feeding study in rats, as point of departure for the risk assessment of SAS particles. This NOAEL is lower than previously proposed [34] but, as summarized in Table 1, is consistent with the outcome (liver atrophy) of a 8-week feeding study and the liver effects (periportal fibrosis) in a 12-week feeding study, both in rats, at daily doses of 810–1000 mg/kg body weight. By applying a default uncertainty factor of 100 (to adjust for interspecies and inter-individual variations in sensitivity), this NOAEL would yield a safe upper level for the lifetime intake of SAS particles of 5 mg/kg body weight per day. The estimated consumption by a European population of 9.4 mg per kg body weight and day would, therefore, suggest that the dietary exposure to SAS particles should be reduced to remain, even with a worst case exposure scenario, below this newly proposed safety threshold of

5 mg/kg daily. Importantly, further studies are needed to investigate local effects of SAS particles in the gastrointestinal system, particularly on the gut-associated lymphoid tissue and embedded dendritic cells. In a broader perspective, mechanistic in vitro studies at different levels of biological complexity are necessary to understand in depth how food-borne nano-particles may influence the delicate balance between immune tolerance and inflammatory responses that depends on the proper function of dendritic cells in the intestinal mucosa. This research direction is crucial to eventually address the concern that the higher occurrence of IBD may be in part a consequence of the lifelong ingestion of nano-sized or nano-structured food additives increasingly used in the modern diet.

Abbreviations

ANS: Scientific Panel on Food Additives and Nutrient Sources added to Food; E 551: synthetic amorphous silica (food additive); ECETOC: European Centre for ecotoxicology and toxicology of chemicals; EU: European Union; EVM: Food Standards Agency Expert group on vitamins and minerals; HDC-ICPMS: hydrodynamic chromatography with inductively coupled plasma mass spectrometry; IBD: inflammatory bowel disease; ICP-AES: inductively coupled plasma atomic emission spectrometry; Ig: immunoglobulin; IL-1β: interleukin-1β; JRC: Joint Research Centre of the European Commission; LOAEL: lowest observed adverse effect level; NDA: Scientific Panel on dietetic products, nutrition and allergies; NOAEL: no observed adverse effect level; OECD: Organzation for Economic Co-operation and Development; ROS: reactive oxygen species; SAS: synthetic amorphous silica.

Authors' contributions

HCW, HN and MS wrote the manuscript. All authors read and approved the final manuscript.

Author details

[1] Institute of Pharmacology and Toxicology, University of Zurich-Vetsuisse, Winterthurerstrasse 260, 8057 Zurich, Switzerland. [2] Immunology Division, Vetsuisse Faculty, University of Zurich, Winterthurerstrasse 260, 8057 Zurich, Switzerland.

Acknowledgements

Research in the author's laboratory was supported by the National Research Program "Opportunities and Risks of Nanomaterials" Grant 406440-141619 and by grant FK-15-053 from the "Forschungskredit" of the University of Zurich.

Competing interests

The authors declare that they have no competing interests.

Received: 1 December 2015 Accepted: 3 May 2016
Published online: 10 June 2016

References

1. Chaudhry Q, Scotter M, Blackburn J, Ross B, Boxall A, Castle L, et al. Applications and implications of nanotechnologies for the food sector. Food Addit Contam Part A. 2008;25:241–58.
2. Puddu M, Paunescu D, Stark WJ, Grass RN. Magnetically recoverable, thermostable, hydrophobic DNA/silica encapsulates and their application as invisible oil tags. ACS Nano. 2014;8:2677–85.
3. Hilty FM, Arnold M, Hilbe M, Teleki A, Knijnenburg JTN, Ehrensperger F, et al. Iron from nanocompounds containing iron and zinc is highly bioavailable in rats without tissue accumulation. Nat Nanotechnol. 2010;5:374–80.
4. US FDA 2015. United States Food and Drug Administration. Code of Federal Regulations Title 21, 21CFR172.480. 2015. http://www.accessdata.fda.gov/scripts/cdrh/cfdocs/cfCFR/CFRSearch.cfm?fr=172.480. Accessed 25 Apr 2016.
5. Union European. Commission regulation (EU) No 1129/2011 of 11 November 2011 amending Annex II to Regulation (EC) No 1333/2008 of the European Parliament and of the Council by establishing a Union list of food additives. Off J Eur Union. 2011;295:1–177.
6. Union European. Commission recommendation of 18 October 2011 on the definition of nanomaterial (2011/696/EU). Off J Eur Union. 2011;275:38–40.
7. Oberdörster G. Toxicology of ultrafine particles: in vivo studies. Philos Trans R Soc A Math Phys Eng Sci. 2000;358:2719–40.
8. Donaldson K, Stone V, Clouter A, Renwick L, MacNee W. Ultrafine particles. Occup Environ Med. 2001;58:211–6.
9. Oberdörster G, Sharp Z, Atudorei V, Elder A, Gelein R, Kreyling W, et al. Translocation of inhaled ultrafine particles to the brain. Inhal Toxicol. 2004;16:437–45.
10. Limbach LK, Li Y, Grass RN, Brunner TJ, Hintermann MA, Muller M, et al. Oxide nanoparticle uptake in human lung fibroblasts: effects of particle size, agglomeration, and diffusion at low concentrations. Environ Sci Technol. 2005;39:9370–6.
11. Lankveld DPK, Van Loveren H, Baken KA, Vandebriel RJ. In vitro testing for direct immunotoxicity: state of the art. Methods Mol Biol. 2010;598:401–23.
12. Landsiedel R, Fabian E, Ma-Hock L, van Ravenzwaay B, Wohlleben W, Wiench K, et al. Toxico-/biokinetics of nanomaterials. Arch Toxicol. 2012;86:1021–60.
13. Mou Y, Chen B, Zhang Y, Hou Y, Xie H, Xia G, et al. Influence of synthetic superparamagnetic iron oxide on dendritic cells. Int J Nanomedicine. 2011;6:1779–86.
14. Napierska D, Thomassen LC, Lison D, Martens JA, Hoet PH. The nanosilica hazard: another variable entity. Part Fibre Toxicol. 2010;7:39.
15. European Union. Comission Regulation (EU) No 231/2012 of 9 March 2012 laying down specifications for food additives listed in Annexes II and III to Regulation (EC) No 1333/2008 of the European Parliament and of the Council. Off J Eur Union. 2012;2012(83):1–295.
16. Marinova KG, Denkov ND, Branlard P, Giraud Y, Deruelle M. Optimal hydrophobicity of silica in mixed oil-silica antifoams. Langmuir. 2002;18:3399–403.
17. Wang P, Zhu Y, Yang X, Chen A. Prolonged-release performance of perfume encapsulated by tailoring mesoporous silica spheres. Flavour Fragr J. 2008;23:29–34.
18. Dekkers S, Krystek P, Peters RJB, Lankveld DPK, Bokkers BGH, van Hoeven-Arentzen PH, et al. Presence and risks of nanosilica in food products. Nanotoxicology. 2011;5:393–405.
19. Fruijtier-Pölloth C. The toxicological mode of action and the safety of synthetic amorphous silica-a nanostructured material. Toxicology. 2012;294.
20. Maynard AD. Old materials, new challenges? Nat Nanotechnol. 2014;9:658–9.
21. SCENIHR 2007. Scientific Committee on Emerging and Newly-Identified Health Risks. The existing and proposed definitions relating to products of nanotechnologies, 29 November 2007. http://ec.europa.eu/health/archive/ph_risk/committees/04_scenihr/docs/scenihr_o_012.pdf. Accessed 25 Apr 2016.
22. ELC 2009. Federation of European Food Additives; Food enzymes and food cultures industries. food additives and nanotechnologies. 2009. http://elc-eu.org/uploads/news_documents/2009-10_Food_additives_and_nanotechnologies_-_ELC_position.pdf. Accessed 25 Apr 2016.
23. ECETOC 2006. European Centre for Ecotoxicology and Toxicology of Chemicals. Synthetic Amorphous Silica (CAS No. 7631-86-9), JACC REPORT No. 51. 2006. http://members.ecetoc.org/Documents/Document/JACC051.pdf. Accessed 25 Apr 2016.
24. OECD 2015. Organization for economic co-operation and development. Dossier on silicon dioxide, Series on the safety of manufactured nanomaterials No. 51. 2015. http://www.oecd.org/chemicalsafety/nanosafety/silicon-dioxide-manufactured-nanomaterial.htm. Accessed 25 Apr 2016.
25. Lewin G. 28-day oral toxicity study of synthetic amorphous silica in wistar (WU) rats. CEFIC, Brussels, Belgium. 2011. Unpublished report, described in OECD 2015. http://www.oecd.org/chemicalsafety/nanosafety/silicon-dioxide-manufactured-nanomaterial.htm. Accessed 25 Apr 2016.

26. Elsea JR. Cab-O-Sil (fluffy), ninety-day dietary feeding, supplement to progress reports dated January 8, and May 6, 1958, final report. Hazleton Laboratories, Falls Church, Virginia. Cabot, Tuscula, Illinois, USA. 1958. Unpublished report, described in SCCS 2015. http://ec.europa.eu/health/scientific_committees/consumer_safety/docs/sccs_o_175.pdf. Accessed 25 Apr 2016.
27. Til H, Hollanders M, Beems R. Subchronic (13 week) oral toxicity study in rats. Evonik Degussa, Germany. 1981. Unpublished report, described in OECD 2015. http://www.oecd.org/chemicalsafety/nanosafety/silicon-dioxide-manufactured-nanomaterial.htm. Accessed 25 Apr 2016.
28. Rutter HA, Shott LD. 13-week dietary administration - rats, silane-treated Cab-O-Sil, final report, project 178-114. Hazleton Laboratories, Falls Church, Virginia. Cabot, Billerica, MA, USA. 1970. Unpublished report, described in ECETOC 2006. http://members.ecetoc.org/Documents/Document/JACC051.pdf. Accessed 25 Apr 2016.
29. Leuschner F. Über die subakute Toxizität von R972. Degussa, Hanau, Germany. 1964. Unpublished report, desribed in ECETOC 2006. http://members.ecetoc.org/Documents/Document/JACC 051.pdf. Accessed 25 Apr 2016.
30. Pliess G. Histologische Befunde bei Versuchsratten, Medikament R972. Laboratorium für Pharmakologie und Toxikologie, Hamburg, Germany. Degussa, Frankfurt am Main, Germany. 1964. Unpublished report, described in ECETOC 2006. http://members.ecetoc.org/Documents/Document/JACC051.pdf. Accessed 25 Apr 2016.
31. So SJ, Jang IS, Han CS. Effect of micro/nano silica particle feeding for mice. J Nanosci Nanotechnol. 2008;8:5367–71.
32. van der Zande M, Vandebriel RJ, Groot MJ, Kramer E, Herrera Rivera ZE, Rasmussen K, et al. Sub-chronic toxicity study in rats orally exposed to nanostructured silica. Part Fibre Toxicol. 2014;11:8.
33. Takizawa Y, Hirasawa F, Noritomi E, Aida M, Tsunoda H, Uesugi S. Oral ingestion of syloid to mice and rats and its chronic toxicity and carcinogenicity. Acta Med Biol. 1988;36:27–56.
34. UK Food Standards Agency 2003. Safe upper levels for vitamins and minerals: report of the expert group on vitamins and minerals. 2003. http://cot.food.gov.uk/sites/default/files/vitmin2003.pdf. Accessed 25 Apr 2016.
35. SCCS 2015. Scientific Committee on Consumer Safety. Opinion on silica, hydrated silica, and silica surface modified with alkyl silylates (nano form). 2015. http://ec.europa.eu/health/scientific_committees/consumer_safety/docs/sccs_o_175.pdf. Accessed 25 Apr 2016.
36. van Kesteren PCE, Cubadda F, Bouwmeester H, van Eijkeren JCH, Dekkers S, de Jong WH, et al. Novel insights into the risk assessment of the nano-material synthetic amorphous silica, additive E551, in food. Nanotoxicology. 2015;9:442–52.
37. NANOGENOTOX 2013. Facilitating the safety evaluation of manufactured nanomaterials by characterising their potential genotoxic hazard. 2013. http://www.nanogenotox.eu/index.php?option=com_content&view=article&id=136&Itemid=158. Accessed 25 Apr 2016.
38. Nel AE, Mädler L, Velegol D, Xia T, Hoek EMV, Somasundaran P, et al. Understanding biophysicochemical interactions at the nano-bio interface. Nat Mater. 2009;8:543–57.
39. Ruh H, Kühl B, Brenner-Weiss G, Hopf C, Diabaté S, Weiss C. Identification of serum proteins bound to industrial nanomaterials. Toxicol Lett. 2012;208:41–50.
40. Cedervall T, Lynch I, Lindman S, Berggard T, Thulin E, Nilsson H, et al. Understanding the nanoparticle-protein corona using methods to quantify exchange rates and affinities of proteins for nanoparticles. Proc Natl Acad Sci U S A. 2007;104:2050–5.
41. Lundqvist M, Stigler J, Elia G, Lynch I, Cedervall T, Dawson KA. Nanoparticle size and surface properties determine the protein corona with possible implications for biological impacts. Proc Natl Acad Sci U S A. 2008;105:14265–70.
42. Nagayama S, Ogawara KI, Fukuoka Y, Higaki K, Kimura T. Time-dependent changes in opsonin amount associated on nanoparticles alter their hepatic uptake characteristics. Int J Pharm. 2007;342:215–21.
43. Kistemaker C, Bouman M, Hulshof K. Consumption of separate products by Dutch population groups-Dutch National Food Consumption Survey 1997–1998. Zeist, TNO-Nutrition Food Res Institute, TNO-report. 1998;98:812.
44. Peters R, Kramer E, Oomen AG, Herrera Rivera ZE, Oegema G, Tromp PC, et al. Presence of nano-sized silica during in vitro digestion of foods containing silica as a food additive. ACS Nano. 2012;6:2441–51.
45. Warheit DB. How meaningful are the results of nanotoxicity studies in the absence of adequate material characterization? Toxicol Sci. 2008;101:183–5.
46. European Food Safety Authority. Scientific opinion of the panel on food additives and nutrient sources added to food on calcium silicate, silicon dioxide and silicic acid gel added for nutritional purposes to food supplements following a request from the European Commission. EFSA J. 2009;1132:1–24.
47. European Food Safety Authority. Opinion of the Scientific Panel on Dietetic Products, nutrition and allergies on a request from the commission related to the tolerable upper intake level of silicon (Request N° EFSA-Q-2003-018). EFSA J. 2004;60:1–11.
48. Ley RE, Hamady M, Lozupone C, Turnbaugh PJ, Ramey RR, Bircher JS, et al. Evolution of mammals and their gut microbes. Science. 2008;320:1647–51.
49. Bogunovic M, Ginhoux F, Helft J, Shang L, Hashimoto D, Greter M, et al. Origin of the lamina propria dendritic cell network. Immunity. 2009;31:513–25.
50. Sass W, Dreyer HP, Seifert J. Rapid insorption of small particles in the gut. Am J Gastroenterol. 1990;85:255–60.
51. des Rieux A, Fievez V, Garinot M, Schneider Y-J, Préat V. Nanoparticles as potential oral delivery systems of proteins and vaccines: a mechanistic approach. J Control Release. 2006;116:1–27.
52. Awaad A, Nakamura M, Ishimura K. Imaging of size-dependent uptake and identification of novel pathways in mouse Peyer's patches using fluorescent organosilica particles. Nanomedicine. 2012;8:627–36.
53. Powell JJ, Thomas-McKay E, Thoree V, Robertson J, Hewitt RE, Skepper JN, et al. An endogenous nanomineral chaperones luminal antigen and peptidoglycan to intestinal immune cells. Nat Nanotechnol. 2015;10:361–9.
54. Bekiaris V, Persson EK, Agace WW. Intestinal dendritic cells in the regulation of mucosal immunity. Immunol Rev. 2014;260:86–101.
55. Toda T, Yoshino S. Amorphous nanosilica particles block induction of oral tolerance in mice. J Immunotoxicol. 2016;18:1–6.
56. Evans SM, Ashwood P, Warley A, Berisha F, Thompson RPH, Powell JJ. The role of dietary microparticles and calcium in apoptosis and interleukin-1β release of intestinal macrophages. Gastroenterology. 2002;123:1543–53.
57. Lomer MCE, Thompson RPH, Powell JJ. Fine and ultrafine particles of the diet: influence on the mucosal immune response and association with Crohn's disease. Proc Nutr Soc. 2002;61:123–30.
58. Mazmanian SK, Round JL, Kasper DL. A microbial symbiosis factor prevents intestinal inflammatory disease. Nature. 2008;453:620–5.
59. Lucendo AJ, De Rezende LC. Importance of nutrition in inflammatory bowel disease. World J Gastroenterol. 2009;15:2081–8.
60. Bates J, Diehl L. Dendritic cells in IBD pathogenesis: an area of therapeutic opportunity? J Pathol. 2014;232:112–20.
61. Rescigno M. Before they were gut dendritic cells. Immunity. 2009;31:454–6.
62. Sallusto F, Cella M, Danieli C, Lanzavecchia A. Dendritic cells use macropinocytosis and the mannose receptor to concentrate macromolecules in the major histocompatibility complex class II compartment: downregulation by cytokines and bacterial products. J Exp Med. 1995;182:389–400.
63. Steinman RM, Lustig DS, Cohn ZA. Identification of a novel cell type in peripheral lymphoid organs of mice. 3. Functional properties in vivo. J Exp Med. 1974;139:1431–45.
64. Banchereau J, Steinman RM. Dendritic cells and the control of immunity. Nature. 1998;392:245–52.
65. Manolova V, Flace A, Bauer M, Schwarz K, Saudan P, Bachmann MF. Nanoparticles target distinct dendritic cell populations according to their size. Eur J Immunol. 2008;38:1404–13.
66. Li A, Qin L, Zhu D, Zhu R, Sun J, Wang S. Signalling pathways involved in the activation of dendritic cells by layered double hydroxide nanoparticles. Biomaterials. 2010;31:748–56.
67. Müller L, Riediker M, Wick P, Mohr M, Gehr P, Rothen-Rutishauser B. Oxidative stress and inflammation response after nanoparticle exposure: differences between human lung cell monocultures and an advanced three-dimensional model of the human epithelial airways. J R Soc Interface. 2010;7(Suppl 1):S27–40.
68. Winter M, Beer H-D, Hornung V, Krämer U, Schins RPF, Förster I. Activation of the inflammasome by amorphous silica and TiO2 nanoparticles in murine dendritic cells. Nanotoxicology. 2011;5:326–40.

69. Tetley TD. Health effects of nanomaterials. Biochem Soc Trans. 2007;35:527–31.
70. Powell JJ, Faria N, Thomas-McKay E, Pele LC. Origin and fate of dietary nanoparticles and microparticles in the gastrointestinal tract. J Autoimmun. 2010;34:J226–33.
71. Hummel TZ, Kindermann A, Stokkers PCF, Benninga MA, ten Kate FJW. Exogenous pigment in Peyer patches of children suspected of having IBD. J Pediatr Gastroenterol Nutr. 2014;58:477–80.
72. Zolnik BS, González-Fernández Á, Sadrieh N, Dobrovolskaia MA. Nanoparticles and the immune system. Endocrinology. 2010;151:458–65.

1.2 Titanium dioxide as food additive

Titanium dioxide TiO_2 anatase is widely used as a white pigment. As a common food additive, it's used since several decades and labelled E171. Food products with E171 were found to contain a nano-sized fraction of TiO_2 particles (Weir et al., 2012). In humans, titanium dioxide particles were shown to be present in the blood within hours after oral administration of food-grade E171 (Pele et al., 2015). Studies in mice have shown that after intratracheal instillation of TiO_2, especially anatase particles could lead to chronic inflammation (Park et al., 2009). In mouse dendritc cells, primed with lipopolysacharides (LPS), TiO_2 particles were able to activate the inflammasome with secretion of IL-1β (Winter et al., 2011). Therefore, we included food-grade TiO_2 anatase particles, and TiO_2 anatase nanoparticles in the initial screening with steady-state DCs to examine the potential ability of this material to trigger IL-1β secretion.

1.3 Iron (III) phosphate for food fortification

Food fortification with iron phosphate nanoparticles ($FePO_4$) NPs could be used in order to reduce iron deficiency and alleviate anemia, because these NPs have a high bioavailability combined with an improved sensory performance (Hilty et al., 2010). In this study, we monitored the response of steady-state DCs exposed to $FePO_4$ to examine the potential ability of this nanostructured material to trigger adverse immune reactions.

1.4 Immunity

Protection of a host against foreign materials and maintenance of tolerance towards nutrients, food antigens and beneficial commensals is crucial for survival. The vertebrate immune system achieves this with three layers: 1. a mechanical/physical barrier working continuously, 2. innate immunity that reacts within hours and 3. adaptive immunity to target invaders specifically within several days. To avoid pathogenic insults, i.e. foreign inflammatory or infectious agents, the immune system reacts rapidly and tightly coordinated.

1.4.1 Dendritic cells

Dendritic cells (DCs) develop from hematopoietic progenitors of the bone marrow under the direction of feline McDonough sarcoma-like tyrosine kinase 3 ligand (Scott et al., 2014). This growth factor is required to generate steady-state DCs that, under homeostatic conditions, reside in lymphoid organs like spleen and migrate to non-lymphoid organs including skin, lung and intestines (Watowich & Liu, 2010; Shortman & Naik, 2007). In the Peyer's patches of mice, several subsets of dendritic cells have been found including conventional DC (cDC), defined by the expression of $CD11c^{+}B220^{-}CD11b^{high}$ $SIRP\alpha^{+}$ or $CD11c^{+}$ $B220^{-}CD11b^{intermediate}SIRP\alpha^{-}$ and plasmacytoid DC (pDC), which are expressing the surface markers $CD11c^{intermediate}B220^{+}$ (Castellaneta et al., 2004). Steady-state DCs are dispersed throughout the mucosa of the intestinal tract where, in their dual antigen-presenting role, these specialized sentinel cells initiate immune reactions in response to pathogenic agents while maintaining tolerance to self-antigens, innocuous food constituents and the beneficial microbiome (Bekiaris et al., 2014; Bogunovic et al., 2009; Varol et al., 2009). As immature DCs in the periphery, they are characterized by their high endocytic activity (Sallusto et al., 1995). Intestinal DCs extend branched and rapidly changing projections across the epithelial barrier into the gut lumen and take up particles. Particles are also delivered directly to dendritic cells after their passage through microfold cells (M-cells) into the Peyer's patches (Rescigno, 2009).

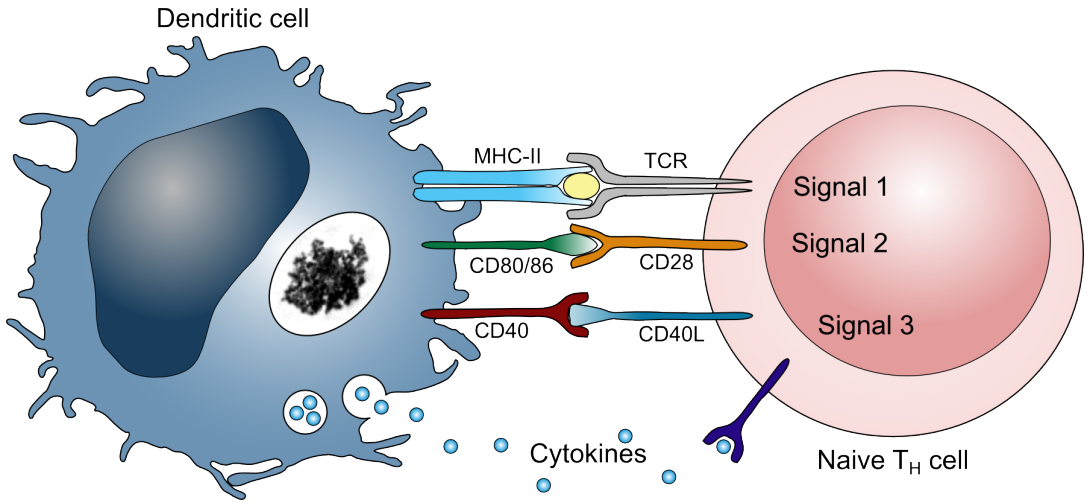

Figure 2. Hypothesis: NPs could disrupt the balance between defense and and tolerance upon internalization in immature DCs. After uptake of NPs, immature DCs may become activated. Presentation of encountered antigen fragments at their cell surface on MHC class II molecules (signal 1) together with up-regulated co-stimulatory cell-surface receptors for T-cell activation such as CD80, CD86 and CD40 (signal 2). In addition, DCs may secrete pro-inflammatory cytokines (signal3).

As specialized antigen presenting cells, DCs are equipped with a plethora of innate pattern recognition receptors (PRRs) such as toll-like receptors (TLRs) and nucleotide-binding oligomerization domain (NOD)-like receptors. TLRs recognize specific chemical motifs found on foreign pathogens. TLR2 and TLR4 for example detect LPS, while TLR3, TLR7 and TLR9 are known to detect DNA motifs (Pandey et al., 2015). Upon encountering foreign materials, immature DCs become activated (Figure 2) and migrate as mature DCs to the lymph nodes. There, they present encountered antigen fragments at their cell surface using MHC class II molecules (Signal 1) together with co-stimulatory cell-surface receptors for T-cell activation such as CD80, CD86 and CD40 (Signal 2). In addition, DCs secrete cytokines, which are required for efficient immune responses (Signal 3). We therefore monitored the response of DCs upon contact with food-grade nanomaterials to examine the potential ability of this material to trigger adverse immune reactions.

2 Aim of the project

Despite the comparably high oral exposure of consumers with food-borne nanoparticles and increasing applications of nanomaterials for food, no *in-vitro* test system to assess the risk of food-borne nanomaterials on intestinal immunity is available.

Therefore, the aim of this thesis was to investigate the effects of food-borne nanomaterials on dendritic cells *in-vitro*. We thus set out to investigate whether nanoparticles interact with steady-state dendritic cells and if this interaction leads to functional implications.

After in depth characterization of the food-grade nanoparticles, we generated immature dendritic cells from mouse bone marrow cultures supplemented with Flt3L. These cells were analyzed by flow cytometry to determine their surface markers. After incubation of the dendritic cells with different nanoparticles, interaction and uptake of nanoparticles were studied by flow cytometry and transmission electron microscopy, respectively.

To determine the consequences of the particle internalization observed, functional assays were conducted. DC were incubated with nanoparticles and analysed for changes in activation and maturation markers. In addition, pro-inflammatory cytokine secretion was monitored in the cell culture supernatant. The mechanism of particle internalization was further delineated using pharmacological inhibitors. This inhibitor effects supported the conclusion that the IL-1β response requires intracellular uptake of SAS particles.

The finding, that pristine SAS particles are able to induce the secretion of IL-1β from immature DCs prompted further experiments addressing the mechanism of pro-IL-1β-induction and IL-1β secretion. These experiments with caspase inhibitors, inhibitors of endosomal acidification and DCs lacking TLR2, TLR3, TLR4, TLR7 and TLR9 provided evidence for an endosomal pattern recognition receptor as the molecular sensor of SAS particles.

3 Results

3.1 Interleukin-1β induction in immature dendritic cells exposed to food-grade synthetic amorphous silica

This paper describes the the pro-inflammatory effects of food-grade SAS particles on immature dendritic cells. We showed that SAS internalization in immature DCs is sufficient to cause induction of the highly pro-inflammatory pro-interleukin-1β and subsequent cleavage and secretion of interleukin-1β. I designed, performed and analyzed the experiments, prepared all figures and co-wrote the manuscript together with H. Naegeli.

Artikel1:
Interleukin-1β induction in immature dendritic cells exposed to food-grade synthetic amorphous silica

Artikel2:
Iron phosphate nanoparticles for food applications do not induce adverse effects in rats or human cell lines

Interleukin-1β induction in immature dendritic cells exposed to food-grade synthetic amorphous silica

Hans Christian Winkler,[†] Julian Kornprobst,[†] Peter Wick,[‡] Lea Maria von Moos,[§] Ioannis Trantakis,[§] Elisabeth Maria Schraner,[‖] Barbara Bathke,[⊥] Hubertus Hochrein,[⊥] Mark Suter,[#] Hanspeter Naegeli[†]*

[†]Institute of Pharmacology and Toxicology, University of Zurich-Vetsuisse, Winterthurerstrasse 260, 8057 Zurich, Switzerland.

[‡]Laboratory for Particles-Biology Interactions, Empa Swiss Laboratories for Materials and Technology, Lerchenfeldstrasse 5, 9014 St. Gallen, Switzerland.

[§]Department of Health Sciences and Technology, ETH Zurich, Schmelzbergstrasse 9, 8092 Zurich, Switzerland.

[‖]Electron Microscopy, Institutes of Veterinary Anatomy and Virology, Winterthurerstrasse 260, 8057 Zurich, Switzerland.

[⊥]Department of Research, Bavarian Nordic GmbH, 82152 Martinsried, Germany.

[#]Immunology Division, Vetsuisse Faculty, University of Zurich, Winterthurerstrasse 204, 8057 Zürich, Switzerland.

*Correspondence to: naegelih@vetpharm.uzh.ch

Manuscript to be submitted.

Abstract

Background: Dendritic cells (DCs) constitute first-line sensors of foreign materials invading the organism. These specialized sentinel cells launch immune reactions against pathogens but also mediate tolerance to self-antigens and, in the intestinal milieu, to nutrients and commensals. A key question in the evaluation of orally ingested nanomaterials is, therefore, whether their contact with DCs in the intestinal mucosa disrupts this delicate homeostatic balance between pathogen defense and tolerance. Here, we generated steady-state DCs by incubating haematopoietic progenitors with feline McDonough sarcoma-like tyrosine kinase 3 ligand (Flt3L) and used the resulting immature DCs to test potential biological responses to food-grade synthetic amorphous silica (SAS) representing a common nanomaterial.

Results: The interaction of completely immature and unprimed DCs with SAS particles and their internalization by endocytosis fails to elicit cytotoxicity and does not trigger the release of interleukin (IL)-1α or tumor necrosis factor-α, which have been recognized as master regulators of acute inflammation in lung-related studies. However, the display of molecular maturation markers on the cell surface shows that SAS particles are able to activate immature DCs. Also, the endocytic uptake of SAS particles into these steady-state DCs leads to induction of the pro-IL-1β cytokine precursor, subsequently cleaved by the inflammasome to secrete highly inflammatory IL-1β. In contrast, neither pro-IL-1β induction nor IL-1β secretion occurs upon internalization of TiO_2 or $FePO_4$ nanoparticles. Pharmacologic inhibitors of the endosomal pathogen recognition pathway like chloroquine and bafilomycin A1 suppress the observed pro-IL-1β induction, indicating that expression of this cytokine precursor takes place in DCs because the nanostructured SAS surface mimics a microbe-associated molecular pattern.

Conclusions: This activation of completely immature DCs with a direct *de novo* induction of a potent inflammatory cytokine, by an unprecedented and unexpected mechanism, implies that the currently massive use of SAS materials as food additives should be reconsidered.

KEYWORDS

E 551, food additive, food toxicology, gut-associated lymphoid tissue, inflammatory bowel disease, nanomaterial, silicon dioxide

Background: Dendritic cells (DCs) develop from hematopoietic progenitors of the bone marrow under the direction of feline McDonough sarcoma-like tyrosine kinase 3 ligand (Flt3L, Additional file 1: Figure S1). This growth factor is required to generate steady-state DCs that, under homeostatic conditions, reside in lymphoid organs like spleen and migrate to non-lymphoid organs including skin, lung and intestines (Watowich & Liu, 2010; Shortman & Naik, 2007). Steady-state DCs are dispersed throughout the mucosa of the intestinal tract where, in their dual antigen-presenting role, these specialized sentinel cells initiate immune reactions in response to pathogenic agents while maintaining tolerance to self-antigens, innocuous food constituents and the beneficial microbiome (Bogunovic et al., 2009; Varol et al., 2009). Although the respiratory toxicity of inhaled nanomaterials gained much attention (Warheit & Donner, 2015; Yazdi et al., 2010), the gastrointestinal tract is exposed to comparably much larger amounts of inorganic particles including nanostructured food additives (Evans et al., 2002; Lomer et al., 2002; Winter et al., 2011; Yada et al., 2014). Silica has currently the highest production volume of all engineered nanomaterials worldwide (Yang et al., 2016). Common applications in the food industry use synthetic amorphous silica (SAS) as anticaking agent in powdered food products, as defoaming agent in beverages, as a thickener in pastes or carrier of flavorings (Dekkers et al., 2011; Peters et al., 2012). Titanium dioxide, containing a minor proportion of particles with a size below 100 nm, serves as a whitening agent in food and toothpastes (Weir et al., 2012). New emerging uses in the food industry include $FePO_4$ particles for iron fortification (Hilty et al., 2010).

Silica particles can lead to acute adverse reactions of the lung after inhalation (Rabolli et al., 2014) and it has been reported that secretion of the pro-inflammatory cytokine interleukin-1β (IL-1β) is necessary for particle-induced pulmonary inflammation (Yazdi et al., 2010; Guo et al., 2013). Because of its potent action, IL-1β biogenesis is tightly regulated. First, an inactive pro-IL-1β precursor is synthesized, which is subsequently cleaved by the intracellular inflammasome complex (comprising caspase-1 and NLRP3) to yield biologically active IL-1β for extracellular secretion (Dinarello, 2011; Netea et al., 2015). The actual trigger of pro-IL-1β induction remains unclear, but in acute lung inflammation a case has been made for IL-1α, released mainly from necrotic macrophages, being a master regulator of pro-IL-1β expression (Rabolli et al., 2014). Another previous report implicated tumor necrosis factor (TNF)-α as a trigger of pro-IL-1β induction (Franchi et al., 2009).

SAS particles withstand gastrointestinal digestion (Peters et al., 2012), reach the intestinal mucosa, penetrate through mucus and epithelial barriers and accumulate in underlying tissues (Evans et al., 2002). Consequently, particle aggregates containing silicon are

detected in the gut-associated lymphoid tissue of humans (Shepherd et al., 1987; Powell et al., 1996). In addition, silica levels of up to 300 μg g^{-1} tissue (a value converted from the actually measured silicon concentration) were found in the spleen of rodents after repeated oral administration of SAS particles (van der Zande et al., 2014). The intestine is less sensitive to irritation compared with lung, but it has been proposed that a life-long contact of the gut-associated lymphoid tissue with deposits of exogenous particles may lead to harmful long-term reactions responsible for chronic inflammatory diseases of the intestinal tract (Lomer et al., 2002; Hummel et al., 2014). To further address this potential hazard, we tested the response of steady-state DCs, representing the most sensitive sentinels of foreign materials, to two kinds of food-grade SAS particles and, as comparators, to TiO_2 and $FePO_4$ nanoparticles of different sizes. This study was instigated by the notion that steady-state DCs, in view of their specialized antigen-presenting function, may respond to nanomaterials by distinctly different mechanisms than macrophages or other previously tested cell types.

RESULTS

Characterization of particles. Food-grade SAS particles were analyzed in depth to determine their shape, specific surface area and hydrodynamic diameter. Under the conditions used for testing of cellular responses, i.e. in cell culture medium, these nanostructured SAS materials with primary particle diameters of 7 and 13 nm form aggregates with a mean diameter of 147 and 127 nm, respectively (Table 1). Nanoparticles of TiO_2 or $FePO_4$ were included in order to have at hand a range of highly defined probes for the comparison of DC reactivity towards different nanomaterials. These reference particles of TiO_2 or $FePO_4$ form aggregates ranging in size between 67 and 352 nm. Traceable 100-nm polystyrene (PS) particles were used exclusively as a size standard for hydrodynamic diameter measurements. Based on a highly sensitive *Limulus* amoebocyte lysate assay, all nanomaterials listed in Table 1 were free of endotoxin contamination except a batch of commercial 50-nm PS particles not used for subsequent biological assays.

Steady-state DCs internalize food-grade nanomaterials. Mouse bone marrow cells were incubated with Flt3L to generate immature DCs from progenitor cells contained in these cultures. These Flt3L-generated DCs were maintained in culture flasks or wells as semi-adherent cell suspensions. The interaction of immature DCs with SAS particles (displaying a primary particle size of 13 nm), $FePO_4$ particles (with a primary size of 11 nm) and TiO_2 particles (with a primary size of 33 nm), suspended in cell culture medium, was first monitored by flow cytometry. The resulting side scatter (SSC) reflects internal cellular structures due to particle uptake whereas the front scatter (FSC) represents cell

Table 1. Particle characterization.

Particle description[a]	Specific surface area[b] [m^2 g^{-1}]	Hydrodynamic diameter [nm] in H_2O[c]	in CM[d]	Shape[e]	Endotoxin contamination[f] [EU per 250 μg particles]
7-nm SAS	326	147 (105-193)[g]	147 ± 5	Irregular	LOD[h]
13-nm SAS	175	182 (130-241)	127 ± 1	Irregular	LOD
11-nm $FePO_4$	188	183 (124-267)	255 ± 35	Irregular	LOD
21-nm $FePO_4$	98	178 (110-258)	230 ± 40	Irregular	0.006
33-nm TiO_2	47	205 (91-335)	67 ± 18	Almost spherical	LOD
140-nm TiO_2	11	Not measured	352 ± 6	Almost spherical	LOD
50-nm PS-NH_2[i]	Not measured	Not measured	Not measured	Spherical	0.043
100-nm PS[k]	Not measured	104 (91-114)	Not measured	Spherical	Not measured

[a]The primary particle diameter was calculated from specific surface area and weight (2.6 kg m^{-3} for SAS, 2.9 kg m^{-3} for $FePO_4$ and 3.9 kg m^{-3} for TiO_2).
[b]Calculated from nitrogen adsorption (Micromeritics Tristar 3000) at 77 K and relative pressure range p/p0 = 0.05-0.25 using the Brunauer-Emmett-Teller (BET) theory.
[c]Determined using Nanoparticle Tracking Analysis 2.3 on a NanoSight instrument (Malvern).
[d]Determined by dynamic light scattering using a Zetasizer Nano ZS (Malvern). CM, complete cell culture medium; values are reported as mean ± standard deviation (n = 3).
[e]Determined by transmission electron microscopy (TEM).
[f]Determined in the Endosafe PTS endotoxin test (Charles River). A control with *Escherichia coli* LPS at the concentration of 10 pg ml^{-1} yielded 0.037 EU ml^{-1}; EU, endotoxin units.
[g]Numbers in parenthesis show the 10% and 90% probability range.
[h]LOD, limit of detection (0.005 EU ml^{-1}).
[i]This endotoxin finding obtained with a purchased batch of polystyrene (PS) particles is included to show an example of contaminated commercial material.
[k]These 100-nm traceable standard particles from Thermo Scientific served as a size standard for hydrodynamic diameter measurements by Nanoparticle Tracking Analysis.

size (Zucker et al., 2010; Wang et al., 2016). Upon incubation with SAS particles, the proportion of DCs with elevated SSC values was increased in a dose-dependent manner (Figures 1a-c). In contrast, the front scatter (FSC) remained unchanged when the DCs

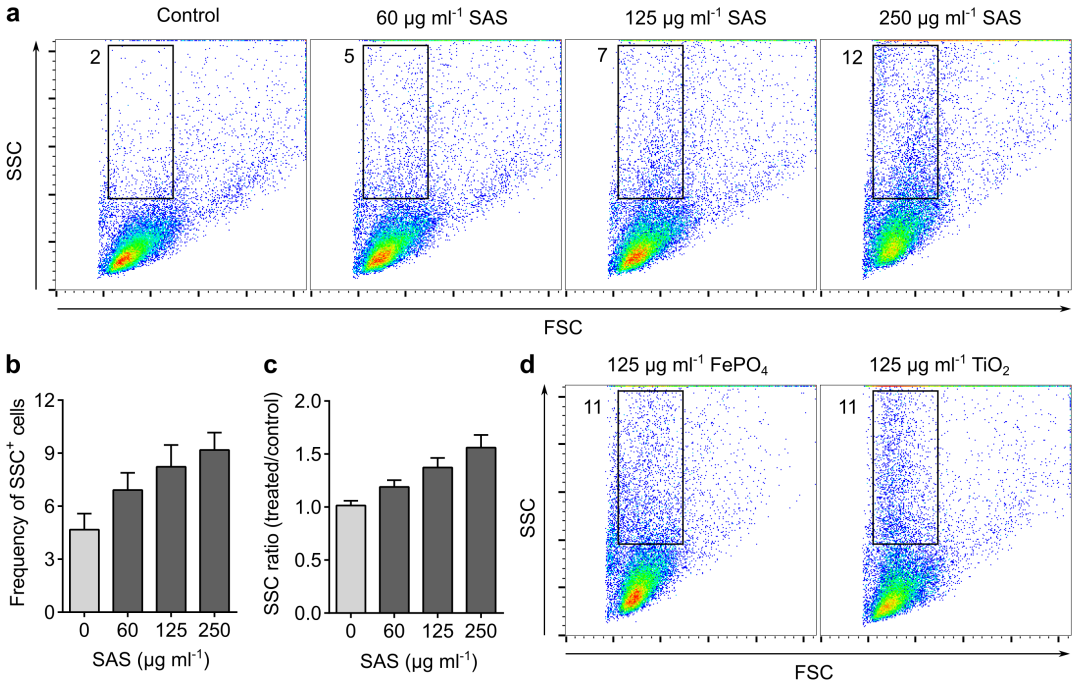

Figure 1. Interaction of steady-state DCs with nanomaterials. Flt3L-generated immature DCs were incubated for 1 h at 37°C with the indicated concentrations of SAS (13-nm primary diameter), 11-nm $FePO_4$ or 33-nm TiO_2 particles, and analyzed by flow cytometry. In culture medium, the SAS particles form aggregates with a mean diameter of 127 nm. The forward scatter (FSC) depends on cell size whereas the side scatter (SSC) reflects intracellular contents like granules (Zucker et al., 2010; Wang et al., 2016). **(a)** Flow cytometry distributions demonstrating a SAS dose-dependent increase of DCs with elevated SSC values. **(b)** Mean percentage of cells in the selected gate (shown in a) with high SSC values. Upon one-way ANOVA, SAS treatments increased the proportion of high-SSC cells in a significant manner ($p < 0.05$, n = 4 experiments with independent bone marrow isolates). Error bars, standard errors of the mean (s.e.m.). **(c)** Ratios of median SSC. Upon one-way ANOVA, SSC values after incubation with SAS particles were significantly higher than controls ($p < 0.05$, n = 4). **(d)** Comparison with SSC increments resulting from incubation of DCs with $FePO_4$ and TiO_2 nanoparticles (quantifications are shown in Additional file 1: Figure S2).

were exposed to SAS particles. Similar responses with elevated SSC and unchanged FSC were observed upon incubation of DCs with the $FePO_4$ and TiO_2 nanoparticles (Figure 1d, Additional file 1: Figure S2). These findings indicate that immature DCs readily interact with all three types of nanomaterials.

The interaction of immature DCs with SAS particles was further investigated by transmission electron microscopy (TEM) after high-pressure cryo-fixation to immobilize biological processes and visualize cellular contents, including membranes, at nanometer

resolution (Figure 2a). This electron microscopy approach revealed multiple protruding dendrites on the cell surface (Figure 2b) indicative of actin-dependent uptake mech-

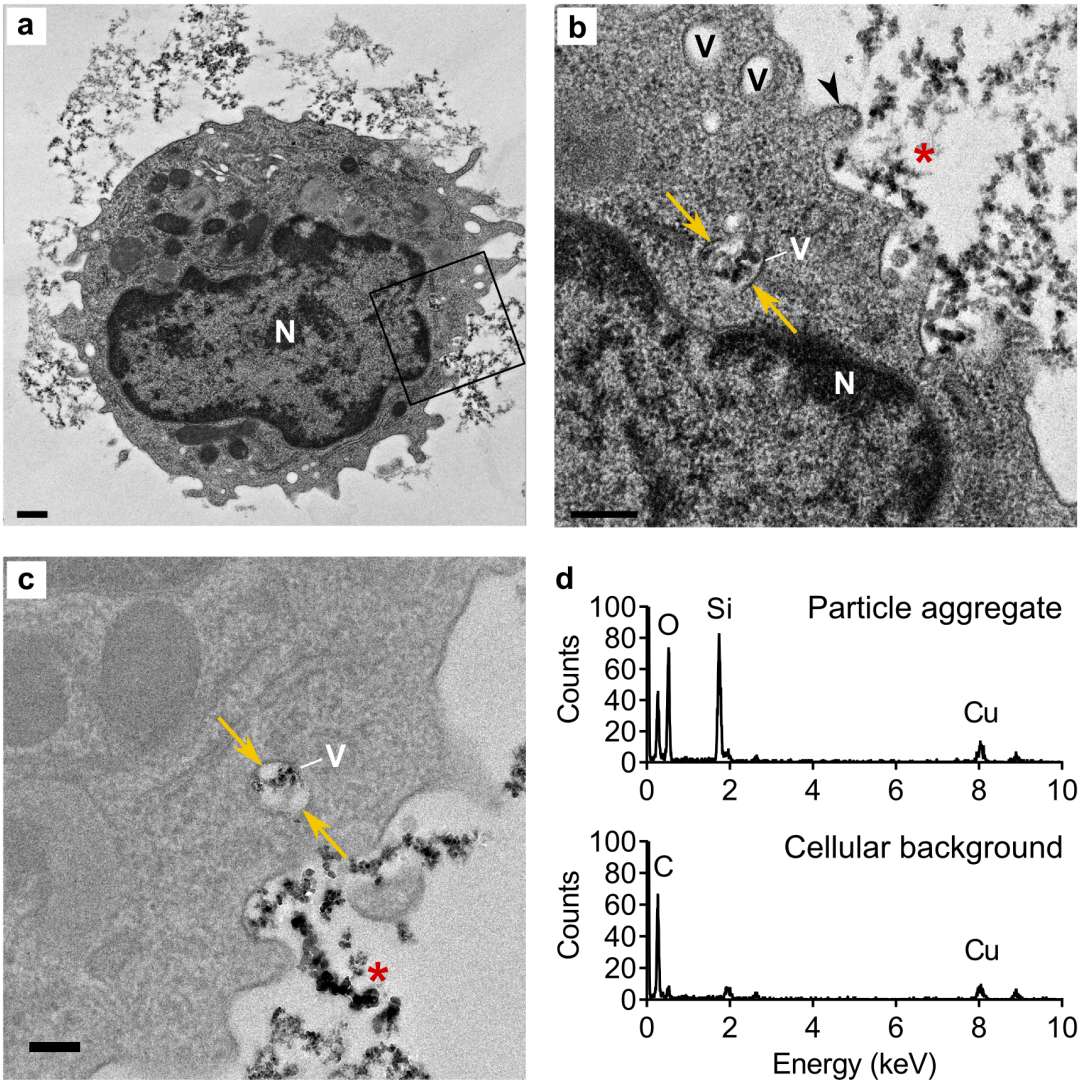

Figure 2. Internalization of nanomaterials by steady-state DCs. Immature DCs were incubated for 2 h at 37°C with 250 μg ml^{-1} SAS particles (13-nm primary diameter) and analyzed by TEM. **(a)** Typical steady-state DC with emerging dendrites interacting with particles. N, nucleus; bar, 0.5 μm. Contrasted with uranyl acetate and lead citrate for 15 min; the rectangle indicates the area selected for higher magnification. **(b)** Magnified region of the DC near its cell surface showing membrane protrusions (arrowhead) in the process of engulfing SAS particles (asterisk). The two arrows indicate internalized particles within a vacuole (V). Scale bar, 0.2 μm. **(c)** Magnified region of a DC in the process of engulfing SAS particles (asterisk) into intracellular vacuoles. Scale bar, 0.2 μm; contrasted with uranyl acetate and lead citrate for 1 min to improve particle visibility. **(d)** Analysis of a representative intracellular SAS particle aggregate and cytoplasmic background by energy-dispersive X-ray spectroscopy (EDX). Internalized $FePO_4$ and TiO_2 particles are shown in Additional file 1: Figure S3.

anisms (Sallusto et al., 1995; Sarkar et al., 2005). By closure of these membrane protrusions, SAS particles become trapped in cytoplasmic membrane-bound vesicles that have the appearances of endosomes (Figure 2c). Analysis of enclosed particle aggregates by energy-dispersive X-ray spectroscopy (EDX) on a scanning TEM instrument confirmed their expected elemental composition, mainly silicon and oxygen (Figure 2d). As a control, analysis of the cellular background, not containing any SAS particles, revealed signals of carbon (a normal biological constituent and part of the embedding resin) and copper (from the TEM specimen support grid). Analogous images showed that immature DCs also internalize $FePO_4$ and TiO_2 nanoparticles and, as observed for SAS particles, localize them to membrane-bound vesicles with the appearance of endosomes (Additional file 1: Figure S3).

Food-grade SAS causes induction of IL-1β in steady-state DCs. To assess functional consequences of this nanomaterial uptake into immature DCs, we determined cell viability and secreted cytokine levels as biomarkers of inflammatory reactions. Propidium iodide staining demonstrated the absence of cytotoxicity when immature DCs were incubated with SAS particles at concentrations of up to 250 μg ml^{-1} (Additional file 1: Figure S4). Despite this lack of cytotoxicity, however, SAS particles initiated IL-1β secretion from immature DCs without any pre-stimulation (usually referred to as "priming") with an inflammatory trigger (Figure 3a). Dose dependence experiments revealed a significantly increased IL-1β secretion at a SAS concentration of 100 μg ml^{-1} (Figure 3b), corresponding to a surface-related nanomaterial density of 50 μg cm^{-2}. This extracellular secretion of IL-1β in response to SAS particles took place without any extracellular release of the cytokines IL-1α (Figure 3c) and TNF-α (Figure 3d).

Since contamination of the SAS batches with endotoxin was excluded by a highly sensitive *Limulus* amoebocyte lysate test (Table 1), it is concluded that SAS particles are sufficient to activate immature DCs and induce the release of a potent inflammatory cytokine. Using small-molecule inhibitors, we next tested whether an intracellular particle uptake is necessary to induce the observed cytokine release. IL-1β production was reduced to baseline levels upon co-treatment of DCs with cytochalasin D, which is a broad inhibitor of actin-dependent processes (Winter et al., 2011), or rottlerin, a selective inhibitor of macropinocytosis (Additional file 1: Figure S5) (Sarkar et al., 2005). These inhibitor effects support the conclusion that the IL-1β responses to SAS particles requires endocytic uptake by actin-mediated mechanisms, primarily macropinocytosis. In contrast, despite their cellular uptake (Additional file 1: Figure S3), $FePO_4$ and TiO_2 nanoparticles elicit no IL-1β response (Figure 3a).

Mechanism of IL-1β induction by SAS particles. Because of its potent inflammatory action, IL-1β biogenesis is tightly regulated. First, an inactive pro-IL-1β precursor is

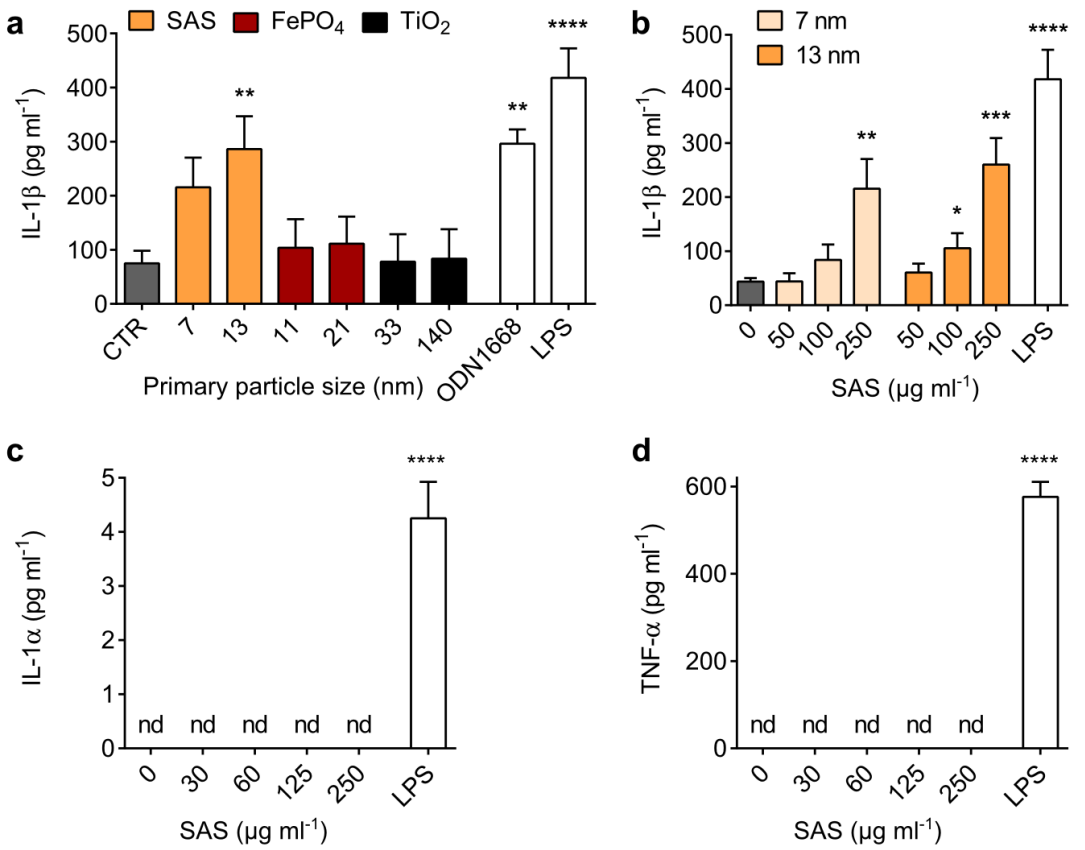

Figure 3. IL-1β secretion induced by food-grade SAS particles. Immature DCs were incubated (18 h, 37°C) with particles to test for IL-1β secretion. Asterisks denote significant differences between SAS treatments and controls ($^{*}p<0.05$, $^{**}p<0.01$, $^{***}p<0.001$, $^{****}p<0.0001$). **(a)** DCs were exposed to particles (250 μg ml^{-1}) and supernatants analyzed for IL-1β. Control reactions contained medium (CTR), 6 μg ml^{-1} ODN1668 (mimicking microbial DNA) or 1 μg ml^{-1} lipopolysaccharide (LPS). One-way ANOVA with Dunnet's correction; n = 3–9; error bars, s.e.m. **(b)** Dose dependence of IL-1β secretion stimulated by SAS particles. Unpaired two-tailed t-test (n = 3–12). **(c)** Release of IL-1α into the cell culture supernatant stimulated by LPS (1 μg ml^{-1}) but not by 13-nm SAS particles. Asterisks denote significant differences between the LPS treatment and controls containing only cell culture medium ($^{****}p<0.0001$). Cytokine levels below detection limit (4 pg ml^{-1}) are indicated as not detectable (nd). One-way ANOVA with Dunnet's correction; n = 4; error bars, s.e.m. **(d)** Release of TNF-α into the cell culture supernatant stimulated by LPS (100 ng ml^{-1}) but not by 13-nm SAS particles. Asterisks denote significant differences between the LPS treatment and controls containing only cell culture medium ($^{****}p<0.0001$). Cytokine levels below detection limit (8 pg ml^{-1}) are indicated as not detectable (nd). One-way ANOVA with Dunnet's correction; n = 4; error bars, s.e.m.

synthesized, which is then cleaved by the intracellular inflammasome complex (involving caspase-1) to yield biologically active IL-1β (Dinarello, 2011; Netea et al., 2015). In line with this well-known pathway, the release of IL-1β upon stimulation with SAS particles was reduced by co-treatment with the caspase inhibitor Z-VAD (Additional file 1: Figure S5), confirming caspase cleavage of pro-IL-1β. Next, we analyzed whole

cell lysates for the presence of pro-IL-1β to understand whether this protein precursor occurs constitutively in immature DCs or is induced following SAS particle uptake. In incubations of 18 h, SAS particles were able like lipopolysaccharide (LPS) to induce the *de novo* production of pro-IL-1β (Figure 4a). Dose dependence experiments revealed a

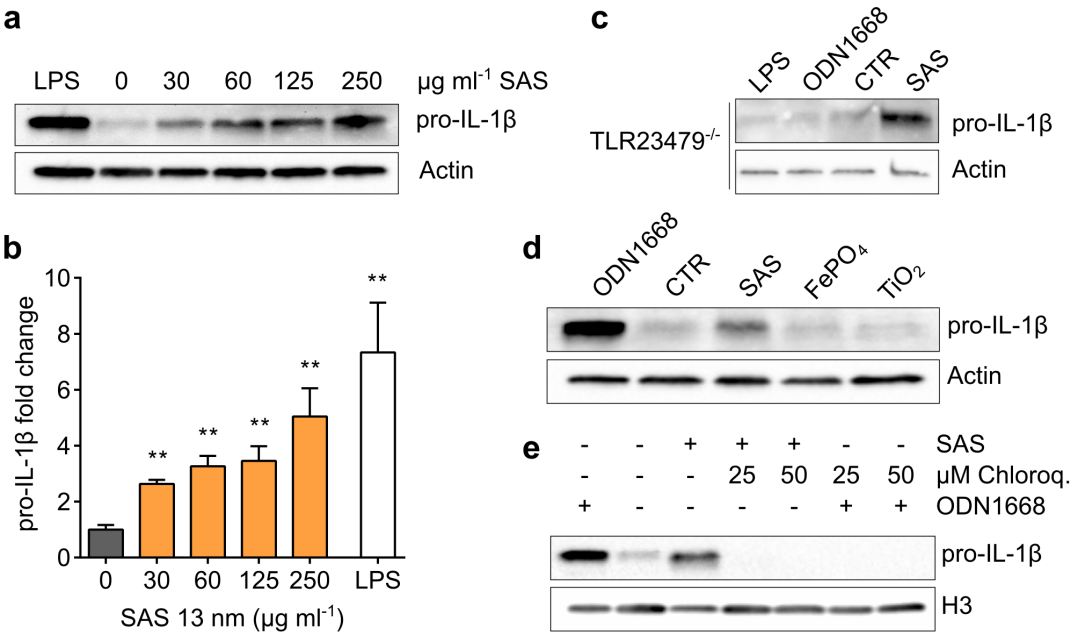

Figure 4. Induction of pro-IL-1β by food-grade SAS particles. Immature DCs were incubated (18 h, 37°C) with the indicated concentration of particles to test for pro-IL-1β induction. Asterisks denote significant differences between SAS treatments and controls (**$p < 0.01$). **(a)** DCs were incubated with LPS (250 ng ml^{-1}) or 13-nm SAS and analyzed for pro-IL-1β (31 kDa) and actin (42 kDa) by immunoblotting. **(b)** Quantification of pro-IL-1β induction by SAS particles (unpaired two-tailed t-test, n = 5). **(c)** Incubation of TLR-2/3/4/7/9$^{-/-}$ DCs with LPS (250 ng ml^{-1}), ODN1668 (600 ng ml^{-1}), medium (CTR) or SAS particles (125 μg ml^{-1}). **(d)** Incubation of wildtype DCs with ODN1668 (600 ng ml^{-1}), medium or particles indicated (125 μg ml^{-1}). **(e)** Effect of TLR inhibition. DCs were incubated with 13-nm SAS (125 μg ml^{-1}) alone or in the presence of chloroquine and analyzed for pro-IL-1β and histone H3 (17 kDa) by immunoblotting. ODN1668 (600 ng ml^{-1}) served as the positive control.

significantly increased pro-IL-1β level at a SAS concentration of 30 μg ml^{-1} (Figure 4b), equivalent to a surface-related nanomaterial density of 15 μg cm^{-2}. Pro-IL-1β was also induced upon SAS treatment of immature DCs lacking Toll-like receptor 4 (TLR4; Additional file 1: Figure S6). Pro-IL-1β was equally induced upon SAS treatment of immature DCs lacking simultaneously TLR2, TLR3, TLR4, TLR7 and TLR9 (Figure 4c). As these particular pattern recognition receptors mediate DC activation by the most abundant pathogen constituents like endotoxin (TLR2 and TLR4) or nucleic acids (TLR3, TLR7 and TLR9) (Pandey et al., 2015) the retained pro-IL-1β induction observed in their absence confirms that this response is not due to microbial contamination. However,

pro-IL-1β is not induced by $FePO_4$ and TiO_2 nanoparticles (Figure 4d). Considering that the particles are detected in endosomes (Figure 2), the mechanism of pro-IL-1β induction by SAS was further delineated using endosomal acidification inhibitors. Pro-IL-1β induction by SAS particles was reduced to baseline levels upon co-treatment with chloroquine (Figure 4e) or bafilomycin A1 (Additional file 1: Figure S7), which both inhibit the endosomal acidification process required for TLR activation (Rutz et al., 2004). This effect points to an endosomal pattern recognition receptor as the molecular sensor of SAS particles.

Concomitant display of maturation markers. Immature DCs are distinguishable from those emerging during inflammation by their molecular phenotype (Dalod et al., 2014). For example, immature DCs are characterized by low surface expression of CD69, but the presentation of this maturation marker is increased upon incubation with SAS particles. CD69 up regulation occurs with both major subsets of steady-state DCs, i.e., with conventional and plasmacytoid DCs (Figure 5a). Conventional DCs are

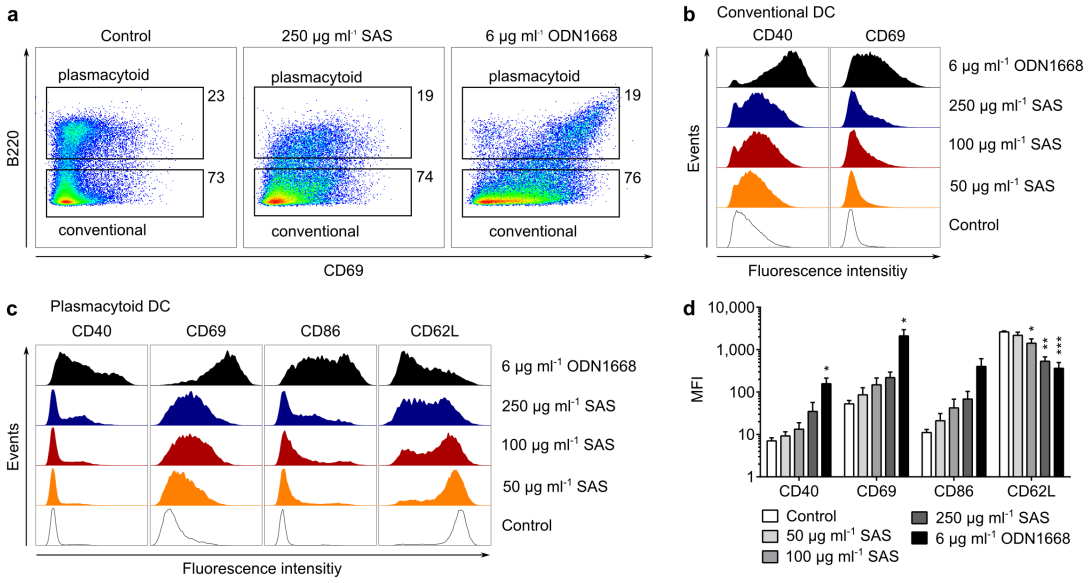

Figure 5. Maturation markers on steady-state DCs. Immature DCs were incubated for 18 h at 37°C with the indicated stimulus and their cell surface markers were analyzed by flow cytometry. **(a)** Increased CD69 on the surface of DCs exposed to SAS particles (13-nm primary diameter) or oligonucleotide ODN1668. Plasmacytoid and conventional DCs are the two major subsets differing in B220 expression. **(b)** Representative histograms showing dose-dependent changes of CD69 and CD40 on conventional DCs exposed to the indicated stimuli. Control, unstimulated DCs in culture medium. **(c)** Representative histograms showing dose-dependent changes in the display by CD69, CD40, CD86 and CD62L on plasmacytoid DCs. **(d)** Quantification of maturation markers by median fluorescence intensity (MFI) on plasmacytoid DCs exposed to SAS particles (13-nm primary size). Statistical significance ($^{*}p<0.05$, $^{**}p<0.01$, $^{***}p<0.001$) was determined by one-way ANOVA with Dunnet's correction, n=3 experiments with independent bone marrow isolates; error bars, s.e.m.

further characterized by low CD40, which is increased upon exposure to SAS particles (Figure 5b). Plasmacytoid DCs are further characterized by low CD40/CD86 and high CD62L, but incubation with SAS particles increased CD40 and CD86 on their surface, whereas CD62L levels were reduced (Figure 5c and 5d). Thus, in response to SAS particles, immature DCs not only induce the synthesis of pro-IL-1β but also undergo a dose-dependent maturation program involving shifts in multiple surface markers. This finding confirms the ability of SAS particles to activate immature DCs.

DISCUSSION

This study is fundamentally different from earlier reports describing the interaction of DCs with nanomaterials in two main aspects. First, the ability of nanomaterials to trigger IL-1β secretion from DCs was previously demonstrated only after priming these cells with LPS to induce expression of the pro-IL-1β precursor. Consequently, these previous reports demonstrated that certain nanomaterials are able to activate the inflammasome, which acts as an enzymatic complex that cleaves preformed pro-IL-1β to liberate the active IL-1β cytokine (Yazdi et al., 2010; Winter et al., 2011). In contrast to our present findings, these earlier studies did not report any pro-IL-1β induction in nanomaterial-exposed DCs. Second, these earlier studies were limited to inflammatory DCs derived from blood or bone marrow cultures stimulated with granulocyte-macrophage colony-stimulating factor (GM-CSF) (Yazdi et al., 2010; Winter et al., 2011). However, GM-CSF drives the differentiation of monocytes towards a special DC subset that sustains inflammation during exceptionally high demand like sepsis (Watowich & Liu, 2010; Varol et al., 2009; Cheers et al., 1988). These inflammatory DCs differ from the Flt3L-derived immature DCs used in our study whose function is to maintain tissue homeostasis by tuning immunologic responses (Watowich & Liu, 2010; Shortman & Naik, 2007; Xu et al., 2007).

Protective immunity is supported by IL-1β but, if not controlled, this highly inflammatory cytokine contributes to autoinflammatory and autoimmune diseases (Dinarello, 2011). Normally, IL-1β production is regulated by two independent signals. A first stimulus, such as LPS, IL-1α or TNF-α, prompts the synthesis of inactive pro-IL-1β by transcriptional induction (Rabolli et al., 2014; Franchi et al., 2009). A second stimulus activates the inflammasome resulting in caspase cleavage of pro-IL-1β to release active IL-1β (Franchi et al., 2009; Yazdi et al., 2010; Winter et al., 2011; Netea et al., 2015). In an animal model of acute pulmonary inflammation, Rabolli et al. (2014) describe a sequential mechanism in which lung-injected silica is taken up by macrophages, thus leading to cytotoxicity. The following release of IL-1α and TNF-α from necrotic

macrophages serves as a stimulus to induce the expression of pro-IL-1β, which is then cleaved upon silica-dependent inflammasome activation for the secretion of bioactive IL-1β (Rabolli et al., 2014). In contrast to this sequential scenario, our analysis with immature DCs (reflecting steady-state DCs in tissues) revealed for the first time that SAS particles are able to directly induce pro-IL-1β expression in the absence of cytotoxic reactions and any IL-1α or TNF-α bursts. This direct pro-IL-1β induction is not dependent on the pattern recognition receptors TLR2, TLR3, TLR4, TLR7 and TLR9. However, we surprisingly observed that the endosomal acidification inhibitors chloroquine and bafilomycin A completely abrogate the pro-IL-1β expression induced by SAS particles. Since the endosomal acidification process – inhibited by these compounds – is required for TLR activation (Rutz et al., 2004), we conclude that another endosomal pattern recognition receptor must constitute the molecular sensor of SAS particles responsible for pro-IL-1β induction. This strict and proven dependence on endosomal acidification also argues against other signaling mechanisms for example associated with cytotoxicity or increased K^+ efflux through the cell membrane (Zhang et al., 2012; Sun et al., 2015).

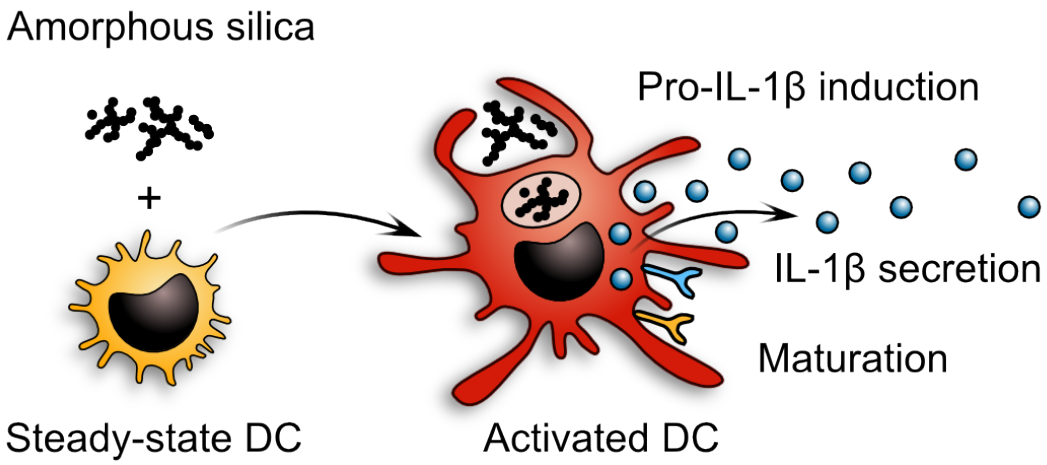

Figure 6. The response of Flt3L-generated immature DCs defines SAS as the first complete inflammatory nanomaterial. In steady-state (immature) DCs, the potent inflammatory cytokine IL-1β is not expressed and secretion is highly regulated by two independent signals. Exposure to food-grade silica causes both pro-IL-1β induction and its cleavage leading to IL-1β secretion. In addition, immature DCs undergo maturation involving shifts in multiple surface markers.

In summary, our findings indicate that the nanostructured surface of food-grade SAS particles, detected by intracellular pattern recognition receptors, mimics both the signal for inducing pro-IL-1β expression and the signal for activating pro-IL-1β cleavage. This study with steady-state DCs, therefore, defines SAS as the first complete inflammatory nanomaterial sufficient for *de novo* induction of IL-1β without needing any additional

cytotoxic or inflammatory trigger (Figure 6). The unprecedented single-hit mechanism of IL-1β induction suggests that SAS particles should be used in food more cautiously than current practice. Based on studies in rodents not assessing immunological endpoints, a lifelong dietary intake of 1.5 g SAS daily (Additional file 1: Figure S8) per adult is currently considered safe (reviewed in Ref. (Winkler et al., 2016)). Even if only a small fraction of the daily ingested SAS materials accumulates over time in lymphoid tissues (Shepherd et al., 1987; van der Zande et al., 2014; Hummel et al., 2014; Awaad et al., 2012), these persisting particles are very likely to reach locally in the tissue the 15 μg cm^{-2} density that in our assays is already sufficient for *de novo* IL-1β induction in DCs, without any accompanying cytotoxicity. An ensuing disruption of the gatekeeping function of DCs may trigger long-term inflammatory responses that contribute to the increased incidence of inflammatory bowel disease or other chronic intestinal disorders (Lomer et al., 2002; Hummel et al., 2014). In view of the unexpected finding that SAS particles cause IL-1β induction by a novel mechanism, as well as the subsequent IL-1β release, we advocate a more prudent use of these nanomaterials to reduce human exposure from food or other sources.

MATERIALS AND METHODS

Particles and Characterization. Food-grade SAS particles, produced by flame hydrolysis according to the Aerosil method (Sepeur et al., 2008), were obtained from Evonik (formerly Degussa). Their mean primary particle sizes are 7 and 13 nm based on measured BET surface areas of 326 m^2 g^{-1} and 175 m^2 g^{-1}, respectively. These same SAS particles were also characterized thoroughly by others (Dekkers et al., 2011; Peters et al., 2012). TiO_2 anatase with an average particle size of 33 nm (based on a measured BET surface area of 47 m^2 g^{-1}) were from Sigma-Aldrich. Food-grade TiO_2 anatase with an average particle size of 140 nm (based on a measured BET surface area of 11 m^2 g^{-1}) was from Sachtleben. $FePO_4$ nanoparticles with an average particle size of 11 and 21 nm (based on measured BET surface areas of 188 m^2 g^{-1} and 98 m2 g^{-1}, respectively) were produced by flame spray pyrolysis (described in the Additional file 1: Supporting Materials and Methods). Amino-modified PS particles with a primary particle diameter of 50 nm were obtained from Bangs Laboratories. The detailed characterization of all nanomaterials is summarized in Table 1.

For endotoxin analyses, particles were suspended in endotoxin-free water (Charles River) by mixing for 30 s on a vortex followed by sonication for 10 min in a Sonorex Digitec waterbath (Bandelin Electronic) at 35 kHz and 80 W. Then particle suspensions were assayed using the Endosafe-PTS test system (Charles River) equipped with highest

sensitivity cartridges with a limit of detection of 0.005 endotoxin units (EU) ml^{-1}. For exposure of cells, particles were suspended in complete cell culture medium [RPMI-1640 GlutaMAX, 10% (vol/vol) heat-inactivated fetal calf serum (from PAA), 100 U ml^{-1} penicillin, 100 μg ml^{-1} streptomycin and 50 μM β-mercaptoethanol (all from Invitrogen)] by mixing and sonication as described above. Fresh particle suspensions were prepared for every experiment and used within 15 min after sonication. SAS suspensions in complete medium remained stable for 24 h, as assessed by hydrodynamic size measurements.

Stimulation of Immature DCs. Immature DCs were generated from mouse bone marrow (Naik et al., 2010). Briefly, femurs and tibiae of C57BL/6 wild-type mice (or TLR-deficient mice on a C57BL/6 background) were flushed with complete culture medium and the released progenitor cells were filtered through a 70-μm cell strainer (BD Falcon), centrifuged, reconstituted in complete medium and incubated for 8 days in the presence of 200 ng ml^{-1} Flt3L (BioXcell). For each culture, the amount of live $CD11c^+$ DCs, the proportion of plasmacytoid DCs (CD11c+B220+) and conventional DCs ($CD11c^+B220^-CD11b^{high}SIRP\alpha^+$ and $CD11c^+$ $B220^-CD11b^{intermediate}SIRP\alpha^+$) were verified by flow cytometry (Additional file 1: Figure S1). Stimulation assays were conducted as previously published (Hochrein et al., 2004). Immature DCs, which grow as cell suspensions, were transferred to 96-well plates (3 x 10^5 cells/well) containing complete cell culture medium (200 μl/well) and challenged with the indicated concentrations of particles suspended in medium for the time indicated. Realistic SAS particle dose concentrations (30 to 250 μg μl^1) were derived from a recent publication, where silica levels of up to 300 μg g^{-1} tissue in the spleen of rodents after repeated oral administration of SAS particles were reported (van der Zande et al., 2014).

Control incubations were carried out with ultra-pure lipopolysaccharide (LPS; *Escherichia coli* 0111:B4, Sigma-Aldrich) or unmethylated deoxyribonucleic acid (DNA) oligonucleotides containing a CpG motif (ODN1668, TIB Molbiol). The inhibitors bafilomycin A1 (InvivoGen), cytochalasin D (Enzo Life Sciences), rottlerin (Sigma-Aldrich) and Z-VAD-FMK (Bachem) were dissolved in dimethyl sulfoxide and added as indicated. Chloroquine diphosphate salt (Sigma-Aldrich) was added as indicated.

DC Phenotype and Maturation. DCs were stained on ice with conjugated antibodies against CD11c (N418, PE-labeled), CD11b (M1/70, PE-Cy7-labeled), B220 (RA3-6B2, APC-eFluor 780-labeled), SIRPα (P84, APC-labeled), CD40 (1C10, PE-labeled), CD62L (MEL-14, APC-labeled), CD69 (H1.2F3, APC-labeled) and CD86 (GL1, PE-labeled) purchased from eBioscience. A FACSCanto II flow cytometry instrument (BD Biosciences) was employed to acquire 50000 events. Dead cells were stained and excluded from analyses using propidium iodide (PI; Sigma-Aldrich). Single-color and

fluorescence-minus-one (FMO) controls were prepared and analyzed along with multicolor samples. Flow cytometry data were analyzed with FlowJo (Version 10, TreeStar).

Cryo-fixation and Electron Microscopy. Immature DCs were transferred to 12-well plates (3 x 106 cells/well) containing complete cell culture medium (1 ml/well). After incubation with particles (250 μg ml^{-1}), cells were prefixed with 0.25% (vol/vol) glutaraldehyde and immediately high-pressure frozen in capillary cellulose tubes using an EM HPM 100 device (Leica). Frozen cells were transferred into a substitution unit (EM-AFS2, Leica) precooled to –90°C for substitution with acetone containing 5% water. The subsequent fixation was carried out with 1 % (wt/vol) osmium tetraoxide, 0.25% (vol/vol) glutaraldehyde raising the temperature to 20°C, then the cells were embedded in epon. Ultrathin (70 nm) sections were contrasted with uranyl acetate and lead citrate for 15 min (for standard contrast) or 1 min (for improved detection of particles)(Roberts, 2002) and examined in a transmission electron microscope (CM12, Philips) equipped with a CCD camera (Ultrascan 1000, Gatan) at an acceleration voltage of 100 kV. Elemental analysis of selected samples was conducted on a scanning transmission electron microscope (G2 Spirit, FEI Tecnai) equipped with a high angle annular dark field detector (HAADF) and an X-Max energy-dispersive X-ray spectroscopy (EDX) detection system for elemental analysis (Oxford). Gatan digital micrograph was used for image acquisition and Oxford INCA for EDX operation and control.

Immunoassays. IL-1β concentrations in cell culture supernatants were detected using the IL-1β DuoSet kit (R&D Systems) following the manufacturer's instructions. Absorbance was measured at 405-nm wavelength (reference wavelength 492 nm) with a SpectraMax Plus 384 microplate reader (Molecular Devices). Mouse IL-1α and TNF$-\alpha$ -concentrations in cell culture supernatants were detected using the IL-1α and TNF$-\alpha$ Ready-SET-Go kits (eBioscience) following the manufacturer's instructions. Absorbance was measured at 450-nm wavelength (reference wavelength 570 nm) with a Epoch 2 microplate reader (BioTek). For Western blotting, cells were washed three times with phosphate-buffered saline (PBS) and whole cell lysates were prepared using M-PER buffer (LifeTechnologies). Equal volumes of cell lysate were resolved on 4-20% (wt/vol) polyacrylamide gradient gels (TGX Stainfree) and the separated proteins were transferred to TurboBlot PVDF membranes (both from BioRad). For immunodetection, membranes were blocked with 10% (wt/vol) milk in Tris-buffered saline, containing 0.1% (vol/vol) Tween-20, for 1 h at room temperature and probed overnight with antibodies against IL-1β (Cell Signaling) and actin (Millipore). After incubation with matching secondary antibodies, chemiluminescence was detected using the ChemiDoc MP gel documentation instrument (BioRad).

Statistical Analysis. Mean and standard error of the mean (s.e.m.) were calculated for

all quantitative parameters using GraphPad Prism 6.0. Results were expressed as mean ± s.e.m. of multiple determinations with independent DC cultures. Comparisons were conducted by one-way ANOVA with Dunnet's correction or unpaired two-tailed t-test, as indicated in the figure legends. A statistically significant difference was assumed for $p < 0.05$.

ASSOCIATED CONTENT

Supporting Information. Detailed information including *in vitro* DC generation, synthesis of $FePO_4$ particles, quantification of the interaction between DC and particles, IL-1β induction in TLR4-deleted DCs, inhibitor assays with cytochalasin D, rottlerin and bafilomycin A1 and TEM images of DC engulfing TiO_2 and $FePO_4$ particles.

AUTHOR INFORMATION

Corresponding Author

*Correspondence to: naegelih@vetpharm.uzh.ch.

Author Contributions

H.C.W., M.S., P.W. and H.N. conceived and designed the experiments. H.C.W. and J.K. carried out the experiments and performed the data analysis. B.B. and H.H. provided the methodology for production and characterization of DCs. L.v.M. and I.T. contributed to particle synthesis and characterization. E.M.S. provided assistance for electron microscopy. H.C.W. and H. N. wrote the manuscript. All authors contributed to the final text and approved the manuscript.

Funding Sources

Supported by the National Research Program "Opportunities and Risks of Nanomaterials" grant 406440-141619 to H.N., M.S. and P.W., and by grant FK-15-053 from the "Forschungskredit" of the University of Zurich to H.C.W.

Notes

The authors declare no competing financial interest.

ACKNOWLEDGMENTS

We thank Zuzana Garajova for excellent technical support, Prof. Thorsten Buch and Filipa Marques Ferreira for providing bone marrow from TLR2/3/4/7/9-deleted mice, Prof. Onur Boyman and Miro Raeber for providing bone marrow from TLR4-deleted mice, Evonik and Sachtleben for providing SAS and TiO_2 particles, the Flow Cytometry Facility and the Center for Microscopy of the University of Zurich for access to instruments. The authors also wish to thank Peter Rast for his contribution to the characterization of $FePO_4$ particles, and Dr. Florentine Hilty and Prof. Sotiris Pratsinis for helpful discussions and critical reading of the manuscript.

Supporting Information

Interleukin-1β induction in immature dendritic cells exposed to food-grade synthetic amorphous silica

Hans Christian Winkler,[†] Julian Kornprobst,[†] Peter Wick,[‡] Lea Maria von Moos,[§] Ioannis Trantakis,[§] Elisabeth Maria Schraner,[∥] Barbara Bathke,[⊥] Hubertus Hochrein,[⊥] Mark Suter,[#] Hanspeter Naegeli[*†]*

[†]Institute of Pharmacology and Toxicology, University of Zurich-Vetsuisse, Winterthurerstrasse 260, 8057 Zurich, Switzerland.

[‡]Laboratory for Particles-Biology Interactions, Empa Swiss Laboratories for Materials and Technology, Lerchenfeldstrasse 5, 9014 St. Gallen, Switzerland.

[§]Department of Health Sciences and Technology, ETH Zurich, Schmelzbergstrasse 9, 8092 Zurich, Switzerland.

[∥]Electron Microscopy, Institutes of Veterinary Anatomy and Virology, Winterthurerstrasse 260, 8057 Zurich, Switzerland.

[⊥]Department of Research, Bavarian Nordic GmbH, 82152 Martinsried, Germany.

[#]Immunology Division, Vetsuisse Faculty, University of Zurich, Winterthurerstrasse 204, 8057 Zürich, Switzerland.

*Correspondence to: naegelih@vetpharm.uzh.ch

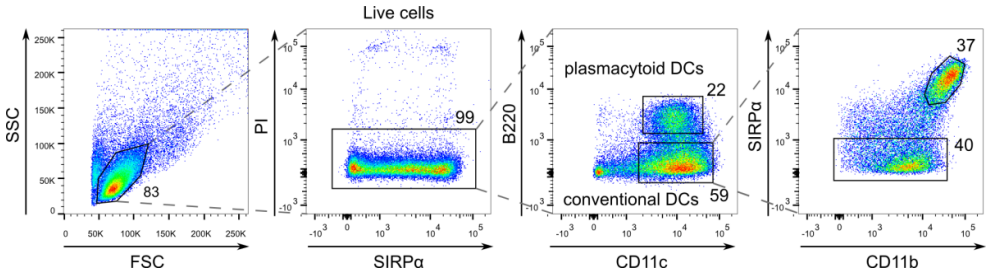

Figure S1. Characterization of steady-state DCs.

Immature DCs, generated from mouse bone marrow progenitors in the presence of Flt3L, were analyzed by flow cytometry. For each culture, the proportion of live $CD11c^+$ DCs, the proportion of plasmacytoid DCs ($CD11c^+B220^+$) and the proportion of conventional DCs ($CD11c^+B220^-$ $CD11b^{high}SIRP\alpha^+$ and $CD11c^+$ $B220^-CD11b^{intermediate}SIRP\alpha^-$) were verified using the respective antibodies. Numbers indicate the percentage of events in each gate. PI, propidium iodide.

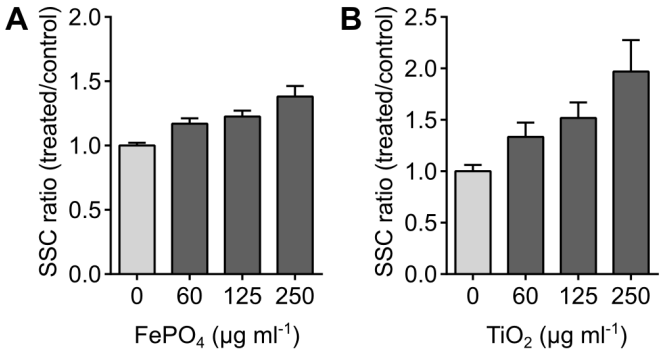

Figure S2. Interaction of steady-state DCs with $FePO_4$ and TiO_2 particles.

Flt3L-generated immature DCs were incubated for 1 h at 37°C with the indicated concentrations of $FePO_4$ (11-nm diameter) or TiO_2 particles (33-nm diameter) suspended in cell culture medium, and analyzed by flow cytometry. The forward scatter signal (FSC) depends on the size of cells whereas the side scatter (SSC) reflects intracellular structures like granules. (**A**) Ratios of median SSC values resulting from incubation of immature DCs with $FePO_4$ relative to controls. (**B**) Ratios of median SSC values obtained from incubation of immature DCs with TiO_2 particles relative to controls. Upon one-way ANOVA, SSC values resulting from the incubation of immature DCs with $FePO_4$ and TiO_2 particles were significantly higher than controls ($p<0.05$, n = 3 experiments with independent bone marrow isolates, error bars indicate s.e.m.).

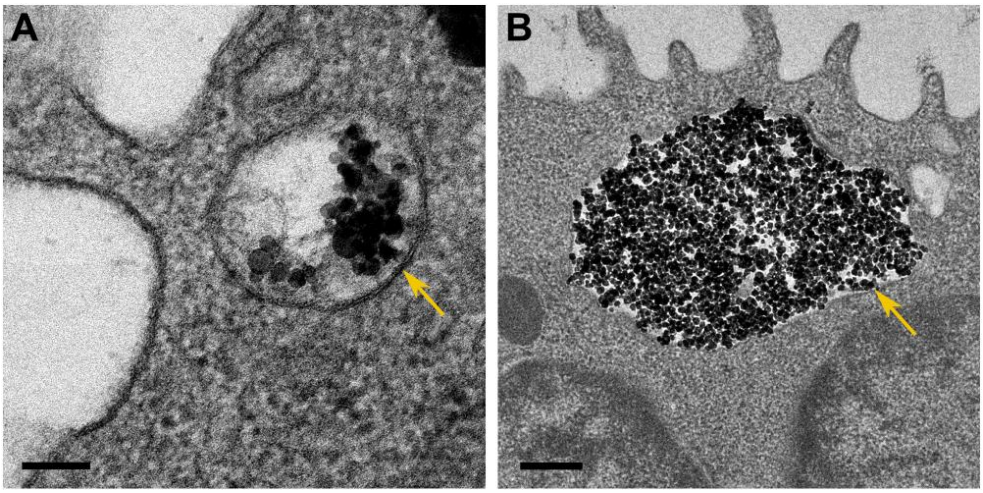

Figure S3. Internalization of $FePO_4$ and TiO_2 nanoparticles by steady-state DCs.

Flt3L-generated immature DCs were incubated for 2 h at 37°C with 250 µg ml^{-1} TiO_2 or $FePO_4$ particles and analyzed by transmission electron microscopy. (**A**) Typical steady-state DC interacting with $FePO_4$ (11-nm primary particle diameter). The arrow indicates internalized $FePO_4$ particles within a cytoplasmic membrane defining a vacuole. Scale bar, 0.1 µm. (**B**) Typical steady-state DC interacting with TiO_2 (33-nm primary particle diameter). The arrow indicates internalized TiO_2 particles within a cytoplasmic membrane defining a vacuole. Scale bar, 0.5 µm.

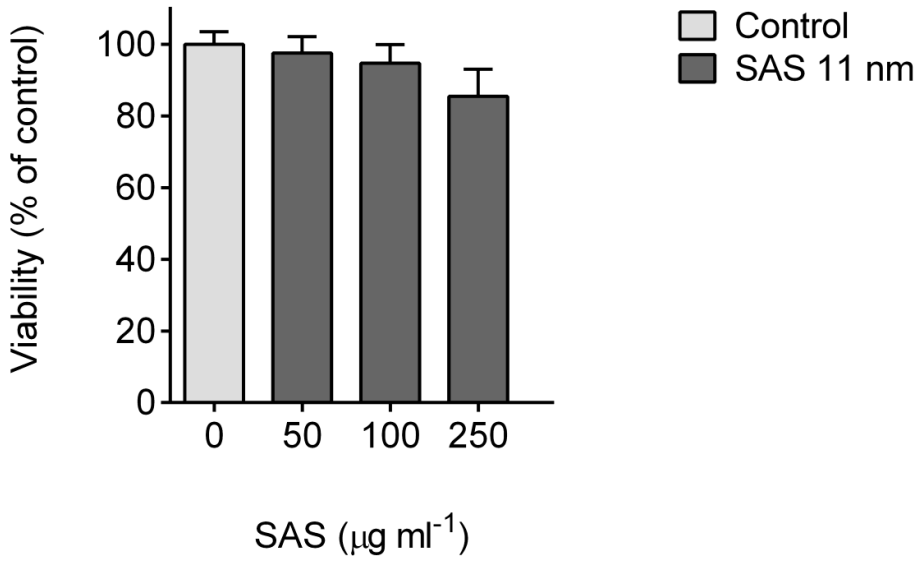

Figure S4. Cell viability upon incubation with SAS particles.

The effect of 13-nm SAS particles on cell viability was analyzed by flow cytometry after propidium iodide staining. Flt3L-generated immature DCs were incubated for 18 h at 37°C with 13-nm SAS particles at the indicated concentrations. Results represent the percentage of viable (propidium iodide-negative) cells relative to medium only control. Upon one-way ANOVA, the viability values resulting from the incubation of immature DCs with SAS particles were not significantly different from controls (one-way ANOVA with Dunnet's correction, n = 5, error bars indicate s.e.m.). Please note that a statistically significant pro-IL-1β induction is observed at a SAS dose of 30 µg ml^{-1}.

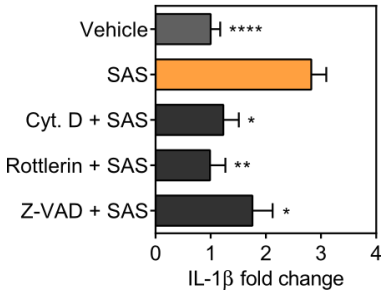

Figure S5. Effect of inhibitors on IL-1β secretion induced by SAS particles.

Flt3L-generated immature DCs were incubated for 18 h at 37°C with 13-nm SAS (250 µg ml^{-1}) alone or in the presence of cytochalasin D (1.5 µg ml^{-1}), rottlerin (1.5 µg ml^{-1}) and Z-VAD (10 µg ml^{-1}). Results represent fold changes relative to vehicle controls (one-way ANOVA with Dunnet's correction, n = 3-12, error bars indicate s.e.m.).

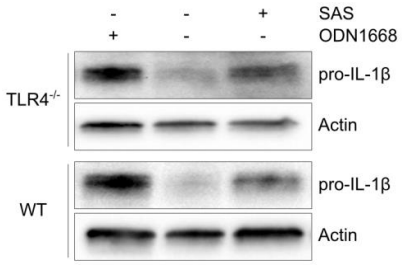

Figure S6. Induction of pro-IL-1β by SAS particles.

Flt3L-generated immature DCs from wildtype (WT) or TLR4$^{-/-}$ mice were incubated for 18 h at 37°C with 13-nm SAS (125 µg ml^{-1}) in cell culture medium, and analyzed by immunoblotting. Control reactions contained medium alone or 600 ng ml^{-1} ODN1668 (mimicking microbial DNA).

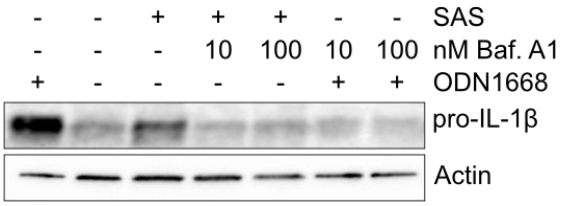

Figure S7. Effect of bafilomycin A1 on pro-IL-1β induction by SAS particles.

Flt3L-generated immature DCs from wildtype mice were incubated for 18 h at 37°C with 13-nm SAS (125 µg ml^{-1}) alone or in the presence of bafilomycin A1 (10 or 100 nM), and analyzed by immunoblotting for pro-IL-1β. Control reactions contained medium alone or 600 ng ml^{-1} ODN1668 (mimicking microbial DNA).

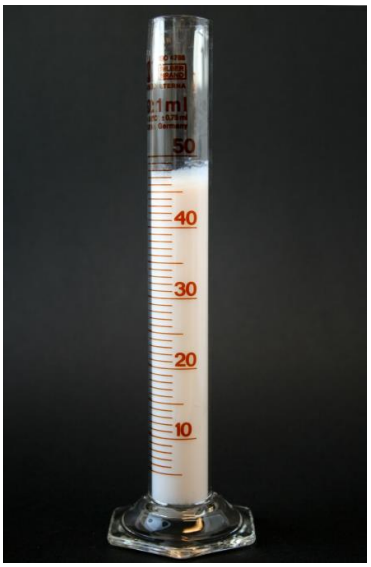

Figure S8. Safe upper limit of nano-structured SAS particles.

The 50-ml measuring cylinder contains 1.5 g of a white fluffy powder consisting of hydrophilic SAS produced by the Aerosil method. This amount of food-grade SAS material is currently considered safe for a 60-kg adult if consumed daily for a lifetime as food additive.[1,2]

Supporting Materials and Methods

Synthesis of $FePO_4$ nanoparticles. $FePO_4$ nanoparticles with an average particle size of 11 and 21 nm (based on measured BET surface areas of 188 $m^2\ g^{-1}$ and 98 $m^2\ g^{-1}$, respectively) were produced by flame spray pyrolysis according to a published method[3] with minor adaptations to obtain the desired particle sizes. Iron nitrate nonahydrate (purity ≥ 97.0%, Riedel-de-Haën/Sigma-Aldrich) and tributyl phosphate (purity 97%; Sigma-Aldrich) were dissolved in a 1:1 (vol/vol) mixture of ethanol (abs. denat. 2% 2-butanone, Alcosuisse) and 2-ethylhexanoic acid (purity ≥ 99%; Sigma-Aldrich) at a total metal concentration of 0.5 mol l^{-1} or 0.4 mol l^{-1} for 21-nm $FePO_4$ and 11-nm $FePO_4$, respectively. This precursor solution was fed at 3 or 7 ml min^{-1} into the FSP spray nozzles by a syringe pump (Lambda, VIT-FIT) and atomized with 5 or 7 l min^{-1} oxygen (pressure drop 1.5 bar). The spray was ignited by a methane/oxygen (2.5 l min^{-1} each) ring-shaped flame. Additionally, 5 l min^{-1} (sheath) O_2 was supplied. All gas flow rates were regulated by mass flow controllers (Bronkhorst, EL-FLOW). Using a vacuum pump (Busch, Mink MM1202 AV), particles were collected on water-cooled teflon membrane-filters (BHA Technologies AG) placed at least 65 cm above the burner.

Supplementary references:

(1) van Kesteren, P. C. E.; Cubadda, F.; Bouwmeester, H.; van Eijkeren, J. C. H.; Dekkers, S.; de Jong, W. H.; Oomen, A. G. Novel Insights into the Risk Assessment of the Nanomaterial Synthetic Amorphous Silica, Additive E551, in Food. *Nanotoxicology* **2015**, *9*, 442–452.

(2) EFSA 2009. European Food Safety Authority. Scientific Opinion of the Panel on Food

3.2 Nanoparticle effects on epithelial cells

This paper describes the effects caused by food-grade $FePO_4$ particles and synthetic amorphous silica in epithelial cells.

I designed, performed and analyzed the electron microscopy experiments and contributed the matching materials and methods part for the manuscript.

Iron phosphate nanoparticles for food applications do not induce adverse effects in rats or human cell lines

Lea M. von Moos[1], Mirjam Schneider[1], Florentine M. Hilty[1], Monika Hilbe[2], Myrtha Arnold[1], Nathalie Ziegler[1], Diogo Sales Mato[1], Hans Winkler[3], Mohamed Tarik[4], Christian Ludwig[4,5], Hanspeter Naegeli[3], Wolfgang Langhans[1], Michael B. Zimmermann[1], Shana J. Sturla[1], Ioannis A. Trantakis*[1]

[1] Department of Health Sciences and Technology, ETH Zürich, Switzerland

[2] Institute of Veterinary Pathology, Vetsuisse Faculty, University of Zurich, Switzerland

[3] Institute of Pharmacology and Toxicology, University of Zurich-Vetsuisse, Switzerland

[4] Energy and Environment Research Division, Paul Scherrer Institut (PSI), Switzerland

[5] École Polytechnique Fédérale de Lausanne (EPFL), ENAC-IIE, Lausanne, Switzerland

Corresponding author: ioannis.trantakis@hest.ethz.ch

Abstract

Nanotechnology offers new opportunities for providing health benefits in foods. Food fortification with iron phosphate nanoparticles ($FePO_4$ NPs) is a promising new approach to reducing iron deficiency because $FePO_4$ NPs combine high bioavailability with superior sensory performance in difficult-to-fortify foods. However, their safety remains largely untested. We fed rats for 90 days diets containing $FePO_4$ NPs at doses at which iron sulfate ($FeSO_4$), a commonly-used food fortificant, has been shown to induce adverse effects. Feeding did not result in signs of toxicity, including oxidative stress, organ damage, excess iron accumulation in organs, or histological changes. These safety data were corroborated by evidence that NPs were taken up by human gastrointestinal cell lines without reducing cell viability or inducing oxidative stress. Our findings suggest $FePO_4$ NPs appear to be as safe for human consumption as $FeSO_4$.

Reducing particle size of essential minerals to the nanoscale may sharply increase their absorption when used as food fortificants and nutritional supplements[1-3]. However, safety concerns arise for orally ingested nanominerals that do not completely dissolve in the stomach and enter the intestines as intact nanoparticles (NPs) that may be taken up, distributed to organs and potentially induce adverse effects[4,5]. Conflicting information regarding the potential toxicity of food relevant NPs has so far hampered the widespread application of nanotechnology in the food sector.

Iron deficiency (ID) affects more than two billion people in industrialized and developing countries[6]. Fortifying food by adding iron can be an effective, sustainable and cost-effective strategy to combat ID[7]. Food fortification with iron is challenging because highly bioavailable iron fortificants such as $FeSO_4$ are chemically reactive and cause unacceptable organoleptic changes, mainly color and taste, in foods[8]. Therefore, iron compounds insoluble in water like $FePO_4$, ferric pyrophosphate ($Fe_4(P_2O_7)_3$ or elemental iron are often used in the food industry. They have less impact on sensory properties but are only poorly absorbed[8]. Reduction of the particle size of such minerals markedly increases their specific surface area (SSA) in relation to mass, leading to improved solubility and *in vivo* bioavailability[9,10]. Reducing iron compounds to the nanoscale further enhances bioavailability while maintaining the low reactivity of the original compounds[11]. Nanostructured iron and iron/zinc compounds produced by flame spray pyrolysis (FSP) were shown to have equivalent iron bioavailability as $FeSO_4$[1,2] without reacting with the food matrix[1,12]. The fate and biological impact of nanostructured iron in the gastrointestinal tract has not yet been thoroughly investigated but is critical for evaluating their safety.

While there is scarce data regarding adverse biological effects of iron phosphate NPs, there are a number of other food relevant NPs that have been shown to induce adverse outcomes after exposure of human intestinal cells or experimental animals to food relevant NPs. Food-grade SiO_2 and TiO_2 NPs are internalized by intestinal epithelial cells and persist biologically[13-15]. They have been shown to induce cytotoxicity, DNA damage and oxidative stress in gastrointestinal cells *in vitro*, however in the absence of blood serum[16,17]. Short-term administration of TiO_2 NPs to mice led to an accumulation of DNA strand breaks in peripheral leukocytes and bone marrow, as well as lipid peroxidation, oxidative DNA lesions, and DNA damage in mouse liver[18,19]. Administration of ZnO NPs by gavage to mice for two weeks led to liver injury associated with lipid peroxidation and DNA damage[20]. Histopathological lesions in liver and kidney, and increased levels of inflammatory cytokines in blood, were reported in mice after oral administration of Al_2O_3 NPs for 13 weeks[21]. In rats, oral exposure to Ag NPs for 13 weeks caused systemic Ag distribution and liver and kidney injury[22]. In a similar study, silica accumulation in spleen and liver fibrosis, but no other adverse effects were observed after administration of SiO_2 NPs via the diet for 12 weeks[23]. Due to the lack

of larger control compounds in the above mentioned studies, it is unclear whether the observed adverse effects were strictly related to the nanoscale size of the particles. No adverse effects were reported, however, after gavage exposure of rats to $Fe_4(P_2O_7)_3$-NPs[24] or Fe_2O_3 NPs[22]. Furthermore, feeding iron deficient rats with a diet containing nanosized iron/zinc compounds (10 or 20 mg Fe kg^{-1}) for 13 days did not result in tissue accumulation of iron[1]. To our knowledge, however, the consequences of sub-chronic exposure to iron NPs incorporated into the diet at dose levels at which non-nanosized iron salts may induce adverse outcomes have never been addressed. Such information is crucial to evaluate whether the administration of $FePO_4$ NPs via a realistic route of exposure may lead to novel adverse outcomes attributable to the nanosize of iron fortificants.

Here we investigate for the first time the responses of human intestinal cell lines to $FePO_4$ NPs as well as the sub-chronic dietary exposure of rats to $FePO_4$ NPs. It was observed that $FePO_4$ NPs can be taken up by human intestinal cell lines, but did not induce cytotoxicity or oxidative stress. In addition, exposing rats to $FePO_4$ NPs at the iron dose in standard rodent diets (35 mg Fe kg^{-1} diet)[25] or at a dose at which $FeSO_4$ has been shown to induce adverse effects (350 mg Fe kg^{-1} diet)[26] for 90 days did not result in any measurable adverse effects. The safety of $FePO_4$ NPs after oral consumption was evaluated in comparison to several food grade control compounds.

Particle characterization

$FePO_4$ NPs were synthesized by FSP; a scalable production process[27] for tailor-made particles with high SSA and well-defined chemical composition[28]. FSP-derived $FePO_4$ NPs had SSAs of 98 $m^2\ g^{-1}$ ($FePO_4$ 98) and 188 $m^2\ g^{-1}$ ($FePO_4$ 188) as determined by nitrogen absorption. A larger food-grade $FePO_4$ compound ($FePO_4$ 27; SSA of 27 $m^2\ g^{-1}$) was included in this study as a control for the effect of particle size. $FeSO_4$ is a highly bioavailable iron compound and was introduced to control for iron toxicity. Food grade SiO_2 NPs (SiO_2 200; SSA of 200 $m^2\ g^{-1}$ and SiO_2 380; SSA of 380 $m^2\ g^{-1}$) were used to control for the effect of non-dissolvable NPs. X-ray diffraction (XRD) indicated that all compounds were amorphous (Supplementary Fig. 1). FSP-produced $FePO_4$ was composed of near-spherical particles in the size range 10-40 nm ($FePO_4$ 98) and 5-10 nm ($FePO_4$ 188), as indicated by transmission electron microscopy (TEM) images (Supplementary Fig. 2). The commercial $FePO_4$ 27 was composed of larger and irregularly shaped particles in the size range 50-200 nm. Assuming dense spherical particles, the calculated primary particle size of $FePO_4$ 27 would be 77 nm, however, as shown in the TEM images, these assumptions are not valid for $FePO_4$ 27 and we therefore do not refer to $FePO_4$ 27 as NPs. Finally, the SiO_2 NPs were irregularly shaped and appeared to be present as aggregates (Supplementary Fig. 2).

***In vitro* hazard characterization**

We investigated the impact of FSP-produced $FePO_4$ NPs on different human gastrointestinal cell lines. By comparing responses in cells derived from a human colon adenocarcinoma (HT29) and its mucus-secreting subclone (HT29-MTX cells),[29] we assessed whether the presence of mucus alters the interactions of NPs with the cells. Additionally, we characterized the responses of human colonic epithelial cells (HCECs), established from noncancerous tissue that retain characteristics of normal epithelial cells. HCEC cells are not tumorigenic, they do not have mutations in hot spot genes and express epithelial as well as stem cell markers[30,31]. In these three human cell models we investigated cellular uptake of $FePO_4$ NPs, their influence on cell viability and their potential to induce oxidative stress.

For *in vitro* evaluation, NPs were dispersed in cell culture media with 10% fetal bovine serum, resulting in agglomerates and polydisperse suspensions with average hydrodynamic diameter from 231 to 615 nm (Supplementary Table 1). Their diameter was unchanged for up to 72 h (Supplementary Fig. 3), suggesting that the dispersion protocol was effective and that changes in agglomerate size during exposure of cells to NPs suspensions were negligible. Zeta potential was around -11 mV (Supplementary Table 1), a common value for various NPs suspended in cell culture media containing serum and related to the formation of a protein corona around the NPs[32].

To assess whether the NPs were taken up by the cells, we characterized $FePO_4$ NP-treated cells by TEM. After exposure to $FePO_4$ NPs for 48 h, internalization of NPs in cells was observed in all three cell lines (Supplementary Fig. 4). Unlike other studies where NPs were also found freely in the cytoplasm[13] or even in the nucleus[14], the $FePO_4$ NPs were exclusively present as large agglomerates and in membrane-enclosed vesicles. Neither HCECs, HT29 nor HT29-MTX are phagocytic cells, therefore the NPs may be taken up through adsorptive endocytosis, a pathway previously hypothesized to be involved in the uptake of iron oxide/hydroxide NPs into Caco-2 cells[33].

Since human intestinal cell lines were active in taking up $FePO_4$ NPs, their impact on metabolic activity and membrane integrity, as well as the potential to induce oxidative stress was characterized. No membrane damage or reduction of metabolic activity appeared to be induced by $FePO_4$ NPs even at high concentrations and exposure times up to 48 h (Supplementary Fig. 5 (24 h), Fig. 1 and Fig.2 (48 h)). Exposure of HCECs to $FePO_4$ 27 led to significant membrane damage (Fig. 1f) and reduction in metabolic activity (Fig. 2f) after 48 h but not after 24 h (Supplementary Fig. 5). All $FePO_4$ particles tested in this study had the same chemical composition and structure. Thus the susceptibility of HCECs towards $FePO_4$ 27 could be related to the different production method, the primary particle size or the agglomerate size. The

FSP-produced $FePO_4$ NPs had a calculated primary diameter of 11 nm ($FePO_4$ 188) and 22 nm ($FePO_4$ 188); however, once suspended in cell culture medium containing serum, both formed agglomerates with a diameter of around 200-300 nm. The larger $FePO_4$ 27 formed agglomerates in suspension with a diameter of 600-700 nm (Supplementary Fig. 3). Since both FSP-produced $FePO_4$ NPs had no impact on cell viability, it seems unlikely that the primary particle size is of direct relevance. It is well known, however, that agglomerate size and density are related to the settling behavior and the effective amount of NPs that come in contact with cells[34]. The larger agglomerates of $FePO_4$ 27 may sediment faster in the cell culture well, resulting in a higher effective concentration of $FePO_4$ 27 compared to the FSP-produced NPs with a smaller agglomerate size, aggravating their biological impact.

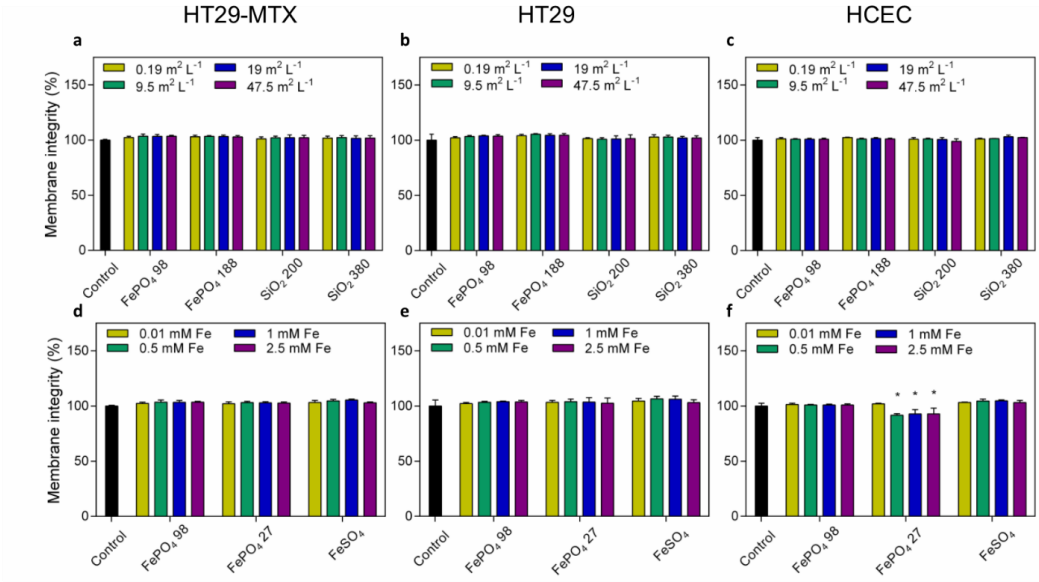

Figure 1. Membrane integrity of intestinal cell lines upon exposure to increasing concentrations of $FePO_4$ NPs for 48 h. a-f) *Membrane integrity of HT29-MTX, HT29 and HCEC cells after exposure to $FePO_4$ NPs. Cells were exposed to equivalent concentrations of **a-c)** SiO_2 NPs to control for the effect of non-dissolvable NPs (concentrations were standardized on SSA) and to **d-f)** larger $FePO_4$ 27 and $FeSO_4$ (concentrations were standardized on molar concentrations of Fe). Results are expressed as mean ± s.d. % metabolic activity relative to untreated cells. Data are from three independent experiments with three technical replicates. Significant differences to untreated control cells were determined with a two way ANOVA and Bonferroni correction, P<0.05, and are indicated by *.*

A small reduction in cell viability was only observed in HCECs upon exposure to $FePO_4$ 27, but not in HT29 and HT29-MTX cells. The difference in cellular responses may be related to the fact that HT29 and HT29-MTX cells are cancer-derived, while HCECs were established from noncancerous tissue. Previous studies have also shown that cancer cells are more resistant to particle-mediated toxicity than non-malignant cells[35]. Under the conditions tested, no influence on metabolic activity or membrane integrity was observed for any of the cell lines exposed to SiO_2 NPs. These observations are in line with previous studies regarding the effect of SiO_2 NPs on intestinal cells under similar exposure conditions[13-15].

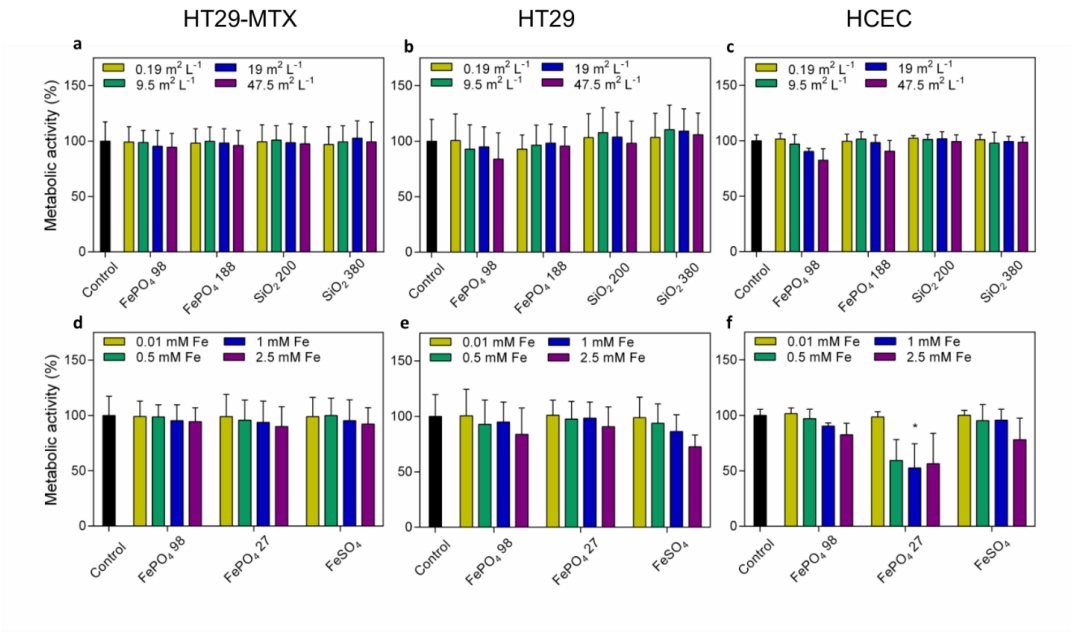

Figure 2. Metabolic activity of intestinal cell lines upon exposure to increasing concentrations of $FePO_4$ NPs for 48 h. a-f) *Metabolic activity of HT29-MTX, HT29 and HCEC cells after exposure to $FePO_4$ NPs. Cells were exposed to equivalent concentrations of* ***a-c)*** *SiO_2 NPs to control for the effect of non-dissolvable NPs (concentrations were standardized on SSA) and to* ***d-f)*** *$FePO_4$ 27 and $FeSO_4$ (concentrations were standardized on molar concentrations of Fe). Results are expressed as mean ± s.d. % metabolic activity relative to untreated cells. Data are from three independent experiments with three technical replicates. Significant differences to untreated control cells were determined with a two way ANOVA and Bonferroni correction, P<0.05, and are indicated by *.*

Oxidative stress is one of the major mechanisms by which NPs are proposed to damage cells[36,37]. Especially iron containing compounds can catalyze the formation of free radicals via the Fenton and Haber-Weiss reactions[38]. We therefore assessed the potential of the $FePO_4$ NPs to induce oxidative stress in

human cell lines by measuring intracellular levels of glutathione (GSH). The tripeptide GSH is a potent and highly abundant free-radical scavenger largely responsible for maintaining cellular redox status and thus protecting cells from oxidative damage[39]. Treatment of the cells with the control compound diethyl maleate (DEM), a GSH scavenger, led to a marked reduction in GSH content (Supplementary Fig. 6). Even though DEM levels were adjusted for each cell line and exposure time, HCECs died after treatment for 6 or 24 h and HT29 and HT29-MTX cells after DEM exposure for 24 h. After short-term (2 h and 6 h) or long-term (24 h) exposure to $FePO_4$ NPs and SiO_2 NPs, no changes in GSH levels were observed in the intestinal cell lines (Supplementary Fig. 6) providing no evidence for the induction of oxidative stress.

During NP-induced oxidative stress, the GSH concentration is expected to decrease, as was observed for HepG2, A549 and A431 cells exposed to Fe_3O_4 NPs[40,41]. Similarly to our results, exposure of primary rat hepatocytes and IMR-90 cells to Fe_3O_4 NPs did not affect GSH levels[40]. Three and 24 h exposure of HT29 cells to 40 and 200 nm SiO_2 NPs did not induce changes in GSH levels, whereas 24 h exposure of HT29 cells to the same SiO_2 NPs as tested in this study led to a 160 % increase in GSH[13]. The dose in that study was slightly higher (500 µg ml^{-1}), but the cell culture media and the assay to measure GSH were very similar to our experiments. The cell confluency during the assay may however explain the observed difference. We exposed cells to the NPs in their exponential growth period while in the previous study cells were approximately 80% confluent when exposed to the NPs[13].

Dietary NP administration to rats

We characterized the impact of sub-chronic dietary exposure to $FePO_4$ NPs in rats. Weanling Sprague-Dawley rats were exposed to $FePO_4$ NPs or control compounds ($FePO_4$ 27, $FeSO_4$ and SiO_2 200) (Fig. 3a) for 90 days (Supplementary Fig. 7). The compounds were incorporated into the diet to simulate the intended route of exposure for food fortification applications. Each compound was delivered at two doses, a low (L) (35 mg Fe kg^{-1} diet) or high (H) dose (350 mg Fe kg^{-1} diet). The low dose was equal to the normal amount of iron in the standard rodent AIN-93G diet.[25] The high dose corresponded to the lowest observable adverse effect level (LOAEL) of $FeSO_4$ previously found after administering $FeSO_4$ to rats in the drinking water for 1 and 4 months[26]. The silica diets contained either 35 or 350 mg Si kg^{-1} diet and 35 mg Fe kg^{-1} diet in the form of $FeSO_4$.

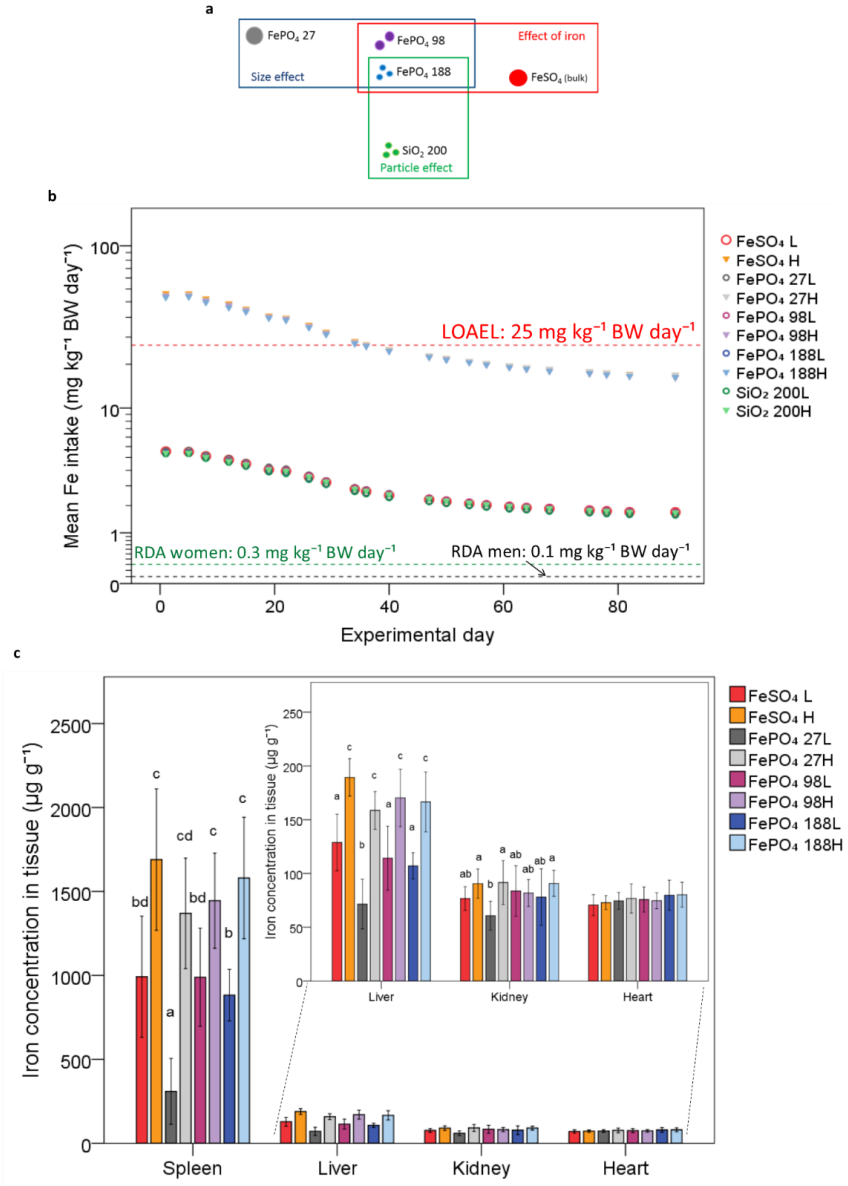

Figure 3. Iron intake during sub-chronic exposure of experimental animals to diets containing $FePO_4$ NPs and iron concentration in tissue upon sacrifice. a) *Compounds used for in vivo study.* ***b)*** *The average iron intake kg^{-1} BW day^{-1} (on a log scale) was estimated based on the body weight and food intake. Non visible error bars are too small to be seen. BW = body weight, LOAEL = lowest observable adverse effect level of $FeSO_4$ in rats, RDA = Recommended Dietary Allowance for humans.* ***c)*** *Total iron concentration in spleen, liver, kidney and heart. n=12 rats per group, except $FePO_4$ 98L n=11. Data points represent mean ± s.d., statistical significance was determined with a two way ANOVA and Bonferroni correction, P<0.05. Bars without a common letter (a, b, c or d) are statistically different.*

The test compounds were administered in the diet at constant concentrations of 35 or 350 mg Fe kg^{-1} diet. The body weight of the rats increased from the start of the study (21 days old) until they were sacrificed after 90 days of study (111 days old) with no apparent differences amongst the feeding groups (Supplementary Fig. 8a). Furthermore, there were no observed differences in food intake amongst groups (Supplementary Fig. 8b). By the time of sacrifice after 90 days of study (111 days old), the animals were on average 544±50 g, about 150 g heavier than anticipated for 105 days-old Sprague Dawley rats[42]. This high weight may have been due to the free access to food and housing in single cages, reducing physical activity[43]. In terms of food intake and body weight, the average iron intake per kg body weight per day ranged from 1.6±0.1 to 5.0±0.1 mg Fe kg^{-1} body weight day^{-1} in the low dose groups and from 16.0±0.3 to 50.0±1.0mg Fe kg^{-1} body weight day^{-1} in the high dose groups, both decreasing as the animals grew over the period of the study (Fig. 3b). At the beginning of the study consumption of iron exceeded the LOAEL for $FeSO_4$ (25 mg Fe kg^{-1} body weight day^{-1}) by up to 25 mg Fe kg^{-1} body weight day^{-1} for the high dose. After 36 days (mid study) intake was equal to the LOAEL and at the end of the study intake decreased to 15 mg Fe kg^{-1} body weight day^{-1}, 10 mg Fe kg^{-1} body weight day^{-1} lower than the LOAEL. The average iron intake was 28.0±0.4 mg Fe kg^{-1} body weight day^{-1}, exceeding the previously reported LOAEL by 3 mg Fe kg^{-1} body weight day^{-1}. The average iron intake was approximately 100 times higher than the recommended dietary allowances (RDA) for humans of 0.1 and 0.3 mg Fe kg^{-1} body weight day^{-1} for men and women, respectively[44].

Potential accumulation of iron in selected organs was studied by measuring the total iron concentration in spleen, liver, kidney and heart upon sacrifice (90 days). The highest iron concentrations were found in the spleen, followed by liver, kidney and heart (Fig. 3c). Iron levels in the spleen were significantly lower in animals fed $FePO_4$ 27L compared to all other groups. Animals receiving diets containing a low dose of iron had significantly lower spleen iron concentrations compared to groups receiving the same compound at high dose. Total liver iron concentration was significantly lower in animals fed $FePO_4$ 27L compared to all other groups and all low-dose groups had significantly lower liver iron concentrations compared to the group receiving the same compound at high-dose. In the kidney, iron concentration for animals fed $FePO_4$ 27L was significantly lower than all high dose groups except those fed $FePO_4$ 98H. No significant differences in iron concentrations in the heart were observed amongst groups. The lower levels of iron in the liver and spleen of animals fed $FePO_4$ 27L indicate smaller iron stores in these animals, potentially related to the lower bioavailability of iron from larger $FePO_4$ particles[2]. Elevated tissue iron concentration in high dose groups confirmed that iron loading through increased dietary iron intake leads to iron accumulation in the liver and spleen[45]. Nevertheless, we did not observe any difference

between the groups receiving iron in the form of NPs or $FeSO_4$, suggesting that iron derived from NPs is stored and deposited in the body like iron from $FeSO_4$.

In animals fed diets containing SiO_2 NPs, potential silicon accumulation was studied by measuring total silicon concentration in spleen, liver, kidney and heart upon sacrifice (90 days) (Supplementary Fig. 9). Silicon concentrations in organs from control animals fed $FeSO_4$ L were below the limit of quantification (10.2±4.7 µg Si g^{-1} tissue). Low tissue levels of silicon were detected in animals fed SiO_2 NPs, but no differences were observed between animals fed SiO_2 200L or SiO_2 200H, indicating that silicon can be taken up from diets containing SiO_2 NPs and can be distributed systemically as was shown previously[23].

To further characterize the iron status of the animals, we measured the number of red blood cells (RBCs), hemoglobin (Hb), hematocrit (Hct) mean corpuscular volume (MCV), mean corpuscular hemoglobin (MCH), total iron binding capacity (TIBC), plasma iron (PI) and transferrin saturation (TSAT) after 45 and 90 days. At both time points, the $FePO_4$ NPs groups did not differ from the group receiving $FeSO_4$ L in any of the measured parameters (Supplementary Table 2) and all hematological parameters were within the normal range in all animals. After 45 days, only the group fed $FePO_4$ 27L differed significantly from the group receiving $FeSO_4$ L, as noted by significantly decreased Hb, MCV, MCH and TSAT levels. Also after 90 days, the levels of Hb, MCV and MCH in the group fed $FePO_4$ 27L were still significantly lower compared to the group receiving $FeSO_4$ L. These findings further corroborate the hypothesis that iron from $FePO_4$ 27 is less bioavailable compared to $FeSO_4$ and the $FePO_4$ NPs.

We assessed the potential of the $FePO_4$ and SiO_2 NPs to cause systemic or local oxidative stress by measuring levels of GSH in RBCs, in the gastrointestinal mucosa and in the liver. All GSH concentrations were very similar to previously reported GSH values in healthy rats[46-48] and there were no differences in GSH concentrations amongst the diet groups (Fig. 4), providing no evidence for induction of oxidative stress. We also investigated potential oxidative DNA damage by quantifying 8-oxo-7,8-dihydro-2′-deoxyguanosine (8-oxo-dG) in the gastrointestinal mucosa and liver. 8-oxo-dG is one of the most common free-radical-induced oxidative DNA lesions, it is highly mutagenic and a biomarker for oxidative stress[49]. Overall, the 8-oxo-dG levels ranged from 17±6 to 23±9 lesions per 10^6 dG and from 10±6 to 20±11 lesions per 10^6 dG in the liver and the gastrointestinal mucosa, respectively (Fig. 4d).

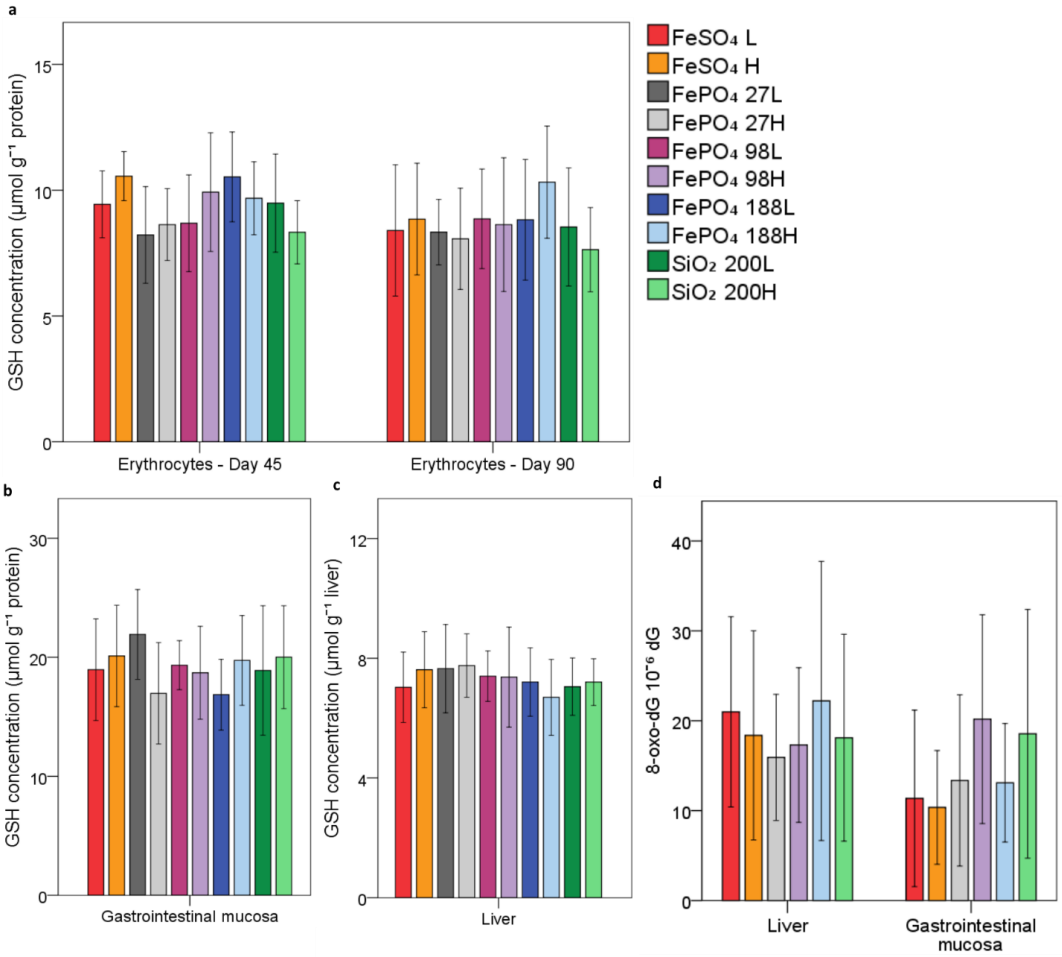

Figure 4. Levels of total glutathione (GSH) and oxidative DNA damage (8-oxo-dG). a) *GSH levels in the erythrocytes after 45 and 90 days.* ***b)*** *GSH levels in the gastrointestinal mucosa.* ***c)*** *GSH levels in the liver.* ***d)*** *Levels of 8-oxo-dG in gastrointestinal mucosa and liver. Bars represent mean ± s.d., statistical significance was determined with a two way ANOVA and Bonferroni correction, P<0.05. For a, b and c) n=12 rats per group, except $FePO_4$ 98L n=11, for d) liver: n=6, gastrointestinal mucosa: n=12 rats per group.*

No differences in 8-oxo-dG levels amongst the treatment groups were observed, providing no evidence for the induction of oxidative damage by $FePO_4$ NPs. These observations are consistent with data from a study in which similarly high $FeSO_4$ intakes did not impact lipid peroxidation, activity of superoxide dismutase, glutathione peroxidase and glutathione S-transferase in the colonic mucosa of rats[50]. In contrast, administration of similar doses of $FeSO_4$ via the diet increased malondialdehyde levels in spleen and gut, induced catalase activity in gut tissue, and decreased glutathione S-transferase activity in spleen and gut[51]. However, those rats were already 15 months old in the beginning of the study and older animals

are generally more susceptible to oxidative stress compared to young animals. In the case of $FeSO_4$ administration in the drinking water, similar $FeSO_4$ intakes were linked to increased lipid peroxidation and reduced GSH levels in the liver and gastrointestinal mucosa of rats[26]. In the water the iron was most likely present as highly reactive Fe^{2+} ions and thus causing oxidative stress. Such damages may not occur during iron administration in solid food containing chelators that might reduce direct toxicity to gastrointestinal mucosa and decrease iron bioavailability[52], resulting in lower liver toxicity.

We further quantified changes in plasma concentrations of alkaline phosphatase (ALP), alanine aminotransferase (ALAT), aspartate aminotransferase (ASAT) and ɣ-glutamyl transferase to assess potential liver damage. Plasma concentrations of urea, creatinine, and uric acid were quantified to estimate potential kidney damage. After 45 and also 90 days, no differences in any of these biomarkers among the different diet groups were observed. This suggests $FePO_4$ NPs do not induce liver or kidney damage (Supplementary Table 3). It was surprising not to find an effect after 45 days because in the high dose groups the administered dose was well above 25 mg Fe kg^{-1} body weight day^{-1}, and administration of the same amount of iron as $FeSO_4$ was reported to increase ALAT, ASAT and ALP levels[26]. As mentioned previously in the context of induction of oxidative stress, this discrepancy might be attributed to the administration via drinking water instead of solid food.

After the sacrifice, histological analysis of organs and tissues was performed and stains for Fe^{2+} and Fe^{3+} were used to assess iron deposition. All tissues stained negatively for Turnbull blue (for Fe^{2+}), while mild positive Prussian blue staining (for Fe^{3+}) was observed in all tissues except heart, brain and testis. The incidence of staining was not influenced by the dose or the composition of the iron compound. The only observed difference in the high dose groups compared to the group receiving $FeSO_4$ L was increased positive iron staining of enterocytes and in cells (macrophages and fibrocytes) of the lamina propria mucosae in the duodenum and the colon (Supplementary Fig. 10 and Supplementary Fig. 11). Despite these apparent iron depositions, no abnormal histological changes were detected.

Conclusions

Food fortification with highly bioavailable $FePO_4$ NPs could play an important role in combatting ID, but safety concerns arising from their small size limit their use. We tested the potential of two $FePO_4$ NPs to induce adverse effects both *in vivo* and in three different gastrointestinal cell lines. The $FePO_4$ NPs did not induce direct toxicity or oxidative stress in human gastrointestinal cell lines regardless of the presence of mucus or the transformational state of the cells. Furthermore, administration of diets enriched with $FePO_4$ NPs – at a dose recommended for laboratory rodents or at a dose at which $FeSO_4$ previously

induced adverse effects – did not lead to any toxicologically relevant adverse outcomes or accumulation of tissue iron. This is the first investigation of the influence of sub-chronic *in vivo* exposure to $FePO_4$ NPs and relation with responses of human cells. The data suggest $FePO_4$ NPs are at least as safe for human consumption as $FeSO_4$, because administration of $FePO_4$ NPs at doses that were approximately 100 times higher than the RDA of iron for women did not result in adverse outcomes. Therefore, these $FePO_4$ NPs and potentially other nanosized minerals should be further explored as food fortificants and supplements.

Acknowledgements

The authors would like to thank F. Krumeich and S. Handschin (ETH Zurich) for performing TEM on some particles and cells, V. Galetti (ETH Zurich) for support with statistical analysis, C. Zeder, P. Rast, L. Posavec, C. Wellenzohn, R. Govender (ETH Zurich), G. Pellegrini, E.M. Schraner, S. Kitz (UZH-Vetsuisse) and Albert Schuler (PSI) for their technical assistance, Evonik for providing the silica particles, Prof. S. Pratsinis for helpful discussions and the Swiss National Science Foundation (Project No. SNF 406440_141610 and CRSII3_136247/2) for funding.

Author contributions

L.v.M., I.T., F.H., M.Z. and S.S. conceived and designed the experiments. L.v.M, M.S. carried out the experiments and analyzed the data. M.A. and W.L. contributed to the animal experiments. M.H. performed the histological analysis. D.S.M., M.T. and C.L. performed the iron and silica analysis. N.Z. contributed to the 8-oxo-dG quantification. H.W. performed TEM analysis of NP and NP uptake by cells. L.v.M, I.T and S.S. wrote the manuscript. All authors contributed to writing and approved the manuscript.

Competing financial interests

The authors declare no competing financial interests.

References

1 Hilty, F. M. *et al.* Iron from nanocompounds containing iron and zinc is highly bioavailable in rats without tissue accumulation. *Nat. Nanotechnol.* **5**, 374-380, doi:10.1038/nnano.2010.79 (2010).

2 Rohner, F. *et al.* Synthesis, characterization, and bioavailability in rats of ferric phosphate nanoparticles. *Journal of Nutrition* **137**, 614-619 (2007).

3 Erfanian, A., Mirhosseini, H., Abd Manap, M. Y., Rasti, B. & Bejo, M. H. Influence of nano-size reduction on absorption and bioavailability of calcium from fortified milk powder in rats. *Food Research International* **66**, 1-11, doi:10.1016/j.foodres.2014.08.026 (2014).

4 Wang, J. X. *et al.* Acute toxicity and biodistribution of different sized titanium dioxide particles in mice after oral administration. *Toxicol. Lett.* **168**, 176-185, doi:10.1016/j.toxlet.2006.12.001 (2007).

5 Mahler, G. J. *et al.* Oral exposure to polystyrene nanoparticles affects iron absorption. *Nat. Nanotechnol.* **7**, 264-U1500, doi:10.1038/nnano.2012.3 (2012).

6 WHO. Guidelines on food fortification with micronutrients. (2006).

7 Baltussen, R., Knai, C. & Sharan, M. Iron fortification and iron supplementation are cost-effective interventions to reduce iron deficiency in four subregions of the world. *Journal of Nutrition* **134**, 2678-2684 (2004).

8 Hurrell, R. F. Fortification: Overcoming technical and practical barriers. *Journal of Nutrition* **132**, 806S-812S (2002).

9 Wegmuller, R. *et al.* Particle size reduction and encapsulation affect the bioavailability of ferric pyrophosphate in rats. *Journal of Nutrition* **134**, 3301-3304 (2004).

10 Swain, J. H., Newman, S. M. & Hunt, J. R. Bioavailability of elemental iron powders to rats is less than bakery-grade ferrous sulfate and predicted by iron solubility and particle surface area. *Journal of Nutrition* **133**, 3546-3552 (2003).

11 Hilty, F. M. *et al.* Incorporation of Mg and Ca into Nanostructured Fe2O3 Improves Fe Solubility in Dilute Acid and Sensory Characteristics in Foods. *J. Food Sci.* **76**, N2-N10, doi:10.1111/j.1750-3841.2010.01885.x (2011).

12 Hilty, F. M. *et al.* Development and optimization of iron- and zinc-containing nanostructured powders for nutritional applications. *Nanotechnology* **20**, doi:10.1088/0957-4484/20/47/475101 (2009).

13 Gehrke, H. *et al.* In vitro toxicity of amorphous silica nanoparticles in human colon carcinoma cells. *Nanotoxicology* **7**, 274-293, doi:10.3109/17435390.2011.652207 (2013).

14 Schubbe, S. *et al.* Size-Dependent Localization and Quantitative Evaluation of the Intracellular Migration of Silica Nanoparticles in Caco-2 Cells. *Chem. Mat.* **24**, 914-923, doi:10.1021/cm2018532 (2012).

15 McCracken, C., Zane, A., Knight, D. A., Dutta, P. K. & Waldman, W. J. Minimal Intestinal Epithelial Cell Toxicity in Response to Short- and Long-Term Food-Relevant Inorganic Nanoparticle Exposure. *Chem. Res. Toxicol.* **26**, 1514-1525, doi:10.1021/tx400231u (2013).

16 Mu, Q. *et al.* Mechanism of cellular uptake of genotoxic silica nanoparticles. *Particle and Fibre Toxicology* **9**, doi:10.1186/1743-8977-9-29 (2012).

17 Gerloff, K., Albrecht, C., Boots, A. W., Foerster, I. & Schins, R. P. F. Cytotoxicity and oxidative DNA damage by nanoparticles in human intestinal Caco-2 cells. *Nanotoxicology* **3**, 355-364, doi:10.3109/17435390903276933 (2009).

18 Trouiller, B., Reliene, R., Westbrook, A., Solaimani, P. & Schiestl, R. H. Titanium Dioxide Nanoparticles Induce DNA Damage and Genetic Instability In vivo in Mice. *Cancer Research* **69**, 8784-8789, doi:10.1158/0008-5472.can-09-2496 (2009).

19 Shukla, R. K., Kumar, A., Vallabani, N. V. S., Pandey, A. K. & Dhawan, A. Titanium dioxide nanoparticle-induced oxidative stress triggers DNA damage and hepatic injury in mice. *Nanomedicine* **9**, 1423-1434, doi:10.2217/nnm.13.100 (2014).

20 Sharma, V., Singh, P., Pandey, A. K. & Dhawan, A. Induction of oxidative stress, DNA damage and apoptosis in mouse liver after sub-acute oral exposure to zinc oxide nanoparticles. *Mutation Research/Genetic Toxicology and Environmental Mutagenesis* **745**, 84-91, doi:http://dx.doi.org/10.1016/j.mrgentox.2011.12.009 (2012).

21 Park, E. J. *et al.* A 13-week repeated-dose oral toxicity and bioaccumulation of aluminum oxide nanoparticles in mice. *Archives of Toxicology* **89**, 371-379, doi:10.1007/s00204-014-1256-0 (2015).

22 Yun, J. W. *et al.* Comparative toxicity of silicon dioxide, silver and iron oxide nanoparticles after repeated oral administration to rats. *Journal of Applied Toxicology* **35**, 681-693, doi:10.1002/jat.3125 (2015).

23 van der Zande, M. *et al.* Sub-chronic toxicity study in rats orally exposed to nanostructured silica. *Particle and Fibre Toxicology* **11**, 19, doi:10.1186/1743-8977-11-8 (2014).

24 Srinivasu, B. Y. *et al.* Beneficiary effect of nanosizing ferric pyrophosphate as food fortificant in iron deficiency anemia: evaluation of bioavailability, toxicity and plasma biomarker. *RSC Adv.* **5**, 61678-61687, doi:10.1039/c5ra07724a (2015).

25 Reeves, P. G., Nielsen, F. H. & Fahey Jr, G. C. AIN-93 purified diets for laboratory rodents: Final report of the American Institute of Nutrition ad hoc writing committee on the reformulation of the AIN-76A rodent diet. *Journal of Nutrition* **123**, 1939-1951 (1993).

26 Toblli, J. E., Cao, G., Olivieri, L. & Angerosa, M. Comparative study of gastrointestinal tract and liver toxicity of ferrous sulfate, iron amino chelate and iron polymaltose complex in normal rats. *Pharmacology* **82**, 127-137, doi:10.1159/000142728 (2008).

27 Strobel, R. & Pratsinis, S. E. Flame aerosol synthesis of smart nanostructured materials. *Journal of Materials Chemistry* **17**, 4743-4756, doi:10.1039/b711652g (2007).

28 Wegner, K. & Pratsinis, S. E. Scale-up of nanoparticle synthesis in diffusion flame reactors. *Chem. Eng. Sci.* **58**, 4581-4589, doi:http://dx.doi.org/10.1016/j.ces.2003.07.010 (2003).

29 Behrens, I., Stenberg, P., Artursson, P. & Kissel, T. Transport of lipophilic drug molecules in a new mucus-secreting cell culture model based on HT29-MTX cells. *Pharm. Res.* **18**, 1138-1145, doi:10.1023/a:1010974909998 (2001).

30 Roig, A. I. *et al.* Immortalized epithelial cells derived from human colon biopsies express stem cell markers and differentiate in vitro. *Gastroenterology* **138**, 1012-1021 e1011-1015, doi:10.1053/j.gastro.2009.11.052 (2010).

31 Constantinescu, S. *et al.* Transcriptomic Responses of Cancerous and Noncancerous Human Colon Cells to Sulforaphane and Selenium. *Chem. Res. Toxicol.* **27**, 377-386, doi:10.1021/tx400427t (2014).

32 Docter, D. *et al.* The protein corona protects against size- and dose-dependent toxicity of amorphous silica nanoparticles. *Beilstein Journal of Nanotechnology* **5**, 1380-1392, doi:10.3762/bjnano.5.151 (2014).

33 Jahn, M. R. *et al.* Iron Oxide/Hydroxide Nanoparticles with Negatively Charged Shells Show Increased Uptake in Caco-2 Cells. *Mol. Pharm.* **9**, 1628-1637, doi:10.1021/mp200628u (2012).

34 Cohen, J. M., Teeguarden, J. G. & Demokritou, P. An integrated approach for the in vitro dosimetry of engineered nanomaterials. *Part Fibre Toxicol* **11**, 20, doi:10.1186/1743-8977-11-20 (2014).

35 Nan, A. J., Bai, X., Son, S. J., Lee, S. B. & Ghandehari, H. Cellular uptake and cytotoxicity of silica nanotubes. *Nano Lett.* **8**, 2150-2154, doi:10.1021/nl0802741 (2008).

36 Nel, A., Xia, T., Madler, L. & Li, N. Toxic potential of materials at the nanolevel. *Science* **311**, 622-627, doi:10.1126/science.1114397 (2006).

37 Oberdorster, G., Oberdorster, E. & Oberdorster, J. Nanotoxicology: An emerging discipline evolving from studies of ultrafine particles. *Environmental Health Perspectives* **113**, 823-839, doi:10.1289/ehp.7339 (2005).

38 Kehrer, J. P. The Haber-Weiss reaction and mechanisms of toxicity. *Toxicology* **149**, 43-50, doi:10.1016/s0300-483x(00)00231-6 (2000).

39 Kosower, N. S. & Kosower, E. M. The glutathione status of cells. *International review of cytology* **54**, 109-160, doi:10.1016/s0074-7696(08)60166-7 (1978).

40 Ahamed, M., Alhadlaq, H. A., Khan, M. A. M. & Akhtar, M. J. Selective killing of cancer cells by iron oxide nanoparticles mediated through reactive oxygen species via p53 pathway. *Journal of Nanoparticle Research* **15**, doi:10.1007/s11051-012-1225-6 (2013).

41 Ahamed, M. *et al.* Iron Oxide Nanoparticle-induced Oxidative Stress and Genotoxicity in Human Skin Epithelial and Lung Epithelial Cell Lines. *Current Pharmaceutical Design* **19**, 6681-6690 (2013).

42 Charles River. *Sprague Dawley® Rat* <http://www.criver.com/products-services/basic-research/find-a-model/sprague-dawley-rat> (

43 Spangenberg, E. M. F., Augustsson, H., Dahlborn, K., Essen-Gustavsson, B. & Cvek, K. Housing-related activity in rats: effects on body weight, urinary corticosterone levels, muscle properties and performance. *Laboratory Animals* **39**, 45-57, doi:10.1258/0023677052886457 (2005).

44 Institute of Medicine. *Dietary reference intakes for vitamin A, vitamin K, arsenic, boron, chromium, copper, iodine, iron, manganese, molybdenum, nickel, silicon, vanadium, and zinc*. (National Academy Press, 2001).

45 Papanastasiou, D. A., Vayenas, D. V., Vassilopoulos, A. & Repanti, M. Concentration of iron and distribution of iron and transferrin after experimental iron overload in rat tissues in vivo: Study of the liver, the spleen, the central nervous system and other organs. *Pathol. Res. Pract.* **196**, 47-54 (2000).

46 Giustarini, D., Dalle-Donne, I., Milzani, A., Fanti, P. & Rossi, R. Analysis of GSH and GSSG after derivatization with N-ethylmaleimide. *Nature Protocols* **8**, 1660-1669, doi:10.1038/nprot.2013.095 (2013).

47 Jonas, C. R. *et al.* Keratinocyte growth factor enhances glutathione redox state in rat intestinal mucosa during nutritional repletion. *Journal of Nutrition* **129**, 1278-1284 (1999).

48 Oztasan, N. *et al.* Endurance training attenuates exercise-induced oxidative stress in erythrocytes in rat. *Eur. J. Appl. Physiol.* **91**, 622-627, doi:10.1007/s00421-003-1029-6 (2004).

49 Kasai, H. Analysis of a form of oxidative DNA damage, 8-hydroxy-2 '-deoxyguanosine, as a marker of cellular oxidative stress during carcinogenesis. *Mutat. Res.-Rev. Mutat. Res.* **387**, 147-163, doi:10.1016/s1383-5742(97)00035-5 (1997).

50 Soyars, K. E. & Fischer, J. G. Iron supplementation does not affect cell proliferation or aberrant crypt foci development in the colon of Sprague-Dawley rats. *Journal of Nutrition* **128**, 764-770 (1998).

51 Arruda, L. F., Arruda, S. F., Campos, N. A., de Valencia, F. F. & Siqueira, E. M. D. Dietary Iron Concentration May Influence Aging Process by Altering Oxidative Stress in Tissues of Adult Rats. *Plos One* **8**, 12, doi:10.1371/journal.pone.0061058 (2013).

52 Cook, J. D. Diagnosis and management of iron-deficiency anaemia. *Best Pract. Res. Clin. Haematol.* **18**, 319-332, doi:10.1016/j.beha.2004.08.022 (2005).

Methods

Materials: Iron phosphate nanoparticles with a specific surface area (SSA) of 188 $m^2 g^{-1}$ ($FePO_4$ 188) and 98 $m^2 g^{-1}$ ($FePO_4$ 98) were produced by flame spray pyrolysis (FSP) as previously described[1] with some adaptations. Iron nitrate nonahydrate (purity. ≥97.0%, Riedel-de-Haën/Sigma-Aldrich), and tributyl phosphate (purity 97%; Sigma-Aldrich), were dissolved in a 1:1 mixture by volume of ethanol (denat. 2% 2-butanone, Alcosuisse) and 2-ethylhexanoic acid (purity ≥99%; Sigma-Aldrich) at a total metal concentration of 0.4 mol L^{-1} or 0.5 mol L^{-1} for $FePO_4$ 188 and $FePO_4$ 98, respectively. This precursor solution was fed at 3 or 7 mL min^{-1} into the FSP spray nozzles by a syringe pump (Lambda, VIT-FIT) and atomized by co-flowing 5 or 7 L min^{-1} of oxygen (purity ≥99.5%; Pangas) at 1.5-1.6 bar pressure drop. The spray was ignited by a methane/oxygen (2.5 L min^{-1}) ring-shaped flame[2]. Using a vacuum pump (Busch, Mink MM1202 AV), product particles were collected on water-cooled Teflon membrane-filters (1TMTF700WHT, BHA Technologies AG) placed at least 65 cm above the burner. Ferric phosphate fine powder (no: 505033003) with SSA of 27 $m^2 g^{-1}$ ($FePO_4$ 27) and dried ferrous sulphate ($FeSO_4$) (no: 501022005480) were purchased from Dr. Paul Lohmann GmbH. Nanostructured fumed silica with SSA of 200 $m^2 g^{-1}$ (SiO_2 200) and 380 $m^2 g^{-1}$ (SiO_2 380) were kindly provided by Evonik Industries (AEROSIL® 200 F and AEROSIL® 380 F, Evonik Industries).

Nanoparticle characterization: SSA was determined by N_2-adsorption (Micromeritics Tristar 3000, Micromeritics Instruments Corp) at 77 K in the relative pressure range p/p0=0.05-0.25 and calculated using Brunauer-Emmett-Teller (BET) theory. Assuming dense spherical particles, the particle diameter (d_{BET}) was calculated from the measured SSA according to $d_{BET} = 6/(\rho \cdot SSA)$, where ρ is the solid particle density ($FePO_4*2H_2O$= 2.87 g cm^{-3})[3]. The crystallinity of the NP powders was investigated by X-ray diffraction (XRD) on a Bruker AXS D8 Advance diffractometer operating with a Cu Kα radiation. For transmission electron microscopy (TEM) analysis, the NPs were dispersed in ethanol or ddH_2O, deposited on a carbon or parlodion foil supported on a copper grid and analyzed on a CM30ST microscope (FEI; LaB6 cathode, operated at 300 kV, point resolution~2 A°) or a CM12 microscope (FEI, operated at an acceleration voltage of 100 kV).

Cell culture: HT29 were obtained from the Leibnitz-Institut DSMZ GmbH (DSMZ ACC299) and HT29-MTX cells were purchased from Culture Collections, UK (ECACC 12040401). Both cell lines were maintained in Dulbecco's Modified Eagle Medium GlutaMax (DMEM) with 10% Fetal Bovine Serum (FBS) (v/v) plus 100 U mL^{-1} Penicillin and 100 µg mL^{-1} Streptomycin (DMEM+; all from Gibco, Life Technologies). HCECs were obtained from Prof. Jerry Shay (University of Texas Southwestern Medical Center, Dallas, Texas, USA) and

cultured under previously reported conditions[4]. All cell lines were incubated at 37 °C in a humidified atmosphere with 5% CO_2. Cell lines were routinely tested for mycoplasma contamination.

Preparation of nanoparticle suspensions: Stock suspensions of $FePO_4$ NPs, SiO_2 NPs and $FeSO_4$ were prepared either in ultrapure water (18.2 MΩ·cm) or in DMEM+ and dispersed by ultrasonic processing in a cup horn sonicator at 200 kJ L^{-1} (Ultrasonic Processor VCX 750, Sonics & Materials Inc.). The hydrodynamic diameter of NPs after ultrasonic processing in ultrapure water or cell culture media was determined by dynamic light scattering (DLS) on a Zetasizer Nano ZS (Malvern). For the cell experiments, dilutions of the stock suspension were prepared in DMEM+ and used for the experiments without further processing. The concentrations were standardized on 1) molar concentrations of Fe for $FePO_4$ 27, $FePO_4$ 98 and $FeSO_4$; 2) SSA for $FePO_4$ 98, $FePO_4$ 188, SiO_2 200 and SiO_2 380.

Nanoparticle uptake: Uptake of $FePO_4$ NPs into HCEC, HT29 and HT29-MTX cells was investigated qualitatively by TEM. Cells were seeded in 6-well plates (HT29 and HT29-MTX: 500000 cells/well, HCECs: 30000 cells/well) on carbon coated sapphire disks (Brügger). After 24 h, cells were exposed for 48 h to $FePO_4$ 27 (75 µg mL^{-1}), $FePO_4$ 98 (75 µg mL^{-1}) and $FePO_4$ 188 (37.5 µg mL^{-1}). Cells were washed three times with PBS and fixed with 2.5% glutaraldehyde in 0.1 M Na/K-phosphate buffer, for 1 hour at 4°C and kept overnight in 0.1 M Na/K-phosphate, postfixed with 1% osmium tetroxide in 0.1 M Na/K-phosphate buffer for 1h, dehydrated in a series of ethanol starting at 70%, and after transferring into acetone embedded in epon followed by polymerization at 60°C for 2.5 days. Sections of 60 to 80 nm thickness sections were stained with uranyl acetate and lead citrate as described in[5] and examined in a transmission electron microscope (CM12, FEI) equipped with a CCD camera (Ultrascan 1000, Gatan) at an acceleration voltage of 100 kV. Digital micrograph (Gatan) was used for image acquisition.

Cell membrane integrity: To determine the extent of damage to the cell membrane, the amount of lactate dehydrogenase (LDH) released into the culture supernatant was determined. Cells were seeded in 96-well plates (3000 cells/well). After 24 h, cells were exposed to $FePO_4$ NPs, SiO_2 NPs and $FeSO_4$ suspensions ($FePO_4$ 27, $FePO_4$ 98 and $FeSO_4$: 0.01, 0.5, 1 and 2.5 mM Fe; $FePO_4$ 98, $FePO_4$ 188, SiO_2 200 and SiO_2 380: 0.19, 9.5, 19 and 47.5 m^2 L^{-1}). After 24 h or 48 h exposure, the LDH release was assessed using the Cytotoxicity Detection Kit for LDH (Roche Diagnostics AG) according to the manufacturer's protocol. 50 µl of supernatant were transferred to a new plate containing 100 µL freshly prepared reagent mix. The amount of formazan formed was determined by measuring the absorbance at 490 nm. The relative membrane integrity was expressed as:

Membrane integrity (%) = 100 – [(experimental value – low control)/(high control – low control)*100]

The low control, which refers to spontaneous LDH release, was determined as the LDH released from untreated cells. The high control, which refers to the maximum LDH release, was determined as LDH released from cells treated with the surfactant Triton X-100 (2%). Results are expressed as mean ± s.d. % membrane integrity relative to untreated cells. Each experiment was preformed independently three times with three technical replicates. Potential interference of NPs and $FeSO_4$ with the LDH assay was tested according to[6] and no interferences were found.

Metabolic activity: Metabolic activity was assessed with the MTS assay (CellTiter 96® AQueous One Solution Cell Proliferation Assay, Promega). Cells were seeded in 96-well plates (2500 cells/well). After 24 h the cell culture medium was removed and cells were exposed to $FePO_4$ NPs, SiO_2 NPs and $FeSO_4$ suspensions ($FePO_4$ 27, $FePO_4$ 98 and $FeSO_4$: 0.01, 0.5, 1 and 2.5 mM Fe; $FePO_4$ 98, $FePO_4$ 188, SiO_2 200 and SiO_2 380: 0.19, 9.5, 19 and 47.5 $m^2 L^{-1}$). After 24 h or 48 h exposure, MTS dye was added to each well and incubated for 4 h. Plates were centrifuged for 10 min at 2000 g to allow NPs to sediment. Then 60 µl of the supernatant were transferred to a new plate and absorbance was measured at 490 nm. Triton X-100 (2%) and untreated cells were used as positive and negative control, respectively. Results are expressed as mean ± s.d. % metabolic activity relative to untreated cells. Each experiment was performed independently three times with three technical replicates. Interference of the NPs with the monitoring of the bioreduction of a tetrazolium salt (MTS; 3-(4,5-dimethylthiazol-2-yl)-5-(3-carboxymethoxyphenyl)-2-(4-sulfophenyl)-2H-tetrazolium) to a formazan product (λmax 490 nm) was tested and no interferences were found.

Glutathione assay: Cells were seeded in 24-well plates (HT29 and HT29-MTX: 350000 cell/well for 2 h and 6 h exposure, 250000 cells/well for 24 h exposure; HCECs: 300000 cells/well for 2 h and 6 h exposure, 200000 cells/well for 24 h exposure). After 24 h, cells were exposed to $FePO_4$ NPs, SiO_2 NPs and $FeSO_4$ suspensions at the highest concentration used in the cell viability assays ($FePO_4$ 27, $FePO_4$ 98 and $FeSO_4$: 2.5 mM Fe; $FePO_4$ 98, $FePO_4$ 188, SiO_2 200 and SiO_2 380: 47.5 $m^2 L^{-1}$). Diethyl maleate (DEM) treated and untreated cells were used as positive and negative control, respectively. After 2 h, 6 h or 24 h, cells were collected and GSH concentration was measured by the enzymatic recycling method, as described previously[7]. Protein content was analyzed using the Pierce™ BCA Protein Assay Kit (Thermo Scientific) according to the manufacturer's protocol. Results are expressed as mean ± s.d. % GSH content relative to untreated cells. Each experiment was preformed independently three times and each sample was analyzed two times.

Animal study

Ethical approval for animal experiment: The study protocol was approved by the cantonal veterinary office of Zurich, Switzerland (authorization no. 26300).

Study outline: Three week old male Sprague-Dawley rats (n=120) (Charles River) were individually housed in stainless steel cages with grid floor in a colony room kept on a 12/12 h light-dark cycle. Twelve animals were randomly assigned to each diet group. Randomization was done according to tables with random numbers generated in EXCEL (Professional Edition, Microsoft). The number of animals per group was based on past similar studies with the same or very similar animal model[8-10]. Feed and water was provided ad libitum throughout the study. Body weight was recorded twice per week. Food intake was recorded at the beginning, around the midpoint and before the end of the study, always for a period of 10 days. After 90 days, rats were anaesthetized by CO_2 inhalation and blood was drawn by cardiac puncture. The rats were euthanized by heart incision. The organs for histopathological analyses (lung, heart, spleen, liver, kidney, stomach, pancreas, duodenum, jejunum, ileum, colon, mesenteric lymph node, brain, sternum and testis) were excised and immediately placed in 4% buffered formaldehyde.

Diets: The experimental diets were based on an iron-free AIN-93G purified rodent diet[11] fortified with either $FeSO_4$, $FePO_4$ 27, $FePO_4$ 98 or $FePO_4$ 188 at two different dose levels. The lower dose was 35 mg Fe kg^{-1} diet which corresponds to the normal iron concentration in the AIN-93G diet[11]. The high dose was aimed to correspond to the LOAEL of $FeSO_4$ in rats and was set at 350 mg Fe kg^{-1} diet. The high dose was based on a study of Toblli et al.[8] where increased oxidative stress and increased plasma levels of biomarkers for liver damage were observed in rats fed 25 mg Fe (as $FeSO_4$) kg^{-1} BW day^{-1}. Assuming an average food intake of 22 g day^{-1}, a body weight of 310 g (average weight at 10 weeks of age) and a Fe concentration of 350 mg Fe kg^{-1} diet, the daily Fe intake would be 25 mg Fe kg^{-1} body weight. To control for the effect of non-biodegradable NPs, diets containing either 35 mg Si kg^{-1} diet or 350 mg Si kg^{-1} diet were also used. In the silica diet, the iron concentration was 35 mg Fe as $FeSO_4$ kg^{-1} diet. All diets were produced by Dyets Inc. and analyzed for their iron content by atomic absorption spectroscopy (AAS) upon arrival.

Blood analysis: At the midpoint and before the sacrifice, a blood sample was drawn from the sublingual vein during light anesthesia with isoflurane. Whole blood was collected 1) in a heparinized capillary for hematological analysis and 2) on heparin for plasma separation. Plasma was separated by centrifugation and erythrocyte pellet and plasma was immediately frozen at -80 °C. The number of red blood cells, hemoglobin levels, hematocrit, mean corpuscular volume and mean corpuscular hemoglobin was

measured in whole blood using a Scil vet abc hematology analyzer (Scil Animal Care Company). The concentrations of alkaline phosphatase, alanine aminotransferase, aspartate aminotransferase, ɣ-glutamyl transferase, urea, creatinine and uric acid were measured in blood plasma using standard enzymatic and colorimetric methods adapted for the Cobas MIRA® autoanalyzer (Hoffman La Roche). Plasma iron concentration and total iron binding capacity were measured as described in[12]. Transferrin saturation was calculated as: plasma iron/TIBC*100. Investigator was blinded to the sample group allocation.

Oxidative stress: Total GSH levels in erythrocytes as well as GSH levels in gastrointestinal mucosa and in liver samples collected at sacrifice were measured by the enzymatic recycling method, as described previously[7]. Protein content was analyzed using the Pierce™ BCA Protein Assay Kit (Thermo Scientific) according to the manufacturer's protocol. Results for GSH in erythrocytes and in gastrointestinal mucosa are expressed as µmol GSH g^{-1} protein while GSH in liver was expressed as µmol GSH g^{-1} liver. The levels of the oxidative DNA lesion 8-oxo-dG in the liver and the gastrointestinal mucosa were quantified according to a previous study[13] with small adaptations. During the entire sample preparation, deferoxamine and butylated hydroxytoluene were added as antioxidants to prevent unwanted formation of 8-oxo-dG and further oxidation thereof[14]. DNA was extracted with the DNA Isolation Kit for Cells and Tissues Version 07 (Roche) according to the manufacturer's protocol except that incubation with proteinase K was done for 1 h at 65 °C and incubation with RNase solution was increased to 1 h. After protein precipitation, the samples were centrifuged at 4000 g for 30 min. DNA concentration was determined by measuring the absorbance at 260 nm with a NanoDrop ND-1000 Spectrophotometer (Thermo Fisher Scientific). Before hydrolysis, 1775 fmol [$^{15}N_5$]8-oxo-dG (Cambridge Isotopes laboratories) was added to each sample as internal standard. Hydrolysis of 50 µg DNA resulted in a final sample volume of 900 µl which was then fractionated chromatographically with HPLC. The HPLC system (Agilent Technologies 1200 Series HPLC) was equipped with a Luna C18 (2) 100Å column (4.6 mm x 250 mm, 5µm, Phenomenex) for purification of 8-oxo-dG and quantification of dG. Solvents and gradient were as previously described[13]. Retention time of 8-oxo-dG as determined by injection of a standard was around 23 min. 8-oxo-dG from the samples was collected 2 min before and 2 min after its retention time. Solvents from the collected fraction were removed by lyophilization. The sample was resuspended in 16 µL ultrapure water and 9.5 µL were injected in a nanoAcquity UPLC (Waters) coupled to a TSQ Vantage triple quadrupole mass spectrometer with ESI source (Thermo Scientific) for quantification of 8-oxo-dG and [$^{15}N_5$]8-oxo-dG. An Atlantis dC18 column (300 µm x 150 mm, 3 µm, Waters) was operated with a linear gradient from 0% acetonitrile + 0.1% formic acid (B) in water + 0.1% formic acid (A) to 9% B in 15 min,

followed by an increase to 90% B in 1 min, at a flow rate of 10µl/min. 8-oxo-dG and the internal standard were quantified as previously described[13]. Investigator was blinded to the sample group allocation.

Metal content in organs: Iron concentration in the different tissues was measured with AAS after acid-assisted digestion. Tissue samples were mineralized in a microwave system (Multiwave GO, Anton Paar) in the presence of 5 mL nitric acid (65%) and 1 mL hydrogen peroxide. After digestion, samples were diluted with water and iron concentration was measured on a SpectrAA-240FS AAS (Varian). Investigator was blinded to the sample group allocation. Silica concentrations were measured with ICP-MS following acid assisted digestion. Tissue samples were mineralized in a microwave system (Multiwave 3000, Anton Paar) in the presence of 5 mL nitric acid (65%) and 2 mL hydrogen peroxide (30%). After digestion, 0.15 mL hydrofluoric acid (48%) was added to dissolve silica, samples were further diluted in water and silica concentration was measured on an Agilent 7700x ICP-MS.

Histology: Histological analyses of lung, heart, spleen, liver, kidney, stomach, pancreas, duodenum, jejunum, ileum, colon, mesenteric lymph node, brain, sternum and testis were done in six rats of the control group ($FeSO_4$ L) and in always six animals of the high dose groups ($FeSO_4$ H, $FePO_4$ 27H, $FePO_4$ 95H, $FePO_4$ 190H and SiO_2 200H). For the analysis by light microscopy, tissues were dehydrated with xylene and a descending alcohol row, paraffin embedded and stained with haematoxylin/eosin, Prussian blue for Fe^{3+} detection and Turnbull blue for Fe^{2+} detection. The histological examination was performed in a blinded manner; the boarded pathologist was unaware of the group assignments.

Statistical analysis: Animal study: Data were processed and analyzed using IBM SPSS Statistics 23 (IBM) and EXCEL (Professional Edition, Microsoft). Values in the text are means + s.d.. For each diet group, data were tested for normal distribution using the Shapiro-Wilk test. Outliers were removed according to the Grubbs criteria with $\alpha=0.05$[15]. To compare means between the treatment groups, one-way ANOVA with Bonferroni post-hoc test was applied to correct for multiple comparisons. Differences were considered significant at $p<0.05$. Cell study: Data was analyzed with Microsoft Excel 2010 and Graph Pad Prism 6. To determine significant differences between treatments and controls, one-way ANOVA with Bonferroni post-hoc test was applied to correct for multiple comparisons. Differences were considered significant at $p<0.05$.

References

1 Rudin, T. & Pratsinis, S. E. Homogeneous Iron Phosphate Nanoparticles by Combustion of Sprays. *Industrial & Engineering Chemistry Research* **51**, 7891-7900, doi:10.1021/ie202736s (2012).

2 Madler, L., Stark, W. J. & Pratsinis, S. E. Flame-made ceria nanoparticles. *J. Mater. Res.* **17**, 1356-1362, doi:10.1557/jmr.2002.0202 (2002).

3 Perry, D. L. & Phillips, S. L. *Handbook of Inorganic Compounds*. (Taylor & Francis, 1995).

4 Roig, A. I. *et al.* Immortalized epithelial cells derived from human colon biopsies express stem cell markers and differentiate in vitro. *Gastroenterology* **138**, 1012-1021 e1011-1015, doi:10.1053/j.gastro.2009.11.052 (2010).

5 Roberts, I. M. Iso-butanol saturated water: a simple procedure for increasing staining intensity of resin sections for light and electron microscopy. *J. Microsc.-Oxf.* **207**, 97-107, doi:10.1046/j.1365-2818.2002.01045.x (2002).

6 Kroll, A., Pillukat, M. H., Hahn, D. & Schnekenburger, J. Interference of engineered nanoparticles with in vitro toxicity assays. *Archives of Toxicology* **86**, 1123-1136, doi:10.1007/s00204-012-0837-z (2012).

7 Rahman, I., Kode, A. & Biswas, S. K. Assay for quantitative determination of glutathione and glutathione disulfide levels using enzymatic recycling method. *Nature Protocols* **1**, 3159-3165, doi:10.1038/nprot.2006.378 (2006).

8 Toblli, J. E., Cao, G., Olivieri, L. & Angerosa, M. Comparative study of gastrointestinal tract and liver toxicity of ferrous sulfate, iron amino chelate and iron polymaltose complex in normal rats. *Pharmacology* **82**, 127-137, doi:10.1159/000142728 (2008).

9 Appel, M. J., Kuper, C. F. & Woutersen, R. A. Disposition, accumulation and toxicity of iron fed as iron (II) sulfate or as sodium iron EDTA in rats. *Food Chem. Toxicol.* **39**, 261-269 (2001).

10 Lund, E. K., Fairweather-Tait, S. J., Wharf, S. G. & Johnson, I. T. Chronic exposure to high levels of dietary iron fortification increases lipid peroxidation in the mucosa of the rat large intestine. *Journal of Nutrition* **131**, 2928-2931 (2001).

11 Reeves, P. G., Nielsen, F. H. & Fahey Jr, G. C. AIN-93 purified diets for laboratory rodents: Final report of the American Institute of Nutrition ad hoc writing committee on the reformulation of the AIN-76A rodent diet. *Journal of Nutrition* **123**, 1939-1951 (1993).

12 Fielding, J. in *Iron, Methods in Hematology* (ed J.D. Cook) (Churchill Livingstone, 1980).

13 Boysen, G. *et al.* Analysis of 8-oxo-7,8-dihydro-2 '-deoxyguanosine by ultra high pressure liquid chromatography-heat assisted electrospray ionization-tandem mass spectrometry. *J. Chromatogr. B* **878**, 375-380, doi:10.1016/j.jchromb.2009.12.004 (2010).

14 Taghizadeh, K. *et al.* Quantification of DNA damage products resulting from deamination, oxidation and reaction with products of lipid peroxidation by liquid chromatography isotope dilution tandem mass spectrometry. *Nature Protocols* **3**, 1287-1298, doi:10.1038/nprot.2008.119 (2008).

15 Grubbs, F. E. SAMPLE CRITERIA FOR TESTING OUTLYING OBSERVATIONS. *Annals of Mathematical Statistics* **21**, 27-58, doi:10.1214/aoms/1177729885 (1950).

Supplementary Information

Iron phosphate nanoparticles for food applications do not induce adverse effects in rats or human cell lines

Lea M. von Moos[1], Mirjam Schneider[1], Florentine M. Hilty[1], Monika Hilbe[2], Myrtha Arnold[1], Nathalie Ziegler[1], Diogo Sales Mato[1], Hans Winkler[3], Mohamed Tarik[4], Christian Ludwig[4,5] , Hanspeter Naegeli[3], Wolfgang Langhans[1], Michael B. Zimmermann[1], Shana J. Sturla[1], Ioannis A. Trantakis*[1]

[1] Department of Health Sciences and Technology, ETH Zürich, Switzerland

[2] Institute of Veterinary Pathology, Vetsuisse Faculty, University of Zurich, Switzerland

[3] Institute of Pharmacology and Toxicology, Vetsuisse Faculty, University of Zurich, Switzerland

[4] Energy and Environment Research Division, Paul Scherrer Institut (PSI), Switzerland

[5] École Polytechnique Fédérale de Lausanne (EPFL), ENAC-IIE, Lausanne, Switzerland

Table of content

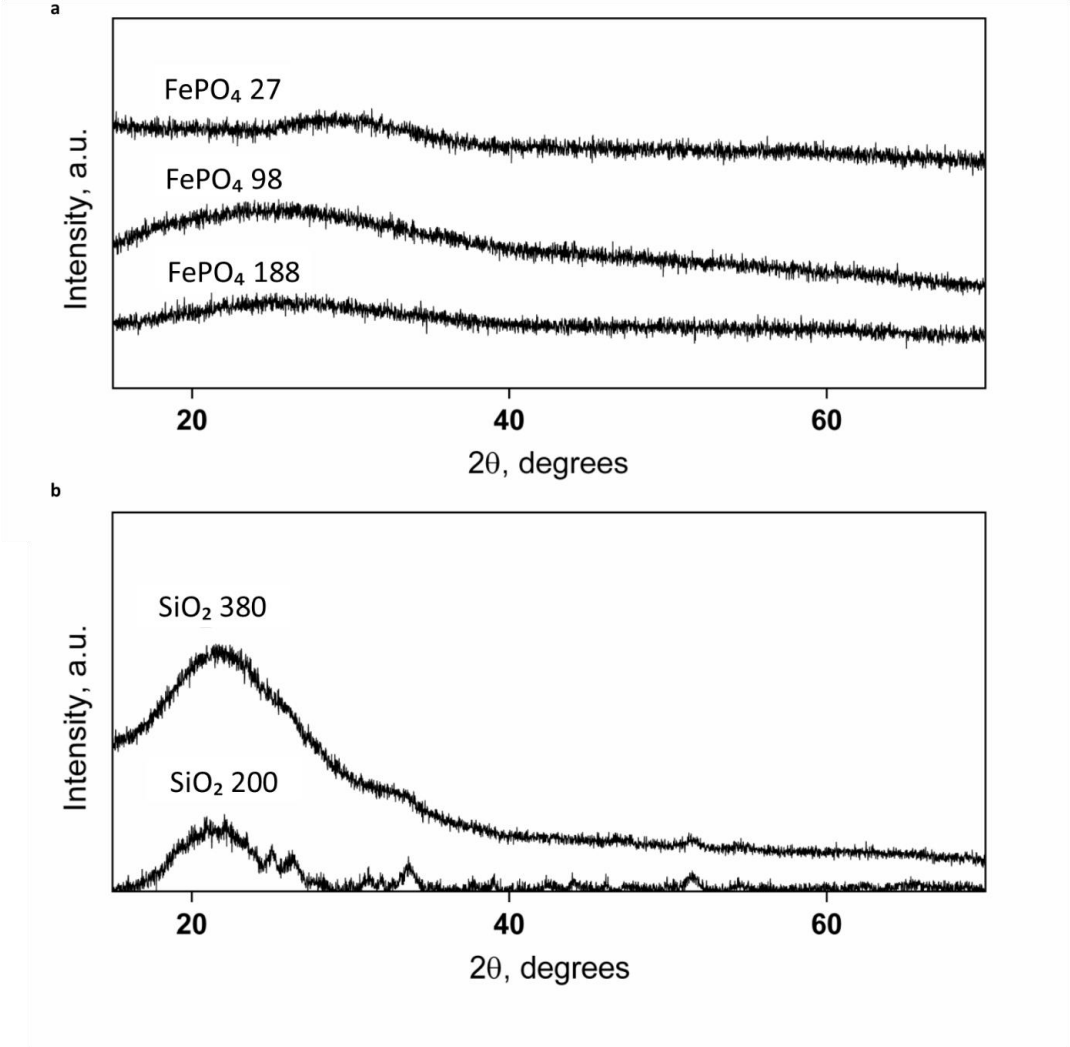

Supplementary Fig. 1. **a)** XRD patterns of $FePO_4$ 27, $FePO_4$ 98 and $FePO_4$ 188. **b)** XRD patterns of SiO_2 200 and SiO_2_380.

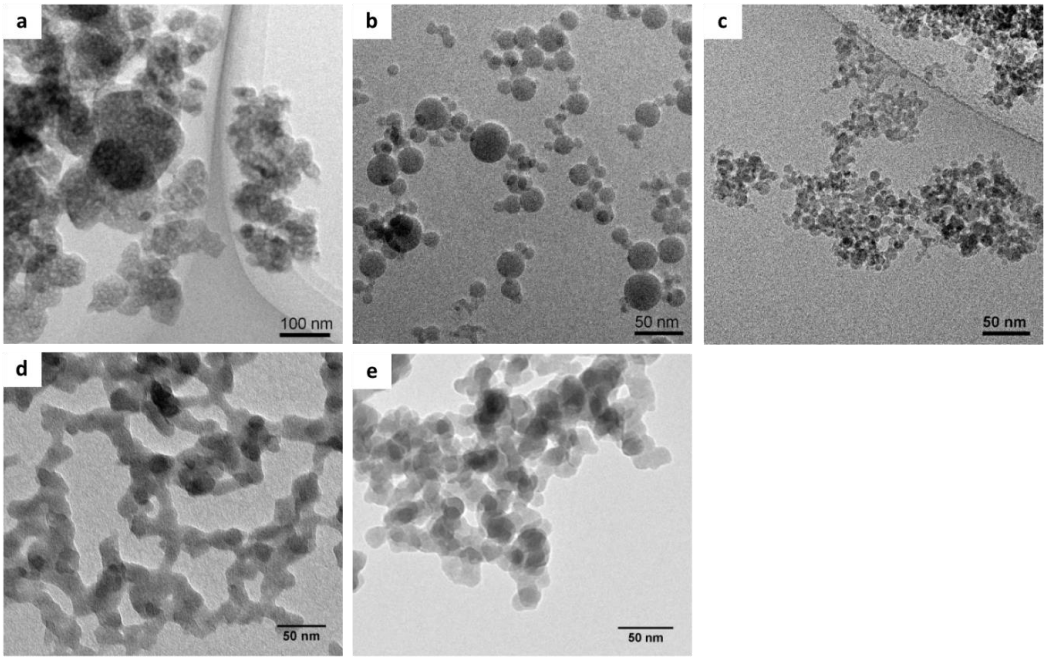

Supplementary Fig. 2. TEM images of **a)** $FePO_4$ 27, **b)** $FePO_4$ 98, **c)** $FePO_4$ 188, **d)** SiO_2 200 and **e)** SiO_2 380.

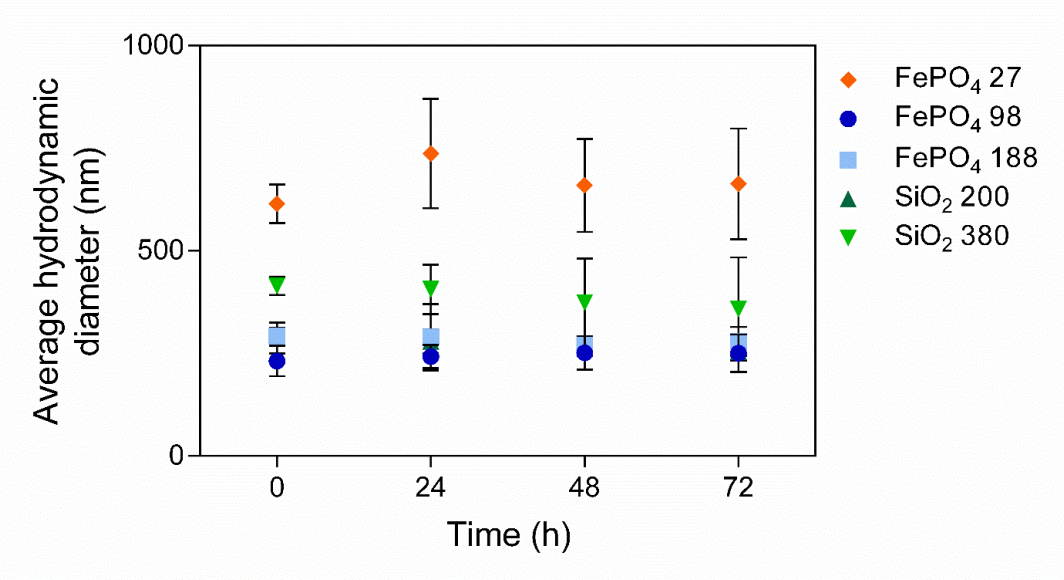

Supplementary Fig. 3. Average hydrodynamic diameter of $FePO_4$ and SiO_2 NPs. The average diameter of $FePO_4$ 27, $FePO_4$ 98, $FePO_4$ 188, SiO_2 200 and SiO_2 380 suspended in DMEM + 10% FBS was measured by DLS directly after ultrasonic dispersion and after 24 h, 48 h and 72 h. Data points represent mean ± SD of three independent experiments.

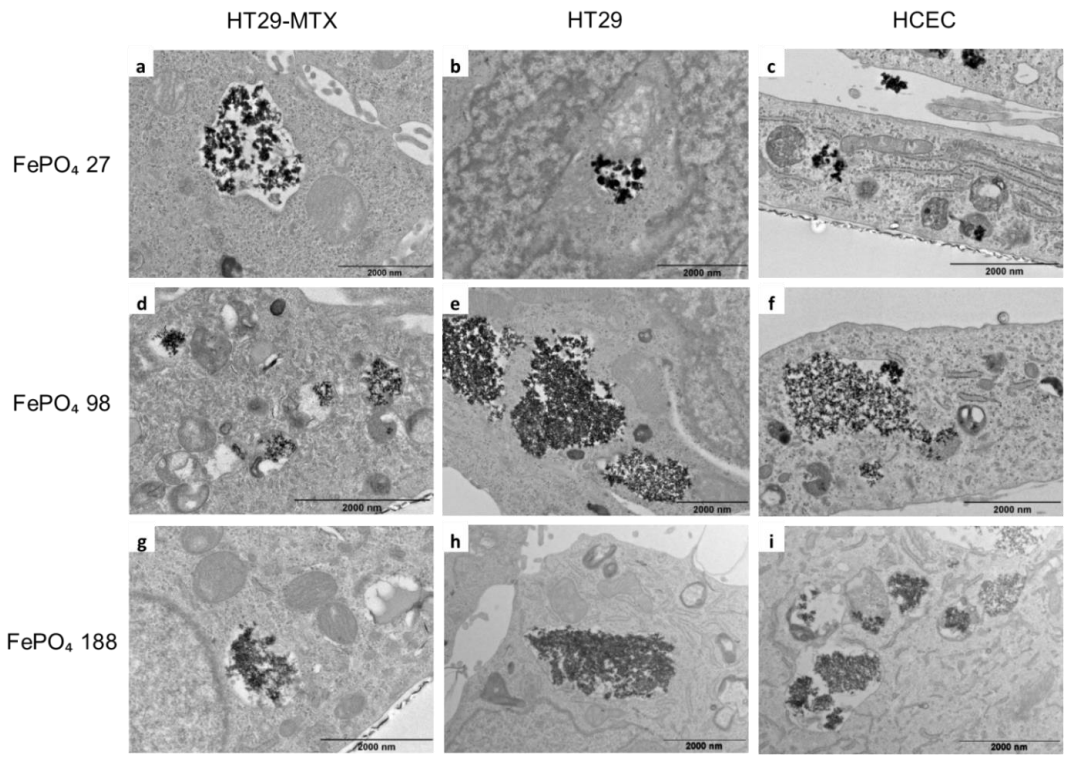

Supplementary Fig. 4. Uptake of $FePO_4$ NPs into intestinal cell lines after 48 h. a) $FePO_4$ 27 in HT29-MTX cells, **b)** $FePO_4$ 27 in HT29 cells, **c)** $FePO_4$ 27 in HCECs, **d)** $FePO_4$ 98 in HT29-MTX cells, **e**) $FePO_4$ 98 in HT29 cells, **f)** $FePO_4$ 98 in HCECs, **g)** $FePO_4$ 188 in HT29-MTX cells, **h)** $FePO_4$ 188 in HT29 cells and **i)** $FePO_4$ 188 in HCECs.

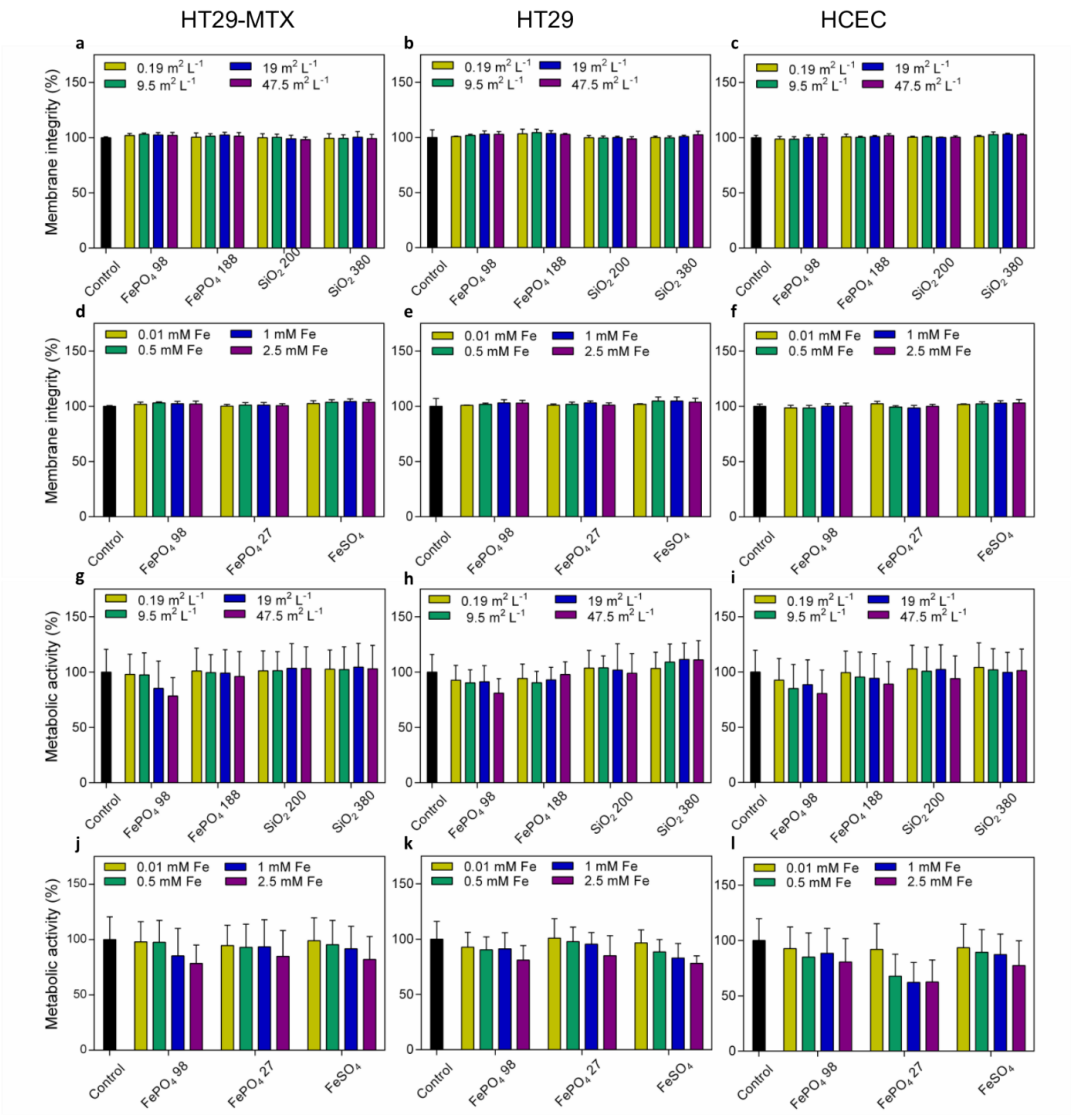

Supplementary Fig. 5. Membrane integrity and metabolic activity of intestinal cell lines upon exposure to increasing concentrations of $FePO_4$ NPs for 24 h. **a-f)** Membrane integrity of HT29-MTX, HT29 and HCEC cells after exposure to $FePO_4$ NPs. As comparison, cells were exposed to equivalent concentrations of **a-c)** SiO_2 NPs (concentrations were standardized on SSA) and to **d-f)** $FePO_4$ 27 and $FeSO_4$ (concentrations were standardized on molar concentrations of Fe). **g-l)** Metabolic activity of HT29-MTX, HT29 and HCEC cells after exposure to $FePO_4$ NPs. As comparison, cells were exposed to equivalent concentrations of **a-c)** SiO_2 NPs (concentrations were standardized on SSA) and to **d-f)** $FePO_4$ 27 and $FeSO_4$ (concentrations were standardized on molar concentrations of Fe). Results are expressed as mean ± SD % metabolic activity relative to untreated cells. Data is from three independent experiments with three technical replicates. Significant differences to untreated control cells were determined with a two way ANOVA and Bonferroni correction, $P<0.05$.

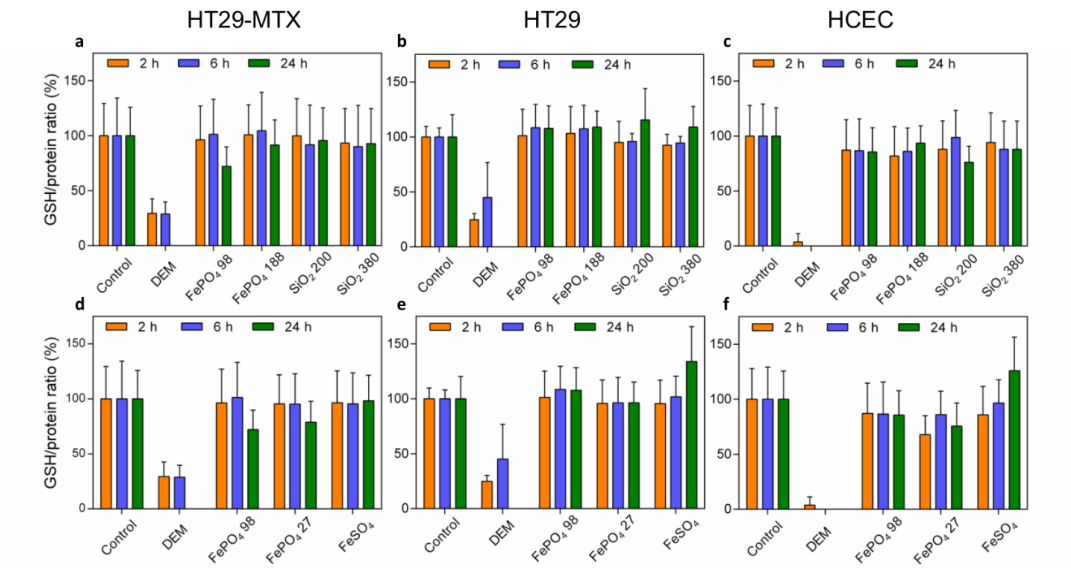

Supplementary Fig. 6. Levels of total glutathione in intestinal cell lines upon exposure to $FePO_4$ NPs. **a-f)** Intracellular GSH concentrations of HT29-MTX, HT29 and HCEC cells after exposure to $FePO_4$ NPs for 2, 6 and 24 h. Cells were also exposed to equal concentrations of **a-c)** SiO_2 NPs (concentration: 47.5 m^2/L) and to **d-f)** $FePO_4$ 27 and $FeSO_4$ (concentration: 2.5 mM Fe). Diethyl maleate (DEM) was used in all experiments as positive control. Results are expressed as mean ± s.d. % metabolic activity relative to untreated cells. Data are from three independent experiments with two technical replicates. Significant differences to untreated control cells were determined with a two way ANOVA and Bonferroni correction, $P<0.05$, and are indicated by *.

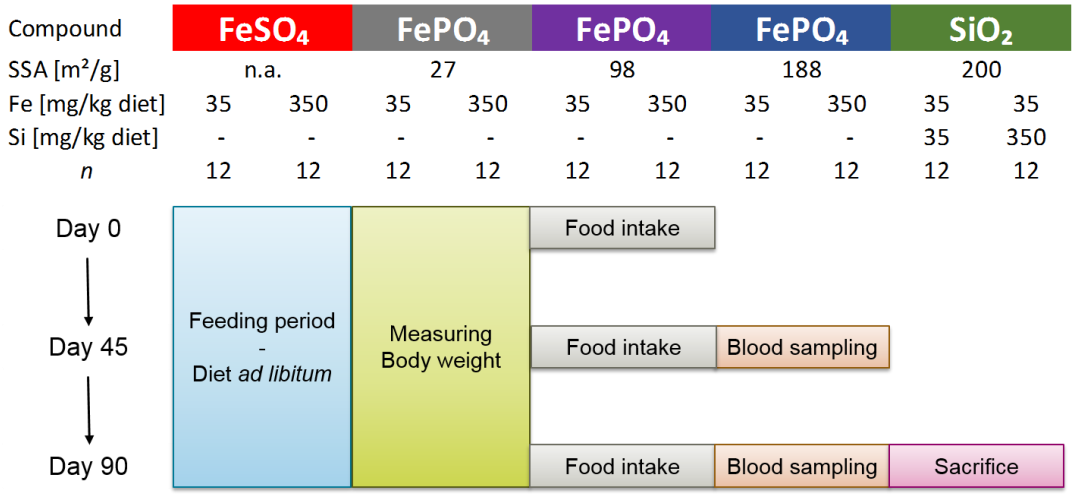

Supplementary Fig. 7. Schematic outline of the sub-chronic exposure study in rats. Animals were fed the corresponding diet for 90 days. Blood was sampled at the midpoint and at the end of the study. Animals were sacrificed after 90 days. n = number of animals per group, SSA = Specific surface area.

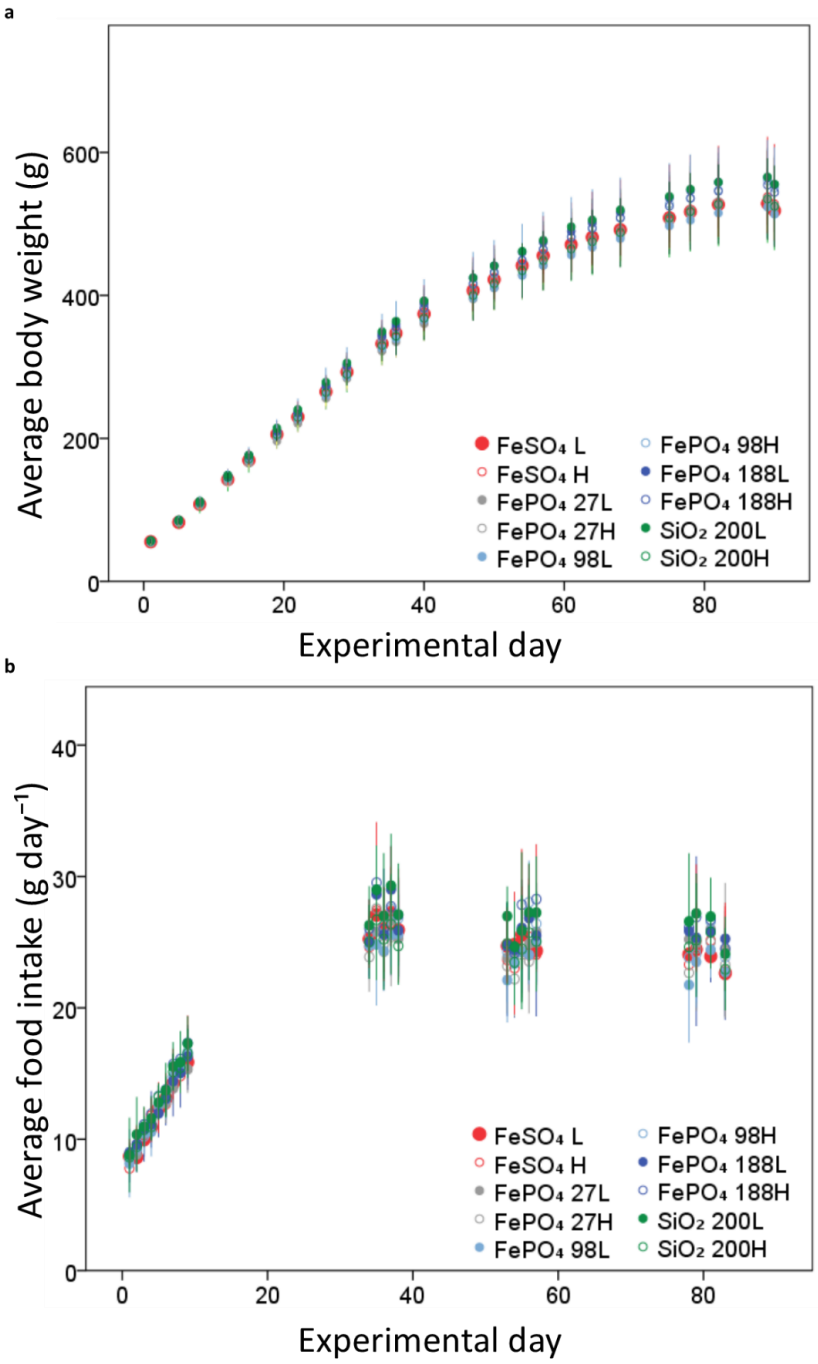

Supplementary Fig. 8. **a)** Body weight of different treatment groups during the study, data points represent mean ± SD. **b)** Food intake of different treatment groups during the study. Data points represent mean ± SD.

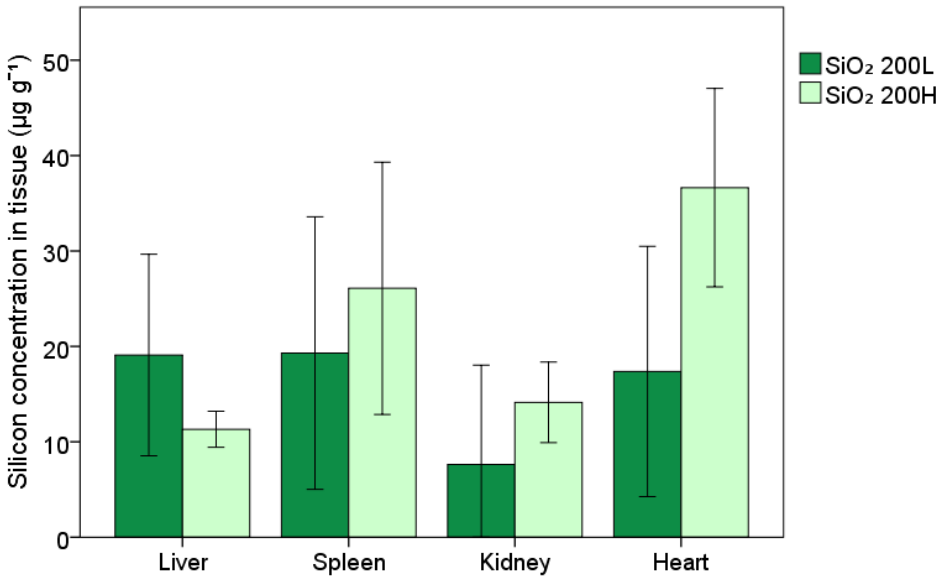

Supplementary Fig. 9. Total silicon concentration in spleen, liver, kidney and heart of animals fed SiO_2 200L and SiO_2 200H. Data points represent mean ± SD. Statistical significance was determined with the Student's t-test, $P<0.05$.

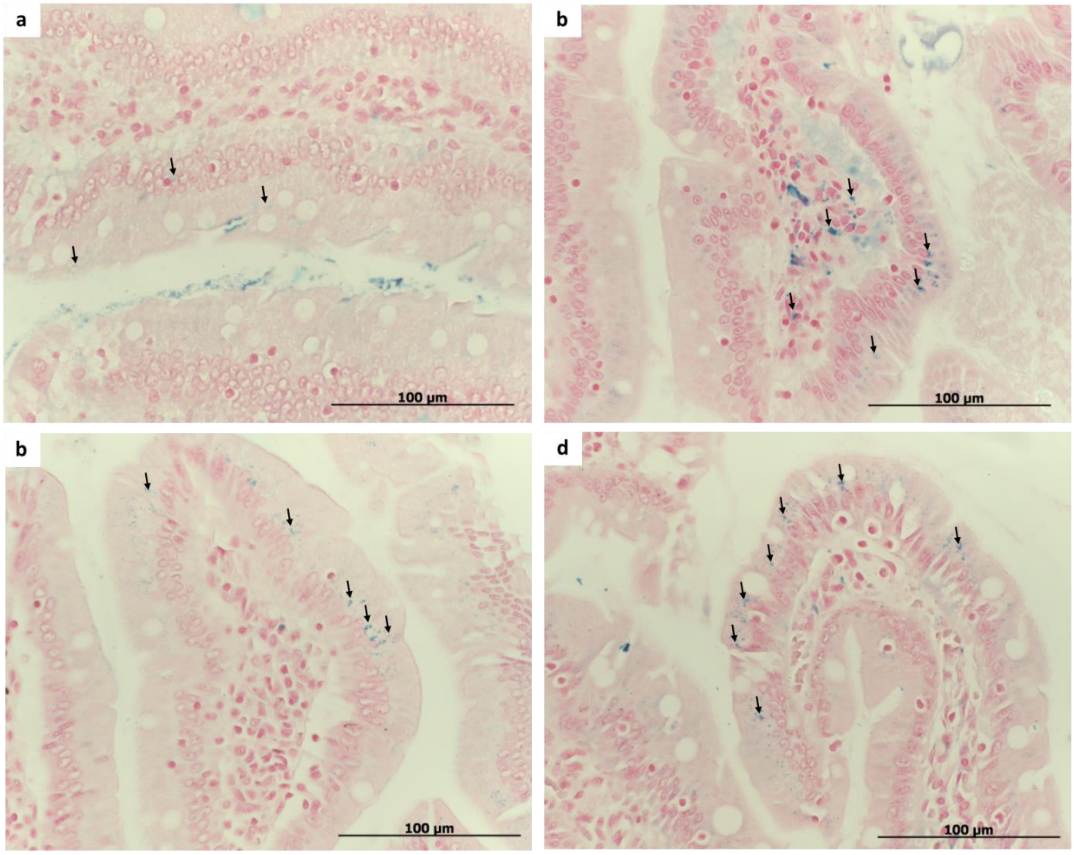

Supplementary Fig. 10. Presence of Fe^{3+} detected by staining with Prussian blue in duodenum of rats fed **a)** $FeSO_4$ H, **b)** $FePO_4$ 27H, **c)** $FePO_4$ 98H, and **d)** $FePO_4$ 188H.

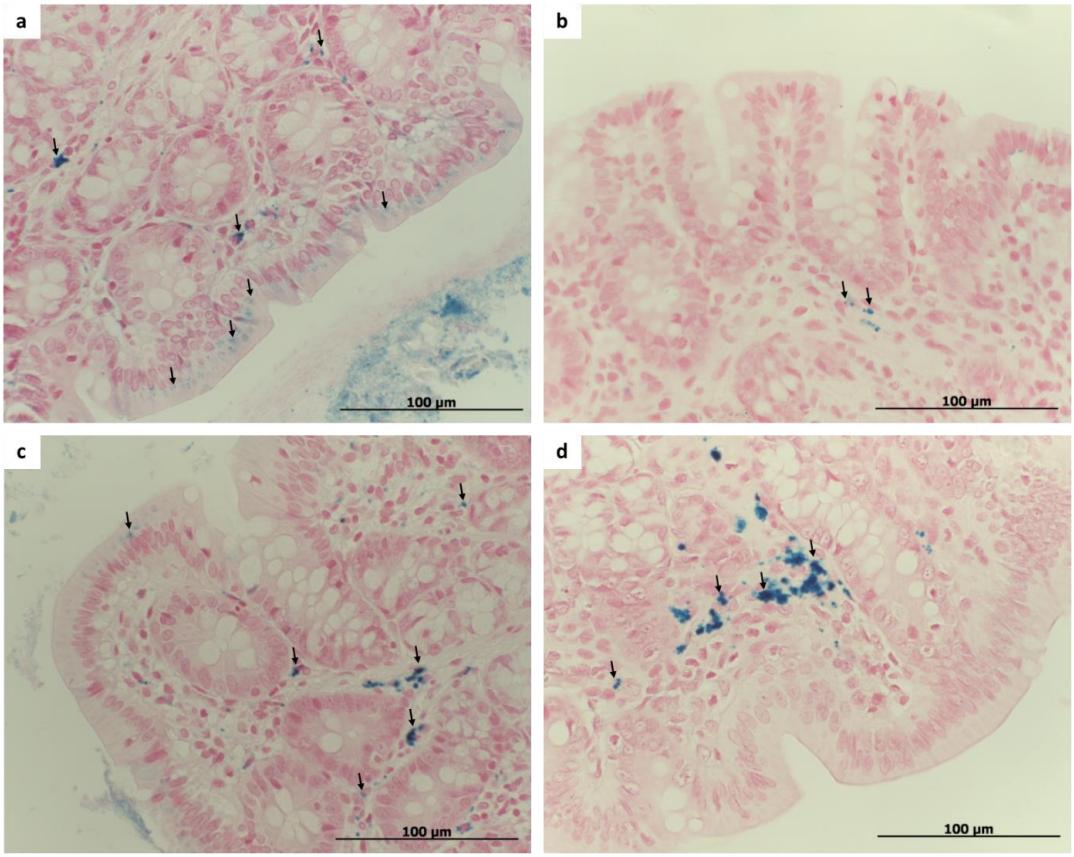

Supplementary Fig. 11. Presence of Fe^{3+} detected by staining with Prussian blue in colon of rats fed **a)** $FeSO_4$ H, **b)** $FePO_4$ 27H, **c)** $FePO_4$ 98H, and **d)** $FePO_4$ 188H.

Supplementary Table 1. Compound characteristics as dry powders and upon suspension in DMEM+.

	SSA[§] (m^2/g)	d_{BET}[¶] (nm)	dH* (nm)	ζ-potential (mV)	PDI[‡]
$FePO_4$ 27	27	77	615±47	-11.9	0.59
$FePO_4$ 98	98±1	21	231±36	-12	0.49
$FePO_4$ 188	188±1	11	292±21	-11.2	0.62
SiO_2 200	175±1	11	287±38	-10.6	0.64
SiO_2 380	326±3	6	415±22	-10.8	0.57

[§]SSA = Specific surface area, [¶]d_{BET} = primary particle size calculated according to the Brunauer–Emmett–Teller theory, assuming dense, spherical particles, *dH = average hydrodynamic diameter, [‡]PDI = Polydispersity index.

Supplementary Table 2. Hematological parameters and biomarkers of iron status

Diet Group	RBC[§], 10^6 mm^{-3}	Hb[¶], g L^{-1}	Hct*, %	MCV[‡], fl	MCH[†], pg	TIBC[ŀ], µg mL^{-1}	PI[Δ], µg mL^{-1}	TSAT[ſ], %
Day 45								
$FeSO_4$ L	6.9 ± 0.6	156.1 ± 9.9^{a}	43.9 ± 3.7	64.0 ± 1.2^{a}	22.8 ± 1.1^{a}	4.8 ± 0.5^{abc}	1.7 ± 0.3^{abcd}	36.1 ± 6.3^{a}
$FeSO_4$ H	6.8 ± 0.4	156.1 ± 7.4^{a}	43.9 ± 2.9	64.8 ± 1.5^{a}	23.0 ± 0.7^{a}	4.8 ± 0.5^{abc}	1.9 ± 0.4^{bd}	40.0 ± 6.6^{a}
$FePO_4$ 27L	7.4 ± 0.3	139.1 ± 14.5^{b}	40.1 ± 4.2	54.5 ± 5.9^{b}	18.9 ± 2.2^{b}	5.2 ± 0.4^{c}	1.2 ± 0.5^{c}	23.3 ± 9.4^{b}
$FePO_4$ 27H	7.0 ± 0.6	158.3 ± 6.2^{a}	44.5 ± 3.0	63.1 ± 2.0^{a}	22.6 ± 1.3^{a}	4.4 ± 0.6^{b}	1.8 ± 0.2^{bd}	38.7 ± 3.0^{a}
$FePO_4$ 98L	6.9 ± 0.5	154.1 ± 7.5^{a}	43.3 ± 2.5	62.4 ± 1.6^{a}	21.9 ± 0.9^{a}	4.5 ± 0.4^{abc}	1.6 ± 0.5^{abcd}	34.5 ± 6.6^{ab}
$FePO_4$ 98H	6.8 ± 0.4	157.0 ± 4.8^{a}	44.3 ± 2.1	65.6 ± 1.2^{a}	23.1 ± 1.5^{a}	4.9 ± 0.6^{abc}	1.9 ± 0.4^{b}	39.5 ± 8.5^{a}
$FePO_4$ 188L	7.0 ± 0.3	155.0 ± 9.5^{a}	42.3 ± 2.1	62.5 ± 1.9^{a}	22.2 ± 1.1^{a}	4.3 ± 0.5^{b}	1.5 ± 0.3^{abcd}	35.2 ± 9.5^{a}
$FePO_4$ 188H	6.7 ± 0.3	157.7 ± 7.6^{a}	43.4 ± 2.1	64.7 ± 1.4^{a}	23.3 ± 0.5^{a}	4.6 ± 0.5^{abc}	1.9 ± 0.2^{bd}	42.6 ± 5.2^{a}
SiO_2 200L	7.0 ± 0.5	153.9 ± 6.3^{a}	43.9 ± 3.1	63.2 ± 1.7^{a}	22.5 ± 1.0^{a}	4.8 ± 0.4^{abc}	1.6 ± 0.4^{abcd}	34.0 ± 8.2^{ab}
SiO_2 200H	7.0 ± 0.2	158.4 ± 6.3^{a}	44.0 ± 2.1	63.4 ± 2.1^{a}	22.9 ± 1.2^{a}	4.5 ± 0.4^{abc}	1.4 ± 0.3^{cd}	31.7 ± 7.5^{ab}
Day 90								
$FeSO_4$ L	8.1 ± 0.4	163.5 ± 10.8^{a}	46.1 ± 2.1	56.9 ± 1.6^{a}	19.9 ± 0.8^{a}	4.7 ± 0.5	1.7 ± 0.4	35.4 ± 8.4
$FeSO_4$ H	8.1 ± 0.4	161.5 ± 9.6^{a}	45.7 ± 3.1	57.4 ± 1.4^{a}	20.3 ± 0.4^{a}	4.7 ± 0.3	1.8 ± 0.1	38.6 ± 3.6
$FePO_4$ 27L	8.2 ± 1.2	148.7 ± 14.2^{b}	43.3 ± 4.6	53.0 ± 3.5^{b}	18.3 ± 1.6^{b}	5.0 ± 0.5	1.6 ± 0.2	30.8 ± 11.0
$FePO_4$ 27H	7.9 ± 0.5	161.1 ± 4.2^{a}	45.6 ± 2.1	56.9 ± 1.7^{a}	20.4 ± 1.2^{a}	4.6 ± 0.6	1.7 ± 0.2	37.8 ± 4.9
$FePO_4$ 98L	8.2 ± 0.3	163.3 ± 6.8^{a}	46.4 ± 1.5	57.4 ± 1.8^{a}	20.2 ± 0.8^{a}	4.8 ± 0.7	1.8 ± 0.3	37.4 ± 6.2
$FePO_4$ 98H	8.0 ± 0.5	167.0 ± 8.0^{a}	47.2 ± 2.6	58.9 ± 1.6^{a}	20.9 ± 1.0^{a}	4.7 ± 0.6	1.9 ± 0.3	40.0 ± 5.3
$FePO_4$ 188L	7.9 ± 0.4	155.5 ± 5.4^{ab}	44.3 ± 1.4	56.3 ± 1.5^{a}	19.5 ± 0.5^{ab}	4.8 ± 0.5	1.6 ± 0.3	33.3 ± 3.6
$FePO_4$ 188H	8.1 ± 0.5	164.5 ± 5.7^{a}	46.5 ± 1.9	57.6 ± 1.6^{a}	20.4 ± 1.0^{a}	4.6 ± 0.5	1.7 ± 0.2	36.7 ± 4.7
SiO_2 200L	8.0 ± 0.4	161.4 ± 6.4^{a}	45.7 ± 1.6	57.1 ± 1.6^{a}	20.2 ± 1.1^{a}	4.8 ± 0.3	1.7 ± 0.3	36.0 ± 6.7
SiO_2 200H	8.2 ± 0.4	164.6 ± 5.1^{a}	47.1 ± 1.6	57.3 ± 1.9^{a}	20.0 ± 0.8^{a}	4.8 ± 0.3	1.8 ± 0.3	37.4 ± 5.8

Values are means ± SD. Statistical significance was determined with a two way ANOVA and Bonferroni correction, $P<0.05$. Values without a common letter (a, b, c or d) are statistically different. [§]RBC = Red blood cells, [¶]Hb = Hemoglobin, *Hct = Hematocrit, [‡]MCV = Mean corpuscular volume, [†]MCH = Mean corpuscular hemoglobin, [ŀ]TIBC = Total iron binding capacity, [Δ]PI = Plasma iron, [ſ]TSAT = Transferrin saturation.

Supplementary Table 3. Plasma biochemistry parameters

Diet Group	ALAT[§], U L^{-1}	ASAT[¶], U L^{-1}	ALP*, U L^{-1}	GGT[‡], U L^{-1}	Urea, mmol L^{-1}	Creatinine, µmol L^{-1}	Uric acid, µmol L^{-1}
Day 45							
$FeSO_4$ L	21.8 ± 4.6	60.4 ± 5.9	236.7 ± 58.3	1.0 ± 0.9	5.1 ± 0.7	21.3 ± 6.5	14.2 ± 10.8
$FeSO_4$ H	23.0 ± 5.4	56.4 ± 7.9	209.6 ± 50.0	0.9 ± 0.4	5.0 ± 0.8	19.3 ± 36.4	20.6 ± 14.1
$FePO_4$ 27L	27.8 ± 5.7	68.2 ± 8.5	231.7 ± 32.0	0.8 ± 0.4	4.5 ± 0.2	19.0 ± 3.3	7.6 ± 3.5
$FePO_4$ 27H	22.3 ± 2.3	58.4 ± 5.6	200.0 ± 32.4	0.7 ± 0.4	5.0 ± 0.5	26.0 ± 23.9	16.9 ± 9.4
$FePO_4$ 98L	21.4 ± 3.5	59.4 ± 5.3	222.4 ± 48.0	0.5 ± 0.3	5.0 ± 0.4	21.0 ± 3.9	17.1 ± 12.0
$FePO_4$ 98H	20.7 ± 3.7	54.0 ± 6.1	194.6 ± 36.9	0.8 ± 0.6	4.9 ± 0.8	20.1 ± 2.4	11.2 ± 4.1
$FePO_4$ 188L	23.0 ± 2.8	59.8 ± 6.5	199.6 ± 63.0	0.8 ± 0.4	4.9 ± 0.6	21.4 ± 6.9	13.2 ± 6.4
$FePO_4$ 188H	22.7 ± 3.3	58.9 ± 6.2	186.4 ± 26.6	0.6 ± 0.4	5.0 ± 0.7	17.9 ± 4.0	13.2 ± 4.5
SiO_2 200L	21.8 ± 4.3	56.6 ± 6.1	219.8 ± 38.1	0.9 ± 0.5	5.3 ± 1.3	20.8 ± 4.4	13.5 ± 8.4
SiO_2 200H	21.9 ± 6.3	59.9 ± 6.1	235.0 ± 34.5	1.1 ± 1.5	5.2 ± 1.0	22.0 ± 7.1	13.8 ± 9.0
Day 90							
$FeSO_4$ L	24.3 ± 3.9	59.6 ± 7.9	125.8 ± 23.3	1.2 ± 0.7	5.6 ± 0.7	24.6 ± 5.2	13.9 ± 6.4
$FeSO_4$ H	22.5 ± 4.8	54.5 ± 6.3	130.0 ± 32.7	1.2 ± 0.7	5.5 ± 0.6	25.8 ± 5.6	14.4 ± 4.7
$FePO_4$ 27L	28.4 ± 6.0	63.8 ± 3.8	131.1 ± 24.3	0.7 ± 0.4	5.4 ± 0.4	22.7 ± 2.9	10.6 ± 3.9
$FePO_4$ 27H	24.8 ± 3.9	58.5 ± 11.0	119.4 ± 20.8	0.9 ± 0.4	5.5 ± 0.7	26.3 ± 3.2	9.5 ± 4.9
$FePO_4$ 98L	22.4 ± 3.3	57.5 ± 4.4	117.1 ± 18.9	0.8 ± 0.3	5.4 ± 0.4	27.4 ± 5.9	10.7 ± 4.9
$FePO_4$ 98H	22.5 ± 4.5	56.9 ± 8.3	115.8 ± 25.3	0.7 ± 0.3	5.5 ± 0.4	26.2 ± 4.2	11.2 ± 4.4
$FePO_4$ 188L	22.4 ± 4.6	60.4 ± 8.2	127.8 ± 40.2	1.5 ± 1.1	5.8 ± 0.4	26.9 ± 5.5	13.8 ± 7.9
$FePO_4$ 188H	24.0 ± 4.5	56.3 ± 4.2	118.7 ± 29.8	0.8 ± 0.6	5.6 ± 0.7	24.6 ± 6.4	10.5 ± 6.2
SiO_2 200L	21.8 ± 3.3	58.8 ± 6.4	117.9 ± 19.4	1.2 ± 0.6	5.6 ± 0.6	29.4 ± 7.2	13.9 ± 6.9
SiO_2 200H	23.6 ± 4.5	59.3 ± 5.0	136.3 ± 10.3	1.1 ± 0.6	5.9 ± 0.6	25.0 ± 5.7	13.9 ± 9.4

Values are means ± SD. Statistical significance was determined with a two way ANOVA and Bonferroni correction, $P<0.05$. Values without a common letter (a, b, c or d) are statistically different. [§]ALAT = Alanine aminotransferase, [¶]ASAT = Aspartate aminotransferase, *ALP = Alkaline phosphatase, [‡]GGT = γ-glutamyl transferase

Additives and Nutrient Sources Added to Food on Calcium Silicate, Silicon Dioxide and Silicic Acid Gel Added for Nutritional Purposes to Food Supplements Following a Request from the European Commission. *EFSA J.* **2009**, *1132*, 1–24.

(3) Rudin, T.; Pratsinis, S. E. Homogeneous Iron Phosphate Nanoparticles by Combustion of Sprays. *Ind. Eng. Chem. Res.* **2012**, *51*, 7891–7900.

4 Materials and Methods

Materials and Methods are listed in the paper in section 3.1. An experimental overview is shown in Figure 1.

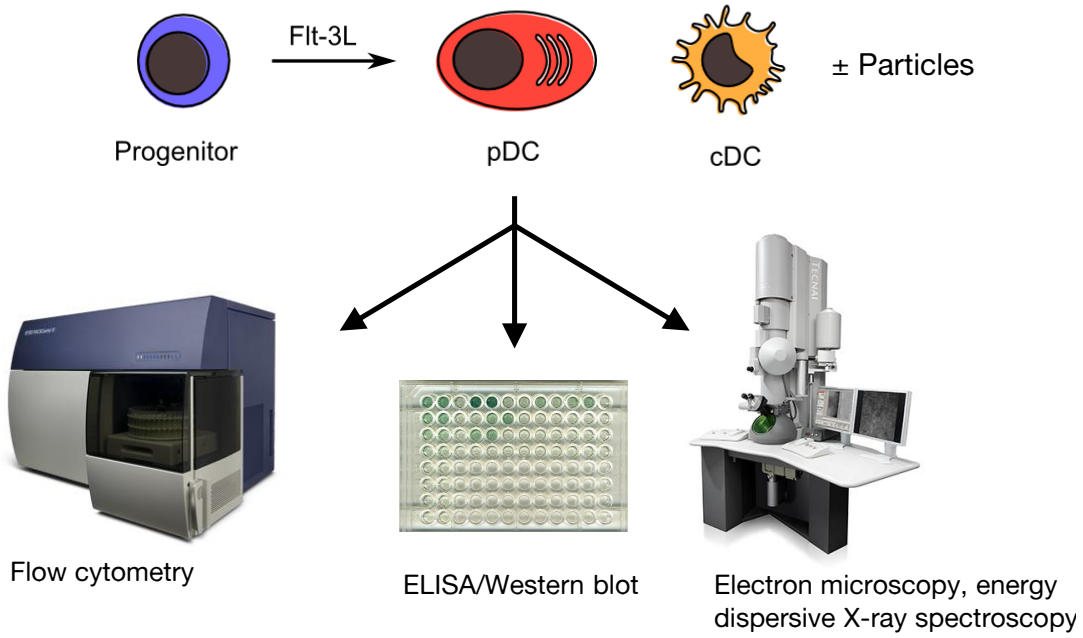

Figure 1. Experimental overview Immature DCs were generated from mouse bone marrow cultures containing hematopoietic progenitors and stem cells. After eight days of incubation with Flt3L, these cells were incubated with food-grade nanoparticles. DC surface and maturation markers were monitored by flow cytometry. Pro-inflammatory cytokine induction and secretion were analyzed by immunoassays (ELISA/western blot). Internalization of particles was analyzed by transmission electron microscopy. Elemental analysis of the particles in DCs was done by energy dispersive X-ray spectroscopy.

4.1 Generation of steady-state DCs from mouse bone marrow

All media were stored at 4°C. Mammalian cells were cultured at 37°C and 5% CO_2, in a humified incubator. Cell culture experiments were performed under a sterile hood.

A modified Neubauer counting chamber and sterile 0.4% trypan blue solution (ICN Biomedicals) were used to determine the exact number of live cells. Immature DCs were generated from mouse bone marrow as described (Naik et al., 2010). Briefly, femurs and tibiae of C57BL/6 mice were flushed with complete culture medium and the released progenitor cells were filtered through a 70-μm cell strainer (BD Falcon), centrifuged, reconstituted in complete medium and incubated for 8 days in the presence of 200 ng/ml Flt3L (BioXcell). For each culture, the amount of live CD11c+ DCs, the proportion of plasmacytoid DCs ($CD11c^+B220^+$) and conventional DCs ($CD11c^+B220^-CD11b^{high}$ $SIRP\alpha^+$ and $CD11c^+$ $B220^-CD11b^{intermediate}SIRP\alpha^-$) were verified by flow cytometry

4.2 Flow cytometry

5×10^5 DCs were harvested by centrifugation for 5 min at 500 g, washed with two times with PBS and stained on ice with conjugated antibodies against CD11c (N418, PE-labeled), CD11b (M1/70, PE-Cy7-labeled), B220 (RA3-6B2, APC-eFluor 780-labeled), SIRPα (P84, APC-labeled), CD40 (1C10, PE-labeled), CD62L (MEL-14, APC-labeled), CD69 (H1.2F3, APC-labeled) and CD86 (GL1, PE-labeled) purchased from eBioscience. A FACSCanto II flow cytometry instrument (BD Biosciences) was employed to acquire 50'000 events. Dead cells were stained and excluded from analyses using propidium iodide (PI; Sigma-Aldrich). Single-color and fluorescence-minus-one (FMO) controls were prepared and analyzed along with multi-color samples. Flow cytometry data were analyzed with FlowJo (Version 10, TreeStar).

4.3 Immunoassays

Immunoassays were performed as described in 3.1. For immunoblots, proteins resolved by SDS-PAGE were transferred from the polyacrylamide gel onto PVDF membrane (Biorad) at a current of 25V for 7 min. After 1 h incubation in blocking solution (10% milk in TBST) to avoid unspecific binding, the membrane was incubated over night with the primary antibody diluted in TBST and 2.5% milk. Afterwards the membrane was washed 3 x with TBST and incubated for 1 h with the appropriate secondary antibody. The membrane was washed again 3 x with TBST, drained and developped with enhanced chemiluminescence (ECL) solution (Fisher Scientific). Chemiluminenscence was detected using a ChemiDoc MP documentation system (Biorad).

4.4 Cryo-fixation and transmission electron microscopy

Immature DCs were transferred to 12-well plates (3×10^6 cells/well) containing complete cell culture medium (1 ml/well). After incubation with particles (250 μg/ml), cells were prefixed with 0.25% (vol/vol) glutaraldehyde and immediately high-pressure frozen in capillary cellulose tubes using an EM HPM 100 device (Leica). Frozen cells were transferred into a substitution unit (EM-AFS2, Leica) precooled to –90°C for substitution with acetone containing 5% water. The subsequent fixation was carried out with 1% (wt/vol) osmium tetraoxide, 0.25% (vol/vol) glutaraldehyde raising the temperature to 20°C, then the cells were embedded in epon. Ultrathin (70 nm) sections were contrasted with uranyl acetate and lead citrate for 15 min (for standard contrast) or 1 min (for improved detection of particles) (Roberts, 2002) and examined in a transmission electron microscope (CM12, Philips) equipped with a CCD camera (Ultrascan 1000, Gatan) at an acceleration voltage of 100 kV. Elemental analysis of selected samples was conducted on a scanning transmission electron microscope (G2 Spirit, FEI Tecnai) equipped with a high angle annular dark field detector (HAADF) and an X-Max energy-dispersive X-ray spectroscopy (EDX) detection system for elemental analysis (Oxford). Gatan digital micrograph was used for image acquisition and Oxford INCA for EDX operation and control.

5 Discussion and outlook

The aim of this thesis was to investigate the effects of food-borne nanomaterials on dendritic cells *in-vitro*. We thus set out to investigate whether nanoparticles interact with steady-state dendritic cells and if this interaction leads to functional implications.

Toxicologists often asked, if the SAS particle concentrations used during this thesis were in a realistic range. While particle concentrations in human Peyer's patches or mesenteric lymph nodes are unknown, a sub-chronic feeding study in rats, with repeated oral administration of 2500 μg/kg SAS per day, detected concentrations up to 300 mg/kg SiO_2 in the spleen (van der Zande et al., 2014). The high silica concentration of 2500 μg/kg SAS per day is equivalent to the NOAEL used for the risk assessment of SAS as a food additive for human consumption (UK Food Standards Agency, 2003; EFSA, 2009). Therefore a range of different particle doses were tested, with the highest dose equivalent to the silica concentration found in the speen of rats orally exposed to SAS particles. This high SAS concentration of 250 μg/ml did not induce cytotoxic effects *in-vitro*. In addition, in our studies, food-grade SAS particles caused significant pro-IL-1β-induction in immature dendritic cells already at the lowest concentration used (30 μg/ml).

While conducting electron microscopy experiments with dendritic cells but also with epithelial cell lines, it became evident that both cell types are able to internalize SAS and $FePO_4$ particles. A very important difference was their uptake kinetics – internalized particles in dendritic cells could be detected already after two hours of incubation, while epithelial cells needed 24-48 hours for particle uptake. This cell type specific property underscores the biological importance of dendritic cells as sentinels of the immune system in the Peyer's patches of the small intestine.

In lung-related studies with alveolar macrophages, no pro-IL-1β-induction could be detected in response to SAS particles without LPS priming (Rabolli et al., 2014). The same authors report further that pro-IL-1β-induction in the lung is dependent on IL-1α secretion. In contrast, in our studies food-grade SAS particles caused pro-IL-1β-induction in unprimed immature dendritic cells without concomitant IL-1α secretion (Figure 1). This points to important organ- and celltype-specific differences, which should be taken

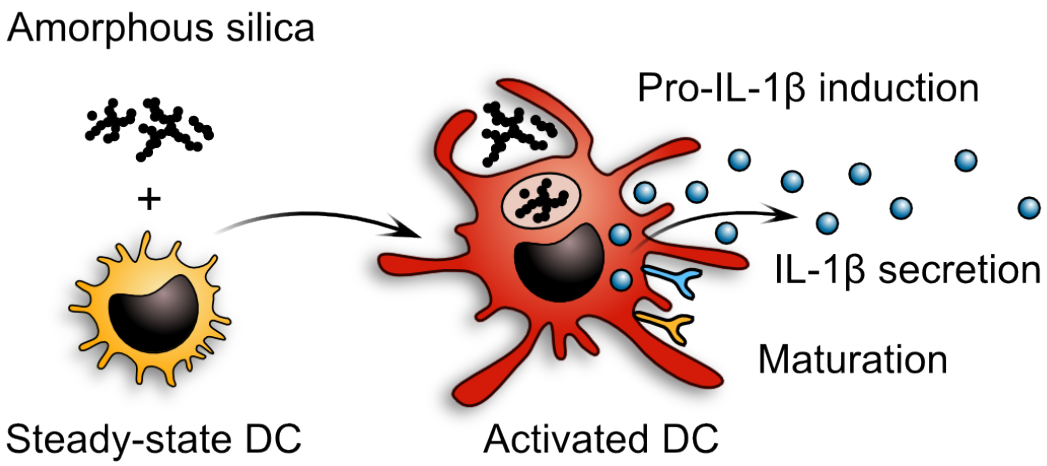

Figure 1. The response of Flt3L-generated immature DCs defines SAS as the first complete inflammatory nanomaterial. In steady-state (immature) DCs, the potent inflammatory cytokine IL-1β is not expressed and secretion is highly regulated by two independent signals. Exposure to food-grade silica causes both pro-IL-1β induction and its cleavage leading to IL-1β secretion. In addition, immature DCs undergo maturation involving shifts in multiple surface markers.

into account for toxicological risk assessments of food-grade nanomaterials and need further investigation on a mechanistic level.

The finding that SAS particles induce pro-IL-1β-induction and IL-1β secretion from immature DCs has several implications. First, the dose dependent induction of the highly regulated inflammatory cytokine pro-IL-1β implies the presence of a cellular receptor for the detection of SAS particles in DCs.

This receptor has to be intracellular and not on the cell surface, as may be concluded from the observation that inhibition of SAS particle internalization by co-treatment with cytochalasin D or rottlerin reduces IL-1β secretion to baseline levels. This hypothesis is supported by electron microscopy data, which demonstrated intracellular localization of SAS particles in endosomes after internalization.

Given that SAS particles are found in the endosome after uptake, it follows that a receptor for monitoring SAS particles would be strategically well placed at the very same location. Therefore, inhibition of endosomal acidification was tested, a prerequisite for endosomal detection by pattern recognition receptors such as TLR9. Chloroquine was previously shown to inhibit acidification of the endosome and detection of single stranded DNA by TLR9 (Rutz et al., 2004). Therefore, the next step was to assess the effects of chloroquine on pro-IL-1β induction. Co-treatment with chloroquine or bafilomycin A1 (another inhibitor of endosomal acidification) reduced pro-IL-1β induction to baseline levels. This indicates that SAS particles are sensed by an endosomal pattern recognition

receptor.

Hence, DC deficient for TLR2, TLR3, TLR4, TLR7 and TLR9 were tested for their ability to induce pro-IL-1β. The observation, that these cells retained the ability to induce pro-IL-1β upon treatment with SAS particles confirmed that this response was not due to microbial contamination with endotoxin or DNA but the identification of the exact receptor remained elusive.

Consequential, activation of a pattern recognition receptor implies that SAS particles mimic or represent a pathogen-associated microbial pattern (PAMP). This could be due to the repetitive surface of SAS particles, which are composed of an ordered pattern of OH^- groups (Zhang et al., 2012) and/or the particulate nature of SAS. With a primary particle size of 10-20 nm SAS particles are in the same size range as non-enveloped small single-stranded DNA viruses such as parvo- or circoviruses. Therefore it seems likely, that SAS particles could act as ”cuckoo's eggs” inside of endosomes. This property suggests that SAS particles may be used as an adjuvant for fine tuning immunological response to vaccines.

On the other hand, the reason for evolution and propagation of a particle specific-sensing mechanism for SAS is of interest. Why did such a mechanism evolve in DCs and is passed on despite it's inherent fitness costs such as energy consumption? On the one hand, particulate sensing could increase the alertness of the immune system in a “dirty” environment already before detection of a specific pathogen. Because the timely defense response towards a pathogen is of high importance for immunity, this could lead to faster and therefore more effective defense reactions. In addition particulate sensing appears to be involved in fine tuning the immunological response. While immature DCs are activated by SAS particles, neither pro-IL-1β induction nor IL-1β secretion is triggered upon internalization of TiO_2 or $FePO_4$ nanoparticles. Follwoing this line of thought, it would be interesting to engineer particles having both the anticaking properties of silica used as food additive combined with the surface characteristics of TiO_2 or $FePO_4$ particles to obtain a less pyrogenic substitue for silica. In addition, it may be worth the effort to investigate the response of dendritic cells towards aluminosilicate particles used often as anticaking agent in food in replacement of SAS particles.

Silica (silicone dioxide) has currently the highest production volume of all engineered nanomaterials worldwide (Yang et al., 2016). Widespread applications in the food industry use synthetic amorphous silica (SAS) as anticaking agent in powdered food products, as defoaming agent in beverages, as a thickener in pastes or carrier of flavorings (Dekkers et al., 2011; Peters et al., 2012). After oral uptake, SAS particles withstand gastrointestinal digestion (Peters et al., 2012) and reach the ileal mucosa. In human subjects, intesti-

nal particle deposits in Peyer's patches were reported to be composed of the elements silicon (Si), titanium (Ti) and aluminum (Al) (Shepherd et al., 1987). While particle concentrations in human Peyer's patches or mesenteric lymph nodes are unknown, a sub-chronic feeding study in rats, with repeated oral administration of 2500 μg/kg SAS per day (equivalent to the NOAEL used for the risk assessment of SAS as a food additive for human consumption (UK Food Standards Agency, 2003; EFSA, 2009)), detected concentrations up to 300 mg/kg SiO_2 in the spleen (van der Zande et al., 2014). This concentration detected *in vivo* is about 10 times higher than the dose which induced significant effects in our *in vitro* assay. Therefore, effects of SAS on DCs seem likely and a reduction of SAS-application in food products may be warranted.

Due to the widespread use of silica in food and it's enormous production volume, our finding that SAS particles induce pro-IL-1β-induction and IL-1β secretion from immature DCs might be relevant for consumers, food industry and regulatory authorities. Highly exposed consumers themselves could reduce their exposure to SAS particles, avoiding food products which contain high amounts of SAS particles. Where possible, food industry may reduce SAS-application in products, or consider substitute products for anticaking or defoaming agents, thickeners or carriers of flavorings. The *in-vitro* test with immature DCs developed during this thesis could be used to screen for a suitable substitute product. For regulatory authorities our finding could have significant value, since it identified a new hazard of SAS particles. As mentioned in the previous paragraph, SAS particles induce significant pro-IL-1β-induction from immature DCs at concentrations about 10 times lower than those detected in the spleen of rodents treated with the NOAEL of SAS. Consequently, future risk assessments of SAS particles for food-products should include an assessment of their effects on local intestinal immunity including DCs. Finally, inclusion of the *in-vitro* test with immature DCs developed during this thesis in planned tiered-testing strategies could benefit the safe application of food-borne nanomaterials.

References

Awaad, A., Nakamura, M., & Ishimura, K. (2012). Imaging of size-dependent uptake and identification of novel pathways in mouse Peyer's patches using fluorescent organosilica particles. *Nanomedicine*, *8*(5), 627–636.

Bekiaris, V., Persson, E. K., & Agace, W. W. (2014). Intestinal dendritic cells in the regulation of mucosal immunity. *Immunol. Rev. 260*(1), 86–101.

Bogunovic, M., Ginhoux, F., Helft, J., Shang, L., Hashimoto, D., Greter, M., Liu, K., Jakubzick, C., Ingersoll, M. A., Leboeuf, M., Stanley, E. R., Nussenzweig, M., Lira, S. A., Randolph, G. J., & Merad, M. (2009). Origin of the lamina propria dendritic cell network. *Immunity*, *31*(3), 513–525.

Castellaneta, A., Abe, M., Morelli, A. E., & Thomson, A. W. (2004). Identification and characterization of intestinal Peyer's patch interferon-alpha producing (plasmacytoid) dendritic cells. *Hum. Immunol. 65*(2), 104–113.

Cheers, C., Haigh, A. M., Kelso, A., Metcalf, D., Stanley, E. R., & Young, A. M. (1988). Production of colony-stimulating factors (CSFs) during infection: separate determinations of macrophage-, granulocyte-, granulocyte-macrophage-, and multi-CSFs. *Infect. Immun. 56*(1), 247–251.

Dalod, M., Chelbi, R., Malissen, B., & Lawrence, T. (2014). Dendritic cell maturation: functional specialization through signaling specificity and transcriptional programming. *EMBO J. 33*(10), 1104–1116.

Dekkers, S., Krystek, P., Peters, R. J. B., Lankveld, D. P. K., Bokkers, B. G. H., van Hoeven-Arentzen, P. H., Bouwmeester, H., & Oomen, A. G. (2011). Presence and risks of nanosilica in food products. *Nanotoxicology*, *5*(3), 393–405.

Dinarello, C. A. (2011). Interleukin-1 in the pathogenesis and treatment of inflammatory diseases. *Blood*, *117*(14), 3720–3732.

EFSA. (2009). European Food Safety Authority. Scientific opinion of the panel on food additives and nutrient sources added to food on calcium silicate, silicon dioxide and silicic acid gel added for nutritional purposes to food supplements following a request from the. *EFSA J. 1132*, 1–24. doi:10.2903/j.efsa.2009.1132

Evans, S. M., Ashwood, P., Warley, A., Berisha, F., Thompson, R. P., & Powell, J. J. (2002). The role of dietary microparticles and calcium in apoptosis and interleukin-1β release of intestinal macrophages. *Gastroenterology*, *123*(5), 1543–1553.

Franchi, L., Eigenbrod, T., & Nunez, G. (2009). Cutting edge: TNF-alpha mediates sensitization to ATP and silica via the NLRP3 inflammasome in the absence of microbial stimulation. *J. Immunol. 183*(2), 792–796.

Guo, J., Gu, N., Chen, J., Shi, T., Zhou, Y., Rong, Y., Zhou, T., Yang, W., Cui, X., & Chen, W. (2013). Neutralization of interleukin-1 beta attenuates silica-induced lung inflammation and fibrosis in C57BL/6 mice. *Arch. Toxicol. 87*(11), 1963–1973.

Hilty, F. M., Arnold, M., Hilbe, M., Teleki, A., Knijnenburg, J. T. N., Ehrensperger, F., Hurrell, R. F., Pratsinis, S. E., Langhans, W., & Zimmermann, M. B. (2010). Iron from nanocompounds containing iron and zinc is highly bioavailable in rats without tissue accumulation. *Nat. Nanotechnol. 5*(5), 374–380.

Hochrein, H., Schlatter, B., O'Keeffe, M., Wagner, C., Schmitz, F., Schiemann, M., Bauer, S., Suter, M., & Wagner, H. (2004). Herpes simplex virus type-1 induces IFN-alpha production via Toll-like receptor 9-dependent and -independent pathways. *Proc. Natl. Acad. Sci. U. S. A. 101*(31), 11416–11421.

Hummel, T. Z., Kindermann, A., Stokkers, P. C. F., Benninga, M. A., & ten Kate, F. J. W. (2014). Exogenous pigment in Peyer patches of children suspected of having IBD. *J. Pediatr. Gastroenterol. Nutr. 58*(4), 477–480.

Lomer, M. C. E., Thompson, R. P. H., & Powell, J. J. (2002). Fine and ultrafine particles of the diet: influence on the mucosal immune response and association with Crohn's disease. *Proc. Nutr. Soc. 61*(01), 123–130.

Naik, S. H., O'Keeffe, M., Proietto, A., Shortman, K., & Wu, L. (2010). CD8+, CD8−, and plasmacytoid dendritic cell generation in vitro using flt3 ligand. *Methods Mol Biol*, *595*, 167–176.

Netea, M. G., van de Veerdonk, F. L., van der Meer, J. W. M., Dinarello, C. A., & Joosten, L. A. B. (2015). Inflammasome-independent regulation of IL-1-family cytokines. *Annu. Rev. Immunol. 33*, 49–77.

Pandey, S., Kawai, T., & Akira, S. (2015). Microbial sensing by Toll-like receptors and intracellular nucleic acid sensors. *Cold Spring Harb. Perspect. Biol. 7*(1), a016246. doi:10.1101/cshperspect.a016246

Park, E.-J., Yoon, J., Choi, K., Yi, J., & Park, K. (2009). Induction of chronic inflammation in mice treated with titanium dioxide nanoparticles by intratracheal instillation. *Toxicology*, *260*(1-3), 37–46.

Pele, L. C., Thoree, V., Bruggraber, S. F. A., Koller, D., Thompson, R. P. H., Lomer, M. C., & Powell, J. J. (2015). Pharmaceutical/food grade titanium dioxide particles are absorbed into the bloodstream of human volunteers. *Part. Fibre Toxicol. 12*, 26. doi:10.1186/s12989-015-0101-9

Peters, R., Kramer, E., Oomen, A. G., Herrera Rivera, Z. E., Oegema, G., Tromp, P. C., Fokkink, R., Rietveld, A., Marvin, H. J. P., Weigel, S., Peijnenburg, A. A. C. M., & Bouwmeester, H. (2012). Presence of nano-sized silica during in vitro digestion of foods containing silica as a food additive. *ACS Nano*, *6*(3), 2441–2451.

Powell, J. J., Ainley, C. C., Harvey, R. S., Mason, I. M., Kendall, M. D., Sankey, E. A., Dhillon, A. P., & Thompson, R. P. (1996). Characterisation of inorganic microparticles in pigment cells of human gut associated lymphoid tissue. *Gut*, *38*(3), 390–395.

Rabolli, V., Badissi, A. A., Devosse, R., Uwambayinema, F., Yakoub, Y., Palmai-Pallag, M., Lebrun, A., De Gussem, V., Couillin, I., Ryffel, B., Marbaix, E., Lison, D., & Huaux, F. (2014, December). The alarmin IL-1α is a master cytokine in acute lung inflammation induced by silica micro- and nanoparticles. *Part. Fibre Toxicol. 11*(1), 69. doi:10.1186/s12989-014-0069-x

Rescigno, M. (2009). Before they were gut dendritic cells. *Immunity*, *31*(3), 454–456.

Roberts, I. M. (2002). Iso-butanol saturated water: A simple procedure for increasing staining intensity of resin sections for light and electron microscopy. *J. Microsc. 207*(2), 97–107.

Rutz, M., Metzger, J., Gellert, T., Luppa, P., Lipford, G. B., Wagner, H., & Bauer, S. (2004). Toll-like receptor 9 binds single-stranded CpG-DNA in a sequence- and pH-dependent manner. *Eur. J. Immunol. 34*(9), 2541–2550.

Sallusto, F., Cella, M., Danieli, C., & Lanzavecchia, A. (1995). Dendritic cells use macropinocytosis and the mannose receptor to concentrate macromolecules in the major histocompatibility complex class II compartment: downregulation by cytokines and bacterial products. *J. Exp. Med. 182*(2), 389–400.

Sarkar, K., Kruhlak, M. J., Erlandsen, S. L., & Shaw, S. (2005). Selective inhibition by rottlerin of macropinocytosis in monocyte-derived dendritic cells. *Immunology, 116*(4), 513–524.

Scott, C. L., Tfp, Z. M., Beckham, K. S. H., Douce, G., & Mowat, A. M. (2014). Signal regulatory protein alpha (SIRPalpha) regulates the homeostasis of CD103(+) CD11b(+) DCs in the intestinal lamina propria. *Eur. J. Immunol. 44*(12), 3658–3668.

Sepeur, S., Laryea, N., Goedicke, S., & Groß, F. (2008). *Nanotechnology: Technical Basics and Applications.* Hannover: Vincentz Network.

Shepherd, N. A., Crocker, P. R., Smith, A. P., & Levison, D. A. (1987). Exogenous pigment in Peyer's patches. *Hum. Pathol. 18*(1), 50–54.

Shortman, K. & Naik, S. H. (2007). Steady-state and inflammatory dendritic-cell development. *Nat. Rev. Immunol. 7*(1), 19–30.

Sun, B., Pokhrel, S., Dunphy, D. R., Zhang, H., Ji, Z., Wang, X., Wang, M., Liao, Y.-P., Chang, C. H., Dong, J., Li, R., Madler, L., Brinker, C. J., Nel, A. E., & Xia, T. (2015). Reduction of Acute Inflammatory Effects of Fumed Silica Nanoparticles in the Lung by Adjusting Silanol Display through Calcination and Metal Doping. *ACS Nano*, *9*(9), 9357–9372.

UK Food Standards Agency. (2003). Safe upper levels for vitamins and minerals: report of the expert group on vitamins and minerals. Retrieved April 25, 2016, from URL: http://cot.food.gov.uk/sites/default/files/vitmin2003.pdf

van der Zande, M., Vandebriel, R. J., Groot, M. J., Kramer, E., Herrera Rivera, Z. E., Rasmussen, K., Ossenkoppele, J. S., Tromp, P., Gremmer, E. R., Peters, R. J., Hendriksen, P. J., Marvin, H. J., Hoogenboom, R. L., Peijnenburg, A. A., & Bouwmeester, H. (2014). Sub-chronic toxicity study in rats orally exposed to nanostructured silica. *Part. Fibre Toxicol. 11*(1), 8. doi:10.1186/1743-8977-11-8

Varol, C., Vallon-Eberhard, A., Elinav, E., Aychek, T., Shapira, Y., Luche, H., Fehling, H. J., Hardt, W.-D., Shakhar, G., & Jung, S. (2009). Intestinal lamina propria dendritic cell subsets have different origin and functions. *Immunity*, *31*(3), 502–512.

Wang, X., Mansukhani, N. D., Guiney, L. M., Lee, J.-H., Li, R., Sun, B., Liao, Y.-P., Chang, C. H., Ji, Z., Xia, T., Hersam, M. C., & Nel, A. E. (2016). Toxicological profiling of highly purified metallic and semiconducting single-walled carbon nanotubes in the rodent lung and E. coli. *ACS Nano*, *10*(6), 6008–6019.

Warheit, D. B. & Donner, E. M. (2015). Risk assessment strategies for nanoscale and fine-sized titanium dioxide particles: Recognizing hazard and exposure issues. *Food Chem. Toxicol. 85*, 138–147.

Watowich, S. S. & Liu, Y.-J. (2010). Mechanisms regulating dendritic cell specification and development. *Immunol. Rev. 238*(1), 76–92.

Weir, A., Westerhoff, P., Fabricius, L., Hristovski, K., & von Goetz, N. (2012). Titanium dioxide nanoparticles in food and personal care products. *Environ. Sci. Technol. 46*(4), 2242–2250.

Winkler, H. C., Suter, M., & Naegeli, H. (2016). Critical review of the safety assessment of nano-structured silica additives in food. *J. Nanobiotechnology*, *14*(1), 44. doi:10.1186/s12951-016-0189-6

Winter, M., Beer, H.-D., Hornung, V., Krämer, U., Schins, R. P. F., & Förster, I. (2011). Activation of the inflammasome by amorphous silica and TiO2 nanoparticles in murine dendritic cells. *Nanotoxicology*, *5*(3), 326–340.

Xu, Y., Zhan, Y., Lew, A. M., Naik, S. H., & Kershaw, M. H. (2007). Differential development of murine dendritic cells by GM-CSF versus Flt3 ligand has implications for inflammation and trafficking. *J. Immunol. 179*(11), 7577–7584.

Yada, R. Y., Buck, N., Canady, R., DeMerlis, C., Duncan, T., Janer, G., Juneja, L., Lin, M., McClements, D. J., Noonan, G., Oxley, J., Sabliov, C., Tsytsikova, L., Vázquez-Campos, S., Yourick, J., Zhong, Q., & Thurmond, S. (2014). Engineered nanoscale food ingredients: evaluation of current knowledge on material characteristics relevant to uptake from the gastrointestinal tract. *Compr. Rev. Food Sci. Food Saf. 13*(4), 730–744.

Yang, Y., Faust, J. J., Schoepf, J., Hristovski, K., Capco, D. G., Herckes, P., & Westerhoff, P. (2016). Survey of food-grade silica dioxide nanomaterial occurrence, characterization, human gut impacts and fate across its lifecycle. *Sci. Total Environ. 565*, 902–912.

Yazdi, A. S., Guarda, G., Riteau, N., Drexler, S. K., Tardivel, A., Couillin, I., & Tschopp, J. (2010). Nanoparticles activate the NLR pyrin domain containing 3 (Nlrp3) inflammasome and cause pulmonary inflammation through release of IL-1α and IL-1β. *Proc. Natl. Acad. Sci. U. S. A. 107*(45), 19449–19454.

Zhang, H. Y., Dunphy, D. R., Jiang, X. M., Meng, H., Sun, B. B., Tarn, D., Xue, M., Wang, X., Lin, S. J., Ji, Z. X., Li, R. B., Garcia, F. L., Yang, J., Kirk, M. L., Xia, T., Zink, J. I., Nel, A., & Brinker, C. J. (2012). Processing pathway dependence of amorphous silica nanoparticle toxicity: colloidal vs pyrolytic. *J Am Chem Soc*, *134*(38), 15790–15804.

Zucker, R. M., Massaro, E. J., Sanders, K. M., Degn, L. L., & Boyes, W. K. (2010). Detection of TiO2 nanoparticles in cells by flow cytometry. *Cytometry. A*, *77*(7), 677–685.

Acknowledgments

First, I would like to acknowledge my supervisor Hanspeter Naegeli for giving me the opportunity to carry out this project at the Institute of Veterinary Pharmacology and Toxicology. Thank you for your support, the friendly and constructive environment at the institute and for being a great mentor. Next, I would like to thank my other supervisors Mark Suter and Peter Wick for advice on DCs and nanoparticle characterization. My PhD committee, Barbara Rothen-Rutishauser and Cornel Fraefel, supported my work through the project, thank you for helpful discussions. A special thank goes to Barbara Bathke and Hubertus Hochrein for teaching me how to generate DCs and always having time to answer my questions. In addition, I would like to highly acknowledge Lea von Moos and Florentine Hilty for a very pleasant collaboration. I also would like to acknowledge all the other "ETH NFP64" members for helpful discussions.

I would like to thank Elisabeth Schraner for introduction to the electron microscope, assistance with high pressure freezing and help with preparing and contrasting ultrathin sections.

I'd like to thank all the colleagues of the Nägeli group. Sandro Imhasly for ROS experiments, Julian Kornprobst for conducting many antigen uptake and NP-DC interaction experiments and Zuzana Garajova for excellent technical support. Chiara Balbo Pogliano, Tamara Codilupi, Elena Clementi, Enni Markkanen, Peter Rüthemann and the members of Professor Meyer's group; thank you for the awesome research atmosphere in lab.

I also would like to highly acknowledge all the other members of the Institute of Veterinary Pharmacology and Toxicology for the friendly working environment. NFP64, Microbiology and Immunology (MIM) PhD program and MD-PhD program organized great scientific and social gatherings, I'd like to thank you for the ones involved.

Above all I would like to thank my family, my dear and incomparable wife Eleni and my friends for the continuous support.

Curriculum Vitae

Surname	WINKLER
Given Names	Hans Christian
Date of birth	March 8, 1986
Place of birth	Winterthur, ZH
Place of origin	Zürich, ZH and Basel, BS

Education

7/2012–present	**PhD,** University of Zürich, Switzerland Microbiology and Immunology PhD program, UZH/ETH, Laboratory of Prof. Dr. Hanspeter Nägeli Thesis: Development of an *in vitro* test to assess the risk of food-borne nanomaterials on dendritic cells
11/2011–10/2012	**DVM,** University of Zürich, Switzerland Laboratory of Dr. Paul O. Hassa Thesis: Identification of macro domain-specific interaction partners of B-aggressive lymphoma proteins (BALs) by mass spectrometry
8/2011–10/2011	**Staatsexamen in Veterinary Medicine**
6/2009–8/2009	**Leadership Program for Veterinary Students**, Cornell University, Ithaca, USA. Laboratory of Dr. Colin Parrish, Baker Institute
2006–2011	**Studies in Veterinary Medicine,** University of Zurich. Major Biomedical Research.
2002–2006	**Alte Kantonsschule Aarau, Aargau** Akzentfach Latein, Schwerpunktfach Biologie und Chemie, Ergänzungsfach Philosophie

Awards and presentations

05/2016	**10. International Nano-Dialogue, Bern, Switzerland** Oral presentation
1/2016-12/2016	**Research grant**, Forschungskredit University of Zürich

2015	**Gordon Research Conference** "Nanoscale Science & Engineering for Agriculture & Food Systems", Boston, USA 1st Place Graduate Poster Presentation
2015	**Travel grant,** Swiss Society of Pharmacology and Toxicology
2009	**Fellowship,** Leadership Program for Veterinary Students, Cornell University, Ithaca NY, USA

Teaching experience

10/2015–02/2016	**Supervision of a master student,** ETH Zürich
2015	**Supervision of a semester student,** ETH Zürich
03/2015	**Cell culture laboratory course,** University of Zurich
2014	**Supervision of a semester student,** ETH Zürich
03/2013	**Cell culture laboratory course,** University of Zurich
2012–2016	**Assistant lecturer MSc in Toxicology course,** University of Basel
2008–2009	**Immunology teaching assistant (Tutor)** for Prof. Dr. Mark Suter, Immunology, Vetsuisse Faculty, University of Zurich

Publications

Winkler HC, Suter M, Naegeli H. (2016). Critical review of the safety assessment of nano-structured silica additives in food. *J. Nanobiotechnology*, 14:44.

Camicia R, **Winkler HC**, Hassa PO. (2015). Novel drug targets for personalized precision medicine in relapsed/refractory diffuse large B-cell lymphoma: a comprehensive review. *Mol. Cancer*, 14:207.

Bachmann SB, Frommel SC, Camicia R, **Winkler HC**, Santoro R, Hassa PO. (2014). DTX3L and ARTD9 inhibit IRF1 expression and mediate in cooperation with ARTD8 survival and proliferation of metastatic prostate cancer cells. *Mol. Cancer*, 13:125.

Rosenthal F, Feijs KLH, Frugier E, Bonalli M, Forst AH, Imhof R, **Winkler HC**, Fischer D, Caflisch A, Hassa PO, Lüscher B, Hottiger MO. (2013). Macrodomain-containing proteins are new mono-ADP-ribosylhydrolases. *Nat. Struct. & Mol. Biol.*, 20(4), 502-507.

Camicia R, Bachmann SB, **Winkler HC**, Beer M, Tinguely M, Haralambieva E, Hassa PO. (2013). BAL1/ARTD9 represses the anti-proliferative and pro-apoptotic IFNγ–STAT1–IRF1–p53 axis in diffuse large B-cell lymphoma. *J. Cell. Sci.*, 126(9), 1969-1980.